Trigger Analysis and Modeling of Very Large Debris Flows in Santa Teresa, Cusco, Southern Peru

Figure 1: Santa Teresa after the debris flows in 1998. Source: Avalos, 2011.

GEO 511: Master Thesis
Department of Geography
University of Zurich

Buis Daniel, S09709338
daniel.buis@sunrise.ch; 079 465 51 56

Supervision by:
PD Dr. Christian Huggel
Dr. Holger Frey
M. Sc. Claudia Giráldez

Responsible Faculty Member:
Prof. Dr. Andreas Vieli

Delivery: 31.01.2014

Summary

The Peruvian Andes have repeatedly been affected by large mass movements such as landslides, avalanches and debris flows. In 1998, two very large debris flows in the region of Machu Picchu (Sacsara and Ahobamba), southern Peru, destroyed the town of Santa Teresa, an important hydropower scheme and further infrastructure. The debris flows on the order of 5 to 25 mill. m^3 volume rank among the largest recently observed events of this type worldwide. Despite their extreme dimensions, these events have not been studied in detail. An important limitation for more insight studies is the remote location of the mass flows and the very sparse information and data available for the study region. Neither triggering processes nor mass flow process characteristics have been understood to date. This thesis tries to fill some of these gaps in understanding that are critical to improved assessment of hazards and eventual risk reduction measures.

For the trigger analysis, data and information from field work; a limited number of ground based meteorological data; and complementary satellite derived data was used. Results indicate that in the case of the Sacsara event, heavy rainfall likely was a main trigger. For Ahobamba, antecedent rainfall as well as snow and ice melt leading to saturation of glacial sediments must have played an important role.

Simulations with a dynamic debris flow model (RAMMS) allowed to constrain a number of flow parameters such as flow height and velocity, runout distance and flow and deposition volumes. Strong surging flow behavior was detected, resulting in very large runout distance (exceeding 20 km); which rather depends on the largest single surge volume, not the total event volume. Based on the identification of potential mass flow sources, several scenarios were modeled. The assessment of related hazards, including a preliminary hazard map, showed that several communities in catchments draining towards Santa Teresa are endangered by mass movements. Monitoring of the hazard situation is strongly recommended. Design and implementation of tailored risk reduction strategies are currently undertaken within an international Peruvian-Swiss project in close collaboration with local communities and the municipality of Santa Teresa.

Zusammenfassung

Die Peruanischen Anden wurden wiederholt von grossen Massenbewegungen wie Erdrutschen, Lawinen und Murgängen heimgesucht. Zwei sehr grosse Murgänge im Jahr 1998 in der Region Machu Picchu (Sacsara und Ahobamba) im südlichen Peru zerstörten das Dorf Santa Teresa, ein wichtiges Wasserkraftwerk und weitere Infrastrukturen. Die Murgänge mit Volumen von 5 bis 25 Mio. m^3 gehören zu den weltweit grössten beobachteten derartigen Massenbewegungen in letzter Zeit. Trotz ihrer extremen Dimensionen wurden diese Ereignisse nie im Detail untersucht. Wichtige Einschränkungen für ausführlichere Studien sind die Abgelegenheit der Murgänge und die nur spärlich vorhandenen Informationen und Daten über das Studiengebiet. Weder Ursachen noch Fliessverhalten wurden bisher untersucht. Diese Arbeit versucht, einige dieser Verständnislücken zu füllen, um die Gefahrenbewertung zu verbessern und die Basis für Risikoreduktionsmassnahmen zu legen.

Für die Ursachenanalyse wurden Daten und Informationen von Feldarbeiten; eine beschränkte Zahl von bodenbasierten meteorologischen Daten; sowie ergänzende satellitenbasierte Daten verwendet. Die Resultate zeigen dass starke Niederschläge vermutlich die Hauptursache des Sacsara-Ereignisses waren. Beim Ahobamba-Ereignis spielten der Vorregen sowie Schnee- und Eisschmelze, welche in Gletschersedimente infiltrierten, eine wichtige Rolle.

Simulationen mit dem dynamischen Murgangmodell RAMMS erlaubten, einige Fliessparameter wie Fliesshöhe und –Geschwindigkeit; Auslaufdistanz und Fliess- und Depositionsvolumen einzugrenzen. Ausgeprägte Fliessschübe wurden festgestellt, was zu sehr grossen Auslaufdistanzen führte (über 20 km). Diese hängen eher vom Volumen des grössten einzelnen Schubes ab als vom Gesamtereignisvolumen. Einige Szenarien wurden basierend auf potentiellen Entstehungsorten von Massenbewegungen modelliert. Eine Gefahrenbewertung möglicher Ereignisse, inklusive einer Gefahrenhinweiskarte, zeigte dass einige Dörfer in Einzugsgebieten um Santa Teresa von Massenbewegungen bedroht sind. Monitoring der Gefahrensituation wird dringend empfohlen. Das Design und die Umsetzung geeigneter Risikoreduktionsstrategien werden momentan innerhalb eines internationalen Peruanisch-Schweizerischen Projekts erarbeitet, in enger Zusammenarbeit mit der Lokalbevölkerung und der Gemeinde Santa Teresa.

Resumen

Los Andes Peruanos repetidamente han sido afectados por grandes movimientos de masa como deslizamientos, avalanchas y aluviones. En 1998, dos grandes aluviones en la region de Machu Picchu (Sacsara y Ahobamba), en el sur de Peru, destruyeron el pueblo de Santa Teresa, una importante central hidroeléctrica e infrastructura adicional. Los aluviones, en el orden de 5 a 25 millones m^3 de volumen, son unos de los mayores eventos recientes observado en todo el mundo. A pesar de sus enormes dimensiones, estos eventos no han sido estudiados en detalle. Las mayores limitaciones para estos estudios son la lejanía a los movimientos de masa y la limitada disponibilidad de información y datos sobre el área de estudio. Ni los causas detonantes ni las características de flujo de los movimientos de masa han sido comprendidos hasta ahora. Esta tesis intenta aumentar la comprensión sobre estos eventos, necesario para mejorar la evaluación de peligros y las medidas de reducción de riesgos.

En la evaluación de las causas detonantes, se han utilizado datos e información de trabajo de campo; uno número limitado de estaciones meteorológicas; y datos satelitales. Los resultados indican que el evento de Sacsara probablemente fue causado por fuerte precipitación. En el evento de Ahobamba, la precipitación antecedente junto con la fusión de nieve y hielo que saturaron los sedimentos glaciales jugaron un papel importante.

Simulaciones con un modelo dinamico para aluviones (RAMMS) ha hecho posible restringir varios parametros de flujo; como la altura y la velocidad de flujo, la distancia recorrida y el volumen de flujo y de deposición. Fueron detectados varios pulsos, que resultaron en muy largas distancias de recorrido (más de 20 km). Estas distancias dependen más del volumen de los pulsos individuales que del volumen total del evento. Basándose en la identificación de posibles orígenes de los movimientos de masa, se modelaron varios escenarios. La evaluación de amenazas, incluyendo un mapa de amenazas preliminar, indica que varias comunidades en las cuencas que drenan hasta Santa Teresa estan en peligro por movimientos de masa. Se recomienda fuertemente el monitoreo de la situación de amenaza. La creación e implementación de estrategias para la reducción de riesgos están siendo efectuadas por un proyecto internacional Peruano-Suizo, en estrecha colaboración con las comunidades locales y la municipalidad de Santa Teresa.

Preface

Glaciology, climate change and natural hazards have fascinated me for years, making this thesis a perfect topic for my interests. This thesis would not have been possible without the help of many. First of all, many thanks to my advisors; Christian Huggel; Holger Frey; and Claudia Giráldez, for all your help setting up this thesis and your tips on various parts of the work flow, e.g. methodology and structure. Your generous help during the last six months was greatly appreciated.

Thanks also to Andreas Vieli, who agreed to this thesis as responsible faculty member. Many thanks to Marc Christen, Yves Bühler, Christoph Graf and Yvonne Schaub, for your patience with my problems with RAMMS. To Demian Schneider, who helped me with RAMMS and the modeling methodology. To Mario Rohrer, for your help with interpreting the sparse climatic data. To César Portocarrero, Felipe Fernandez and Victor Carlotto from Peru, for your information on both the study area and the events in 1998. To Christoph Rohner, helping me out with Matlab and Excel; and to Marco Walser, for your literature list. Finally, thanks to everyone who reviewed this thesis: Maëlle Mühlethaler; Adrian Duss and my parents.

Daniel Buis
Zürich, 23.01.2014

Contents

List of Abbreviations

ASTER GDEM2:	Advanced Spaceborne Thermal Emission and Reflection Radiometer Global Digital Elevation Model Version 2
CARE:	Cooperative for Assistance and Relief Everywhere
CCA DRR:	Climate Change Adaptation and Disaster Risk Reduction
CGIAR:	Group on International Agricultural Research
DEM:	Digital Elevation Model
DesInventar:	Disaster Inventory System
EPFL:	École Polytechnique Fédérale de Lausanne
GIS:	Geographic Information System
GLOF:	Glacier Lake Outburst Flood
IGN:	Instituto Geográfico Nacional
IR:	Infrared
Lidar:	Light Detection and Ranging
PACC:	Programa de Adaptación al Cambio Climático
PET:	Peru time
PR:	Precipitation radar
Radar:	Radio Detection and Ranging
RAMMS:	RApid Mass MovementS
RMSE:	Root Mean Square Error
SDC:	Swiss Agency for Development and Cooperation
SENAMHI	Servicio Nacional de Meteorología e Hidrología del Perú
SLF:	Swiss Federal Institute for Snow and Avalanche Research
SRTM:	Shuttle Radar Topography Mission
TMI:	TRMM Microwave Imager
TMPA:	TRMM Multi-satellite Precipitation Analysis
TM5:	Thematic Mapper Version 5
TRMM:	Tropical Rainfall Measuring Mission
UGRH:	Unidad de Glaciología y Recursos Hídricos
USGS:	United States Geological Survey
UTC:	Coordinated Universal Time
UTM:	Universal Transverse Mercator)
UZH:	University of Zurich
VAR:	Variable rain rate
WGS:	World Geodetic System

1 Introduction

1.1 Context

In the Peruvian Andes, many large mass movements caused natural disasters, claiming nearly 30,000 lifes since 1941. Exposure to large mass movements and climate change related glacier recession is very high (Carey, 2005). The region around Santa Teresa, northwest of Machu Picchu, Cusco, Peru was repeatedly affected by large debris flows (DesInventar, 2013).
Two very large debris flows in 1998 destroyed the old village of Santa Teresa, forcing inhabitants to rebuild the village in a zone of lower risk (CARE & UZH, 2011). The first event, starting from Sacsara valley, reached Santa Teresa on January 13th, 1998 and demolished over 80% of the buildings (Carlotto et al., 1999). A second, even larger event, started from Ahobamba valley and reached Urubamba valley on February 27th, 1998 (CARE & UZH, 2011), dammed Urubamba River and destroyed a hydropower station (Frey et al., 2012). Around four months later, the event continued along the main valley, destroying what was left of Santa Teresa as well as the access road and the railway line between Cusco and Quillabamba (Hermoza et al., 1998; CARE & UZH, 2011). These two events belong to the largest debris flows known worldwide (Giráldez et al., 2013). Still, little is known about triggering processes and flow characteristics of these events (Huggel et al., 2012a). After these events, hazard assessment and monitoring of the study region was strongly recommended by Hermoza et al. (1998).
In the context of climate change, debris flow activity in the region is assumed to increase (Clague, 2009). Additional to high physical vulnerability, local communities often live within reach of large hazard potentials like Glacier Lake Outburst Floods (GLOF), mud- or debris flows or large rock- or ice avalanches (CARE & UZH, 2011). This thesis is part of the first component of a current climate change adaptation and disaster risk reduction (CCA DRR) project, which aims to mitigate climate change impacts in high-mountain areas in Peru.

1.2 Motivation

High mountain areas are a sensitive and fast-changing environment, climate change being both cause and promoter for this fact (Huggel et al., 2004). Conditions are probably changing as fast as research is being done, making it a challenging and interesting topic. Living in Switzerland, hearing from disastrous mass movements in mountains cannot be avoided. But while in Switzerland research, risk management and adaptation measures concerning high-mountain hazards are highly advanced; in other, equally endangered countries like Peru people still find their livelihood threatened by mass movements. This is a big motivation to participate in the CCA DRR project in Peru, in order to contribute to improve disaster risk reduction locally. Cooperating with researchers from Switzerland and Peru, including communicating in English and Spanish, also makes this thesis a welcome language skill exercise. An intriguing aspect is that trigger conditions of both debris flows are still unclear (Huggel et al., 2012a), making their clarification a challenging part of this thesis.

1.3 Goals

In order to set the basis for future risk mitigation measures, the following goals were defined for this thesis:

1) Analysis of climatic and geomorphologic conditions in Santa Teresa area (Chapter 3).
2) Analysis of trigger conditions for two very large debris flows (from Sacsara and Ahobamba valley) in 1998 in Santa Teresa area (Chapter 6).
3) Reconstruction of the 1998 debris flows with the RApid Mass MovementS (RAMMS) model to calibrate model parameters (Section 7.3), based on study region conditions and trigger analysis, including a short DEM evaluation (Section 7.1) and a sensitivity analysis of model input parameters (Section 7.2).
4) Development of hazard scenarios (small, medium, large) for the catchments of Ahobamba, Sacsara and Salcantay based on reconstruction; modeling of hazard scenarios with RAMMS (Sections 8.1 to 8.3).
5) Creation of a preliminary hazard map for Santa Teresa (Section 8.4).

1.4 Focus of Study

In this thesis, only debris flows, mudflows or hyperconcentrated flows are looked at in detail. Other high-mountain hazards like rock, ice or snow avalanches or landslides are only included when cascading processes potentially leading to debris flows are involved. The main focus lies on two very large debris flows in 1998 (January 13th and February 27th) and the area of Santa Teresa (see Chapter 3) – other events that happened in the area will not be assessed in detail. The oldest data considered is from 1965, the newest from 2012. Literature from 1955 to 2014 is taken in account.

2 Background

In this chapter, background information on the context of the thesis (Section 2.1), debris flows (Section 2.2) and modeling (Section 2.3) is given.

2.1 The CCA DRR Project

The Climate Change Adaptation and Disaster Risk Reduction (CCA DRR) Project is a joint project between the University of Zurich (UZH) and the Cooperative for Assistance and Relief Everywhere (CARE) in Peru. It is funded by the Swiss Agency for Development and Cooperation (Salzmann et al., 2009) and coordinated by the UZH (UZH, n.d.). UZH has subcontracts with Meteodat and École Polytechnique Fédérale de Lausanne (EPFL), forming a scientific consortium. CARE has subcontracts with the national meteorological agency in Peru (SENAMHI, for Servicio Nacional de Meteorología e Hidrología del Perú); the glaciology department (UGRH, for Unidad de Glaciología y Recursos Hídricos) as well as several Peruvian universities, schools, NGOs and local governments (CARE & UZH, 2011).

The CCA DRR project focuses on two areas: (1) the Pampa Shonguil and Carhuaz in the province of Ancash and (2) Santa Teresa in the province of Cusco (CARE & UZH, 2011). The main goal of the CCA DRR project is to improve climate change adaptation and disaster risk reduction capacity in the context of retreating glaciers, based on local risk management (CARE & UZH, 2011). The implementation strategy includes four aspects: (1) climate change resistant livelihood; (2) disaster risk reduction; (3) local capacity building and (4) approach causes for vulnerability (CARE & UZH, 2011). The CCA DRR project consists of three components (CARE & UZH, 2011): (1) glacier risks and multi-purpose project; (2) academic capacity building and (3); institutional enforcement. This thesis is part of the first project component; “glacier risks and multi-purpose project”. Expected results of this project component are an early warning system for Pampa Shonguil and Santa Teresa, scenario studies and adaptation measures based on them, management committees and an education plan in schools (CARE & UZH, 2011). This thesis gives first rough scenario studies and a basis for later research for Santa Teresa.

2.2 Debris Flows

After a classification of mass movements, a working definition for debris flows is introduced (Section 2.2.1). Then, debris flow characteristics are listed (Section 2.2.2), before the formation of debris flows is looked at (Section 2.2.3).

2.2.1 Classification and Definition

The wide variety of mass movement processes makes a conclusive definition of debris flows very difficult; existing mass movement definitions are often ambiguous (see Costa, 1984; Pierson & Costa, 1987; Coussot & Meunier, 1996 & Lorenzini & Mazza, 2004). The distinction of these processes is further hindered as they exist in a continuum of classifications (Lorenzini & Mazza, 2004), which are often contradictory or incapable of including all phenomena (Coussot & Meunier, 1996). Well-known classification schemes were done by Varnes (1978); Pierson & Costa (1987); Davies (1988); Coussot & Meunier (1996); and Takahashi (2007a).

A list of mass movements is given in alphabetical order (after Coussot & Meunier, 1996; Takahashi, 2007a; Pierson & Costa, 1987; Lorenzini & Mazza, 2004; Costa, 1984):

- Debris avalanche: Large-scale collapse of mountain bodies with large runout (Takahashi, 2007a), can be saturated (Hungr, 2005).
- Debris flood: Rapid, surging flow of water heavily charged with debris (Hungr, 2005).
- Debris flow (viscous & inertial, immature & mature): Definition see below.
- Granular flow: Flow with large enough sediment concentration that solids are not liquefied (e.g. debris avalanches, grain-/earth flows). Three types exist: Frictional (viscous stress, slow); inertial (collision stress, fast); rapid inertial (collision stress, very fast) (Pierson & Costa, 1987).
- Hyperconcentrated flow: Mixtures of water and sediment with measurable yield strength, flowing like a liquid (Coussot & Meunier, 1996).
- Lahar: Volcanic debris flows (Takahashi, 2007a).
- Landslide: "Gravitational mass down slope motions of rock, debris or earth." (Sassa, 2003 (original in Japanese); cited after Takahashi, 2007a).
- Land slips (cliff failures): Shallow surface soil motion (in contrast to landslide, which stands for deep seated earth block motion) (Takahashi, 2007a).
- Mudflow: Fine-grained debris flows (Hungr, 2005).
- Pyroclastic flow: Flow of volcanic origin with larger mobility, material fluidized by volcanic gas ejections (Takahashi, 2007a).
- Rapid mass movement: Landslide with high velocity, including rock avalanches, debris avalanches and debris flows (Schneider, 2011).
- Slope failure (fall, slide or slump) (Lorenzini & Mazza, 2004).
- Slurry flow: Saturated solid-liquid mixture. Two types exist: viscous (Bingham-plastic-behavior) and inertial (dilatant fluid model) (see Section 2.2.2). Debris flows also are slurry flows (Pierson & Costa, 1987).
- Snow avalanche.
- Solifluction: Slow, continuous movement of saturated soil (Lorenzini & Mazza, 2004).
- Streamflow (& flood): Flowing water with small sediment concentration, flow behavior unaffected by sediment (Lorenzini & Mazza, 2004).
- Tillflow: Debris flows originating from glaciers (Costa, 1984).

As no classification scheme is conclusive, several schemes are summarized here, with focus on debris flows. Davies (1988) made a sediment flow classification in a tertiary diagram based on water, fine solid and coarse solid content (see Fig. 2.1).

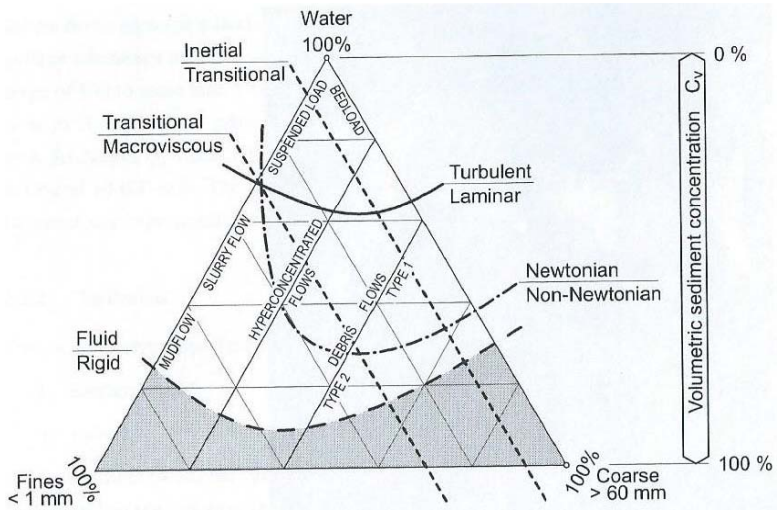

Figure 2.1: Debris flow classification according to Davies (1988). Source: Schatzmann, 2005.

This classification was chosen as it is simple and illustrates the various transitions of mass movements well. The classification of Coussot & Meunier (1996) is somewhat similar, but they add that debris flows are "intermediate phenomena between hyperconcentrated stream flows and landslides", landslides being undersaturated and rigid (Legros, 2006; Wrachien et al., 2010) and hyperconcentrated flows having a lower solid fraction than debris flows (1 - 25% compared to 50 - 90%). In hyperconcentrated flows, coarse particles tend to flow at the bottom, while in debris flows, everything is mixed (Coussot & Meunier, 1996).

Pierson & Costa (1987) plotted sediment concentration and mean velocity (as a replacement for shear rate when the material is subjected to shear stress). With given strain rate, deformation mainly depends on sediment concentration. Boundaries are approximated and depend on physical parameters that have to be estimated (criticized by Coussot & Meunier, 1996). Sediment concentration in debris flows is small enough for the material being liquefied due to high pore fluid pressure (as opposed to granular flows) but large enough to give it a measurable yield strength (the stress at which a material starts to deform), giving them non-Newtonian flow behavior (as opposed to streamflows) (Pierson & Costa, 1987; Takahashi, 2007a). A fluid has Newtonian flow when "the relationship between applied stress and shear rate is constant" (Lorenzini & Mazza, 2004).

Based on above differentiation, debris flows can be defined as mixtures of water and loose, saturated material, flowing rapidly and driven by gravity. This definition is broadly interpreted and based on Costa (1984); Pierson & Costa (1987); Davies (1988); Iverson (1997); Hungr (2005) and Takahashi (2007a). Mudflows, tillflows and lahars are included in this definition, as all of them are possible in Peru. Hyperconcentrated flows have lower solid concentration (Coussot & Meunier, 1996) and are stated separately. The term "rapid mass movement" developed by Schneider (2010) was discarded as it also includes processes not composed of saturated material.

2.2.2 Debris Flow Characteristics

Flow behavior of debris flows is non-Newtonian (Pierson & Costa, 1987). Sediment concentration is usually in the range of 50 - 90% by weight (Coussot & Meunier, 1996), water and fines stay mixed throughout the flow (Costa, 1984). Debris flows are highly unsteady (Davies, 1988) and involve a wide range of grain sizes (Ayotte & Hungr, 2000). They have large runout (Takahashi, 2007a) and can be very erosive and highly destructive (Costa, 1984). Debris flows form from static sediment masses, are transformed into a liquid-like state and deposit again as nearly rigid deposits (Iverson, 1997). Debris flows are a two-phase solid-fluid mixture (Takahashi, 2007a) but can appear to flow as a one-phase material (Ancey, 2003), especially viscous flows. Coarse solids are sustained in the flow by inter-particle collisions, fine solids are suspended within the interstitial fluid (Takahashi, 2007a).

Debris flow volumes vary between 0.1 m^3 and over 10^6 m^3 (Costa, 1984). As estimations based on empirical relationships are difficult, volume is often overestimated (Rickenmann, 1999). Solid volume concentration in debris flows varies from 25 to 86% (Costa, 1984) but is mostly over 50%, highest at the front and decreasing smaller towards the tail (Lorenzini & Mazza, 2004). Most debris flows contain only small amounts of silt or clay. Bulk densities vary between 1.4 g/cm^3 for fluid flows and 2.5 g/cm^3 for dry flows (Costa, 1984).

Discharge is larger compared to water floods (Costa, 1984) and can be estimated using empirical relations. For a volume of 5 mill. m^3, discharges vary between 2,200 m^3/s and 42,700 m^3/s, being on the lower range for muddy flows (Mizuyama et al., 1992; Walder, 1997; Jakob, 2005a). More formulas are given by:

- Evans (1986): $0.72*V^{0.53}$. (2.1)
- Costa & Schuster (1988): $0.063*(PE)^{0.42}$; PE = dam height * volume * g (9,800 N/m^2). (2.2)
- Rickenmann (1999): $0.1*^{V5/6}$. (2.3)

Velocity ranges from 0.5 to 32 m/s (Pierson & Costa, 1986; Rickenmann & Zimmermann, 1993; Rickenmann, 1999; Ayotte & Hungr, 2000 & Lorenzini & Mazza, 2004) and depends on size, concentration and sorting of material and channel geometry (shape, slope, width, sinuosity) (Costa, 1984) as well as water content (Konagai et al., 2007). Rickenmann (1999) found that velocity increases with discharge as follows: $v = 2.1Q^{0.33}S^{0.33}$, (2.4)

With *v* velocity, *Q* discharge and *S* slope.

Debris flows are often categorized based on their rheology. Rheology studies flow and deformation properties of bodies under stress (Lorenzini & Mazza, 2004). Two main approaches for debris flow rheology exist in literature:

1) Classical debris flow rheology assumes that the fluid-particle mixture is a homogeneous continuum (Takahashi, 2007b). The debris flow is steady with uniform and constant properties (Lorenzini & Mazza, 2004). It is a suspension of force-free particles in a viscous fluid and considered to be one-phase (Coussot & Meunier, 1996).
2) As debris-flows are multi-phase systems, a two-phase fluid flow model based on mixture theory was developed by Iverson (1997). Constant volume fractions are assumed, meaning that the mixture system is formally one-phase. However, phase interaction is implemented (Kowalski, 2008).

Takahashi (2007a) added a different approach; multilayer models for inertial debris flows. He assumes that the flow is composed of a collision-dominated lower layer and a turbulent suspension in the upper layer. A stony debris flow only consists of only the former, a muddy debris flow of only the latter, depending on relative depth. Most flows are hybrid.

Two main types of debris flows exist: Inertial and viscous debris flows (Pierson & Costa, 1987; Davies, 1988; Iverson, 1997 & Takahashi, 2007a). Flow regimes are distinguished based on the four dominating forces: viscosity (viscous), sliding friction (frictional), turbulence (turbulent-muddy), and particle collision (stony) (Jan & Shen, 1997).

Inertial debris flows are faster (Pierson & Costa, 1987), less mobile and have steeper fan slopes (Scheidl & Rickenmann, 2009). Inertial forces dominate (Pierson & Costa, 1987). Takahashi (2007a) divides inertial debris flows into stony (particle collision stress dominates) and turbulent-muddy flows (turbulent mixing stress dominates), containing finer particles. Here, inertial debris flows are used synonymously for stony debris flows, neglecting turbulent-muddy flows. Inertial debris flows have densities between 1.4 and 2.3 g/cm^3 (Takahashi, 2007a).

Viscous debris flows (called macroviscous by Davies (1988)) are slower (Pierson & Costa, 1987), with higher mobility and smoother fans (Scheidl & Rickenmann, 2009). Viscous forces dominate (Pierson & Costa, 1987). Iverson (1997) divides viscous flows using clay content: viscous forces dominate with high content, frictional forces with low content. Densities vary from 1 g/cm^3 in the beginning to 2 g/cm^3 in the end of an event. Viscous debris flows generally have more fine material than inertial flows (Takahashi, 2007a).

Transitional debris flows between inertial and viscous also exist (Davies, 1988; Iverson, 2003; Takahashi, 2007a). Flow transformations within different debris flow types or even between mass movements (e.g. from debris flow to flood), can occur within one flow event (Costa, 1984), making a classification of debris flows extremely difficult.

The most important rheological models for debris flows are Bingham (modeling the viscoplastic flow regime, for viscous debris flows) and Bagnold (modeling the collisional regime, for inertial debris flows) (Iverson, 1997). Turbulent-muddy debris flows are best represented with the viscoplastic regime.
In a Bingham model, viscosity is inactive before deformation takes place; an initial shear strength must be exceeded. After that, the relationship between shear rate and stress is constant as in a Newtonian fluid (Pierson & Costa, 1987). Other models are the Coulomb-viscous model (a modification of the Bingham model) and the Herschel-Bulkley fluid model (Takahashi, 2007b). The Bagnold model is also called dilatant model. A dilatant fluid shows an increase in velocity with shear rate (shear thickening), as opposed to a pseudoplastic fluid used by the Herschel-Bulkley model (see above) (Pierson & Costa, 1987).

As debris flows have different rheological properties in different parts and different flow stages (Lorenzini & Mazza, 2004) and interactions between solids and fluids as well as sediment concentration play a crucial role in debris flow behavior (Costa, 1984; Coussot & Meunier, 1996 & Iverson, 1997), mixture theory was developed by Iverson (1997) as an alternative to classical rheology.
Mixture theory uses separate equations for solid and fluid parts as well as their interactions. This way, the entire debris flow process can be modeled consistently, without the definition of rheological parameters. The basic assumption of mixture theory is that granular solids in debris flows behave as Coulomb frictional material (with discrete particles) and inter-granular fluids behave as Newtonian viscous fluids (behaving as a continuum) (Iverson, 2003). Material properties are not assumed to be constant but are functions of volume and mass distribution (Lorenzini & Mazza, 2004). Mixture theory also considers granular temperature (analogous to thermodynamic temperature in gases; derived from grain fluctuation kinetic energy), which represents the energy per unit mass. The higher granular temperature, the higher the fluidity of a debris flow (Iverson, 1997).

Hungr (2005) divides a debris flow path into an initiation, transport and deposition zone, which are looked at in the following sections.

2.2.2.1 Starting zone

For debris flow formation, a starting zone slope higher than 15° is critical and higher than 40° very critical (Takahashi, 2007a, Lehmann & Or, 2012). Zimmermann (1990) distinguishes two starting zone types: Slope type, where water availability is crucial; and valley type, where sediment availability is crucial. On slopes, debris flows either start in steep, loose talus slopes (Type 1) or the contact zone of rock wall and talus slope (Type 2). In valleys, debris flows start in rock gullies filled with debris (Type 3) or temporary debris accumulations in channels (Type 4). Type 1 and 3 produce the largest starting volumes (Zimmermann et al., 1997). Areas with finer-grained soils produce viscous or viscoplastic flows, areas with coarse grained material produce stony debris flows (Lorenzini & Mazza, 2004) – the threshold concentration being 0.1 (ratio between clay concentration and coarse-grained particle concentration) (Coussot & Meunier, 1996).

2.2.2.2 Transport

In the transport zone, the debris flow reaches maximum velocity. The flow process of debris flows is influenced by the starting zone conditions and path characteristics (Ayotte & Hungr, 2000). Interactions between solid and fluid parts are crucial (Iverson, 2005). Velocity is highest in the central and the upper part of the flow (Takahashi, 2007a), at the base of the flow being roughly one third of the mean velocity (Voellmy, 1955). Flow resistance is given by the dominating forces of flow behavior (see above) and increases with increasing particle concentration (Takahashi, 2007a). Debris flow motion is governed by pore fluid pressures and the granular temperature (see below) (Lorenzini & Mazza, 2004). Pore fluid pressures are nearly zero at the head and very large in the flow body (Iverson, 1997).

Debris flows can move as a single surge but usually come in several surges. This surge behavior is caused by temporal damming and breaching of channels by debris (Costa, 1984). A surge consists of three parts (Kowalski, 2008): the precursory surge with a granular front or head, the body of the flow and the tail, which is often a hyperconcentrated flow or mudflow. Velocity is largest at the front and gradually decreases with length (Takahashi, 2007a). Especially viscous debris flows show strong surging behavior; up to several hundred surges are possible, the whole event lasting up to one day. Consecutive surges with turbulent fronts overflow the previous one, smoothing the bed until an equilibrium state of deposit thickness is reached. The smoothened bed gets eroded again by a final surge, leaving the channel as rugged as before (Takahashi, 2007a).

The front of a debris flow is characterized by low fluid pressure (Iverson, 1997), high friction, dilation and coarse particles (Iverson et al., 2010) and can contain large boulders. It is usually the part with the largest flow depth (Costa, 1984) and density (Lorenzini & Mazza, 2004). The front develops due to (1) loss of water due to adhesion at the channel; (2) inverse grading; and (3) the plastic behavior slowing the flow. Inverse grading increases friction and means that the coarsest particles are on top of the flow. Due to higher velocity at the top, coarse particles are transported to the front (Lorenzini & Mazza, 2004). The tail is fine-grained, nearly liquefied and has very high fluid pressures (Iverson, 1997).

Inertial debris flows usually have large boulders at the front, whereas viscous flows rarely carry boulders exceeding 1 m in diameter (Schatzmann, 2005; Takahashi, 2007a). Boulders are held in place by the fine-grained matrix due to cohesion, buoyancy, dispersive pressures, turbulence and structural support (Costa, 1984).

2.2.2.3 Deposition

Deposition is governed by resistance at the head and lateral boundaries of the debris flow, reducing granular temperature to zero (Iverson, 1997). Reasons for stopping are decreasing slope, lateral spreading and escaping pore fluids which increase internal friction (Costa, 1984). Debris flows can also be deposited in channels, potentially forming temporary dams which can be remobilized by the next debris flow surge (Costa, 1984).
In the deposition area (depending on slope, volume and debris flow strength), the debris flow front slows down, steepens, builds elongated ridges (called levees) and forms a deposition fan (Costa, 1984). Levees are formed as the coarsest particles deposit first, hindering fine-coarse particles behind (Lorenzini & Mazza, 2004). This also causes inverse grading in depositions, except for very large boulders which are deposited early (Takahashi, 2007a).

Runout of debris flows can be very far-reaching (Costa, 1984; Lorenzini & Mazza, 2004; Takahashi, 2007a). Possible reasons for this large runout are: volume effect (Heim, 1932); velocity dependency on slope and flow thickness (Legros, 2002); friction reduction with increasing velocity (Voellmy,

1955); pore pressure increase by fluidization or lubrication (Korup et al., 2012); dynamic rock fragmentation (Davies et al., 1999); granular agitation (Savage & Hutter, 1991); buoyancy (Takahashi, 2007a); clay content (Costa, 1984); high water content (Legros, 2006; Takahashi, 2007a); shearing of the mixture (Takahashi, 2000) or incorporation of ice (Schneider, 2011). Large clay content explains the much larger runout distance of lahars (Costa, 1984).

Overall slopes of 15 - 30% are common, but even 3% was observed (Lorenzini & Mazza, 2004). Overall slope (H/L) is defined as the slope between the uppermost point of the starting zone and the bottom of the deposition zone (also called reach angle by Hürlimann et al., 2008). Minimum overall slope observed in Switzerland was 19% for coarse-grained debris flows (Rickenmann & Zimmermann, 1993). The overall slope decreases with increasing catchment area or volume (Zimmermann et al., 1997). Rickenmann (1999) found that the travel distance (L) of a debris flow depends on volume (V) and the lowest point of the deposition (H) as follows: $L = 1.9M^{0.16}H^{0.83}$. Rickenmann (2005) found that the overall slope is smaller for fine-grained debris flows compared to coarse-grained. Lowest overall slopes were observed in Canada (0.07, Rickenmann, 2005).

2.2.3 Formation and Triggers

Zimmermann et al. (1997) defines “disposition” as the susceptibility of an area to form distinct processes, e.g. debris flows. He distinguishes basic and variable disposition and triggering events. These terms are used to describe the preconditions and triggers of debris flows in this thesis. Similar concepts are used by Petrakov et al. (2008) or Wieczorek & Glade (2005).

2.2.3.1 Basic disposition

Basic disposition describes the general susceptibility of a catchment or starting zone, the magnitude and the spatial occurrence of debris flows (Zimmermann et al., 1997). It depends on aspects that do not change rapidly over time like geomorphology, geology, relief, hydrology and glaciology and can be assessed rather easily (Zimmermann et al., 1997).

Basic conditions for debris flows are (Zimmermann et al., 1997):

- Exposition and height: influence on frost erosion and debris production.
- Slope: 15° or higher (Takahashi, 2007a).
- Debris type: Erodible bedrock or loose, permeable sediments with low clay content can become unstable fast (Hungr, 2005); clay-rich sediments are cohesive and poorly permeable but easily eroded by debris flows (Rickenmann & Zimmermann, 1993).
- Type of debris production: continuous production by weathering (small flows) or deposited debris (e.g. moraines) and weathered bedrock (large flows).
- Stability: Depends on porosity, permeability, permafrost occurrence, lithology and grain size.

Smaller and steeper basins are more prone to form debris flows as they are higher and proportionally more rain can fall locally (Costa, 1984). Usually, debris flows occur in semiarid (main trigger: rain), alpine (main trigger: snowmelt) or volcanic (main trigger: eruption) areas (Lorenzini & Mazza, 2004). All these environments are present near Santa Teresa. Additionally, alpine areas have larger sediment availability (Rickenmann & Zimmermann, 1993). Basic disposition is not always as constant as it seems. Large-scale climate variations can strongly influence topography, due to their influence on slope stability, especially in high-mountain areas (Huggel et al., 2012b) (see “Variable disposition”).

2.2.3.2 Variable disposition

Variable disposition (also called pre-event condition) explains medium-term variability in the susceptibility to debris flow formation and determines the temporal occurrence of debris flows (when & how often) and their magnitude. As it can vary seasonally or within days, it is very hard to assess (Zimmermann et al., 1997).

Variable factors enhancing debris flow potential are:

- Hydro-meteorological conditions (Zimmermann et al., 1997).
- Sediment availability (Costa, 1984; Zimmermann et al., 1997).
- Glacier debuttressing (Strom, 2009) due to glacier melting (Haeberli et al., 2010).
- Permafrost thaw (Strom, 2009); decreases internal strength (Haeberli et al., 2010).
- Human activity leading to an increase in gradient (Lorenzini & Mazza, 2004).
- Soil properties and their groundwater response to precipitation events (Lorenzini & Mazza, 2004; DeGraff & Ochiai, 2009).
- Slope modification and land-use change (Marui & Nadim, 2009).
- (Absence of) vegetation cover (Costa, 1984).

Many of these factors affect glacial and periglacial environments. Glaciers and high-mountain environments are especially susceptible to many natural hazards (Haeberli et al., 2010). Unstable steep glaciers, an abundance of erodible material, process chains, volcano-ice interactions and high mass turnover rates enhance debris flow potential (Schneider, 2011). Glacier melt leads to the formation of many new lakes, which have to be assessed carefully due to their high hazard potential (Haeberli et al., 2010).
Climate exerts a strong control on hydro-meteorological conditions, as snowmelt and rain both infiltrate soils (Chen et al., 2010). Large-scale climatic variations such as the El Niño phenomenon – especially strong from 1997 - 1999 – increase debris flow activity in the study region by increasing temperature and precipitation (Curtis et al., 2001; Wieczorek & Glade, 2005). Many large slope failures were preceded by especially high temperatures, mainly due to higher snowmelt and infiltration into the soil (Huggel et al., 2012b).
Variable disposition causes debris flows to show a certain periodicity, as debris availability changes after each event (Zimmermann et al., 1997). Medium-term susceptibility to debris flow formation can be increased with climate change.

2.2.3.3 Triggering events

Triggering events are short-term and highly variable stresses on the system (Zimmermann et al., 1997). Basic and variable conditions define how strong a triggering event has to be in order to produce debris flows. When debris is saturated, a smaller trigger is necessary (Zimmermann et al., 1997). A debris flow is triggered when the gravitational force is stronger than the resisting force (Lorenzini & Mazza, 2004).

Possible triggers for debris flows are:

- Addition of moisture to loose debris in steep slopes due to (Costa, 1984) precipitation events (most common) and snowmelt (Zimmermann et al., 1997).
- Earthquakes (Zimmermann et al., 1997).
- Volcanic eruptions (Takahashi, 2007a) and pyroclastic flows (Iverson, 1997).
- Floods incorporating sediments (Iverson, 1997).
- Landslides (Rickenmann & Zimmermann, 1993) and slope failure (Iverson, 1997).
- Glacial lake outburst floods (Costa, 1984).

Two main initiation processes can be distinguished for these triggers (based on Takahashi, 2000):

1) Shallow and deep-seated slope instabilities (Channel-bed erosion following surface runoff and landslides transforming into a debris flow) (Section 2.2.3.4).
2) Dam failure (Section 2.2.3.5).

In mountainous terrain like the Santa Teresa area, debris flows from moraines or landslides are more common, whereas in the lowlands, channel-bed erosion occurs more often (Zimmermann et al., 1997; Haeberli et al., 2012). Complex process chains and interactions are common (Haeberli et al., 2010). Triggers can occur simultaneously or affect a large area, causing several flows at the same time (Hungr, 2005). Debris flows are either mobilized when the soil fails and pore pressure increases fast (sudden liquefaction) or when complete liquefaction does not take place until the mass is in movement (slow failure) (Iverson et al., 1997).
Not only landslides but various other mass movements (e.g. rock- and ice avalanches) can transform into a debris flow (Evans et al., 2006; Schneider, 2011). Especially critical are combinations of triggers, e.g. an earthquake hitting after rainfall saturated the soil (Sassa et al., 2007). Ice can melt when incorporated to debris, causing debris flows (Schneider, 2011).
Earthquakes are an important trigger for landslides or debris flows (Gruber & Pike, 2008). Also, they destabilize slopes for up to several years, which might lead to landslides and flows during the next strong storm (Kazuo et al., 2009; Marui & Nadim, 2009). Volcanic eruptions and floods incorporating sediments are not considered within this thesis, as they did not cause the debris flows of Santa Teresa in 1998.

2.2.3.4 Slope instabilities

Takahashi (2007a) distinguishes two types of slope instabilities: Shallow (triggered during intense rainfall) and deep-seated (often after rainfall). Shallow slope instabilities contain a lot of water and occur suddenly, whereas deep-seated slope instabilities take a long time until the ground water level is high enough to destabilize a whole earth block. Slope instability is used as a synonym for landslide (as used in Takahashi, 2007a); landslides as used in Takahashi (2000) are referred to as “deep-seated slope instabilities. Channel-bed erosion is termed “shallow slope instability”. Debris flows are a type of shallow landslide (Gruber & Pike, 2008).

Shallow slope failure on steep slopes due to water inflow is the most common debris flow trigger (Iverson et al., 1997). Failure occurs as particles loose cohesion due to increased pore water pressures (Costa, 1984). This happens when rigid debris gets deformed by fast volumetric compression (Wrachien et al., 2010) and becomes saturated, meaning that the void space between particles is filled (Takahashi, 2007a). Water can infiltrate via surface runoff and groundwater infiltration due to rain and snowmelt (Costa, 1984; Iverson, 1997; Iverson et al., 1997; Zimmermann et al., 1997). Steeper slope lowers critical pore pressure (Klubertanz et al., 2000) and critical runoff (Tognacca et al., 2000), but with pore water pressures above a critical threshold, slope is of minor importance (Klubertanz et al., 2000). Critical water amount in soil depends on the soil’s permeability (Klubertanz et al., 2000). Mass movement only occurs when a local soil part fails and exceeds the strength of neighboring soil it leans against (Lehmann & Or, 2012). Debris flow formation is also possible without saturation on steep slopes (Tarantino & Bosco, 2000; Coe et al., 2008). Also, high pore pressures do not always liquefy the soil (Iverson et al., 1997).

Rainfall increases debris moisture content and pore water pressures, inducing slope instability (Garland & Olivier, 1993). High intensity, short duration rainstorms mostly produce too little infiltration to generate high pore water pressures. Low intensity, long duration storms cause rising groundwater but do not enhance pore water pressure much. Medium intensity storms of several hours to few days’ du-

ration cause pore water pressure to increase above a critical threshold (Garland & Olivier, 1993; Klubertanz et al., 2000; Wieczorek & Glade, 2005; Takahashi, 2007a). This antecedent rainfall is crucial for debris flow formation (BAFU, 1991; Garland & Olivier, 1993; Wieczorek & Glade, 2005), except for arid or semi-arid regions (Coe et al., 2008).
Snowmelt is an important trigger for debris flows in glacial environments, as water percolates into the ground for a long period of time (Saemundsson et al., 2003; Haeberli et al., 2010). Many slope failures occurred after exceptionally warm periods with subsequent refreezing of melt water in rock fissures, what increased pore pressures (Haeberli et al., 2010).
Surface runoff caused by rainfall or snowmelt can incorporate debris and progressively destabilize a bed, producing a debris flow (Tognacca & Bezzola, 1997; Takahashi, 2007a). Groundwater upwelling can cause liquefaction of debris from the bottom to the top (Takahashi et al., 2003), causing a deep-seated landslide (see below).

Several authors (Caine, 1980; Garland & Olivier, 1993; Zimmermann et al., 1997; Hürlimann et al., 2003; Saemundsson et al., 2003; Guzzetti et al., 2007a and 2007b) worked out critical precipitation amounts as thresholds for triggering debris flows. These amounts vary strongly for different geographical regions (Zimmermann et al., 1997; Wieczorek & Glade, 2005). Until now, no threshold value for Peru exists (see for example Guzzetti et al., 2007a; Guzzetti et al., 2007b or IRPI, 2013).

When a deep-seated landslide starts, its soil structure is destroyed, with a liquefied layer at the bottom and a solid earth block on top. The solid earth block moves on top of the liquefied layer and moves faster, leaving the liquefied layer behind, which goes down as ad debris flow (Takahashi, 2007a). Deep-seated landslides usually start slow, reduce shear strength and increase pore water pressure. This can increase debris flow potential substantially (Reid et al., 2003). Landslides are a common trigger for debris flows, especially in mountainous areas (Rickenmann & Zimmermann, 1993; Wrachien et al., 2010). Landslides are triggered for mainly the same reasons as debris flows (Sassa et al., 2007). According to Iverson et al. (1997), landslides can generate debris flows in three ways (separately or simultaneously): (1) Coulomb failure within a soil; (2) liquefaction of the mass by high pore fluid pressures and (3); conversion of landslide translational energy into internal vibrational energy (granular temperature).

2.2.3.5 Dam Failure

Schuster (2000) classified natural dams in four types: Landslide dams, glacial moraine dams, glacier ice dams and volcanic dams (see below). Sooner or later, many fail, caused by the same reasons as debris flows (Schuster, 2000). Natural dams can fail in three ways (Takahashi, 2007a): (1) Overtopping caused by impact from ice or rock falls or landslides (Schuster, 2000); (2) sudden and (3); progressive falls caused by seepage of the dam. When the lake overflows, an initial breach is formed, which is progressively enlarging until the dam fails (Worni et al., 2012; Evans et al., 2006). All these dam failure types are connected to high water levels (Haeberli et al., 2010). Floods resulting from dam failures can transform into debris flows when travelling downslope and incorporating erodible material (Clague, 2009).

Landslide dams form mostly in steep mountain valleys, which can be destroyed by an upland flash flood, causing sediment re-mobilization and a debris flow (Schuster, 2000) or cascading landslide breaks, leading to a larger event (Cui et al., 2010).
Glacial moraine dams form where glaciers are retreating. They have an especially high hazard potential as they (Zimmermann et al., 1997; Schuster, 2000): (1) are close to unstable glaciers or rock walls; (2) consist of easily erodible material; (3) are steep; (4) are bare of vegetation; (5) can incorporate loose debris downstream; (6) have large peak discharges; and (7) can occur totally unexpectedly. Peak

discharge is usually very large and controlled by the lake volume, dam height and width, material properties, failure mechanism, sediment availability and downstream topography (Clague, 2009). Also called GLOFs (glacial lake outburst floods) (Schuster, 2000), these dam failures are very common in Peru and show complex interactions and usually result from cascading processes (Worni et al., 2012).
Glacier ice dams can exist on, beneath or behind a glacier, damming water upstream. Rapid draining of these dams causes floods, incorporating sediment and transforming into debris flows (Costa, 1984; Schuster, 2000). Due to recent climate-related glacier recession, several supra-, sub- or periglacial lakes are formed due to melting snow and ice (Clague & Evans, 2000).
Volcanic dams are stream blockages by lava or pyroclastic flows or dammed crater lakes. Their failure causes lahars, as material is incorporated easily in the flood (Schuster, 2000).

2.3 Numerical Modeling

Debris flow modeling is used to gain information on starting zones, flow paths, runout, volume, return period, velocity, flow height and duration (Zimmermann et al., 1997) of real and potential debris flow events. Modeling is especially important in remote areas such as the Santa Teresa region in Peru, where field data is largely missing and experiments too difficult or expensive to carry out (Huggel et al., 2002; Huggel, 2004; Schneider, 2011). Debris flow models should consider their viscous nature, fluid-sediment interactions and friction (Lorenzini & Mazza, 2004). Two-phase models are expected to give better results (Hürlimann et al., 2008; Wrachien et al., 2010).
Many models for debris flows exist in literature. The most important modeling approaches are empirical and flow direction models as well as dynamic flow models (based on Hürlimann et al., 2008, see sections below). An alternative approach is the finite volume approach (Kowalski, 2008), which assumes no constant mixture but discretizes small control volumes, including a rate of exchange between volumes. Each control volume's velocity and movement is calculated. The main advantage is that this model can calculate discontinuous solutions and does not require a structured mesh.

In simulation models, two kinds of error and uncertainty sources have to be distinguished (Heuvelink, 1998): (1) DEM data contains uncertainties (input error) and (2) the model contains uncertainties (model error). A model error can arise when complex processes get simplified or when applied algorithms are faulty (Andres, 2010). Also model parameters can have a significant uncertainty, as they are often poorly constrained (Ghilardi et al., 2003).

2.3.1 Empirical models

Empirical models try to estimate important parameters like maximum runout distance, volume, angle of reach, deposition area etc. using empirical relationships. They are very fast and simple in computation, but do not consider catchment characteristics. Also, the initiation point must be specified (Hürlimann et al., 2008). Empirical approaches are based on the assumptions that past events represent possible future events (Crosta et al., 2003) – this assumption is challenged when including climate change impacts. When modeling the runout of a debris flow, the overall slope concept is often used (see Section 2.2.2.3).

2.3.2 Flow direction models

Flow direction models can be distinguished in single and multiple flow direction models. The best known example for a single flow direction model is D8, where the flow always follows the steepest path to a neighboring cell (O'Callaghan & Mark, 1984). In multiple flow direction models, the flow can invade several neighboring cells, based on various algorithms (Hürlimann et al., 2008). Huggel et al. (2003a!) developed a modified single flow direction model (MSF) based on D8, where a flow spreading of 45° from the steepest path is possible. Flow direction models are fast and can calculate debris-flow trajectories. However, volume and intensity cannot be implemented and maximum runout cannot be calculated directly (Hürlimann et al., 2008). Also, MSF does not have a physical basis of debris flow behavior (Huggel et al., 2003a). Another well-known model of this type is LAHARZ (Iverson et al., 1998).

2.3.3 Dynamic Flow Models

Dynamic (also called physical) flow models simulate the debris flow process based on physically derived parameters (Zimmermann et al., 1997; Rickenmann, 2005; Huggel, 2004). Dynamic flow models mainly differ in their implementation of flow rheology. They can simulate total runout distance, flow depth and velocity, kinetic energy, momentum, frictional work rate, flow pressure and final deposition height for each step (Schneider, 2011; Hürlimann et al., 2008).
One-dimensional dynamic flow models (e.g. AVAL-1D from Christen et al., 2002) are very useful for modeling, but have several drawbacks. It is necessary to define the flow direction and width in advance, which adds uncertainty (Christen et al., 2008). 1D-models only calculate along predefined topographic profiles, while 2D-models can use DEMs for determining debris flow properties over an area (Hürlimann et al., 2008). Dynamic flow models need to be calibrated with rheological parameters, which increase simulation speed and need less input data and technical know-how. However, flow process dynamics can be strongly simplified, and parameters are often poorly constrained, which is the main drawback of dynamic flow models (Rickenmann, 2005; Gruber & Pike, 2008; Hürlimann et al., 2008). Rheological tests can help constrict parameters better (Coussot & Meunier, 1996). There is a trade-off between complex models giving sophisticated results and simple models giving simplified results.

Many dynamic flow models exist (for some examples see Ayotte & Hungr (2000); Bozhinskiy & Nazarov (2000); Klenov (2000); Liu & Lai (2000) & Ghilardi et al. (2001)). Well-known examples are RAMMS (Bartelt et al., 2013, see Section 5.2.2), DAN-3D (McDougall & Hungr, 2004) and FLO-2D (O'Brien et al., 1993). Only few of these models look at very large events, such as Lahars and GLOFs (Worni et al., 2013) or the debris flows in Peru. In a comparison, FLO-2D showed slightly better results than RAMMS (Cesca & D'Agostino, 2008), but requires more unconstrained physical and empirical input parameters, limiting its use for Peru, as data availability is poor.

3 Study Region

This chapter analyses the study region in terms of social (Section 3.1) and environmental (Sections 3.2 and 3.3) aspects as well as past (Section 3.4) and potential (Section 3.5) hazards. As glaciology changes fast under the influence of climate change, it was attributed to the variable disposition. This chapter is based on various studies that have been carried out near the study region (Huggel et al., 2003b; Carey, 2005; Hegglin & Huggel, 2008; Suarez, 2010; Navarro, 2011; Carey et al., 2011; Giráldez, 2011; Klimeš, 2011; CARE & UZH (n.d., 2011, 2012, 2013a and 2013b); Frey et al., 2012; Haeberli et al., 2012; Huggel et al., 2012a and 2012c ; Giráldez et al., 2013; Huggel et al., 2013; Schauwecker et al., 2012; Vicuña, n.d.).

Fig. 3.1 shows the Study Region, consisting of three subcatchments (from west to east: Sacsara, Salcantay (or Santa Teresa; Salkantay), Ahobamba (or Aobamba)) and a small part of Urubamba (or Vilcanota) catchment (north). From now on, “Sacsara”, “Salcantay”, “Ahobamba” and “Urubamba” refer to the catchments/ valleys of the corresponding rivers. “Santa Teresa” refers to the village.

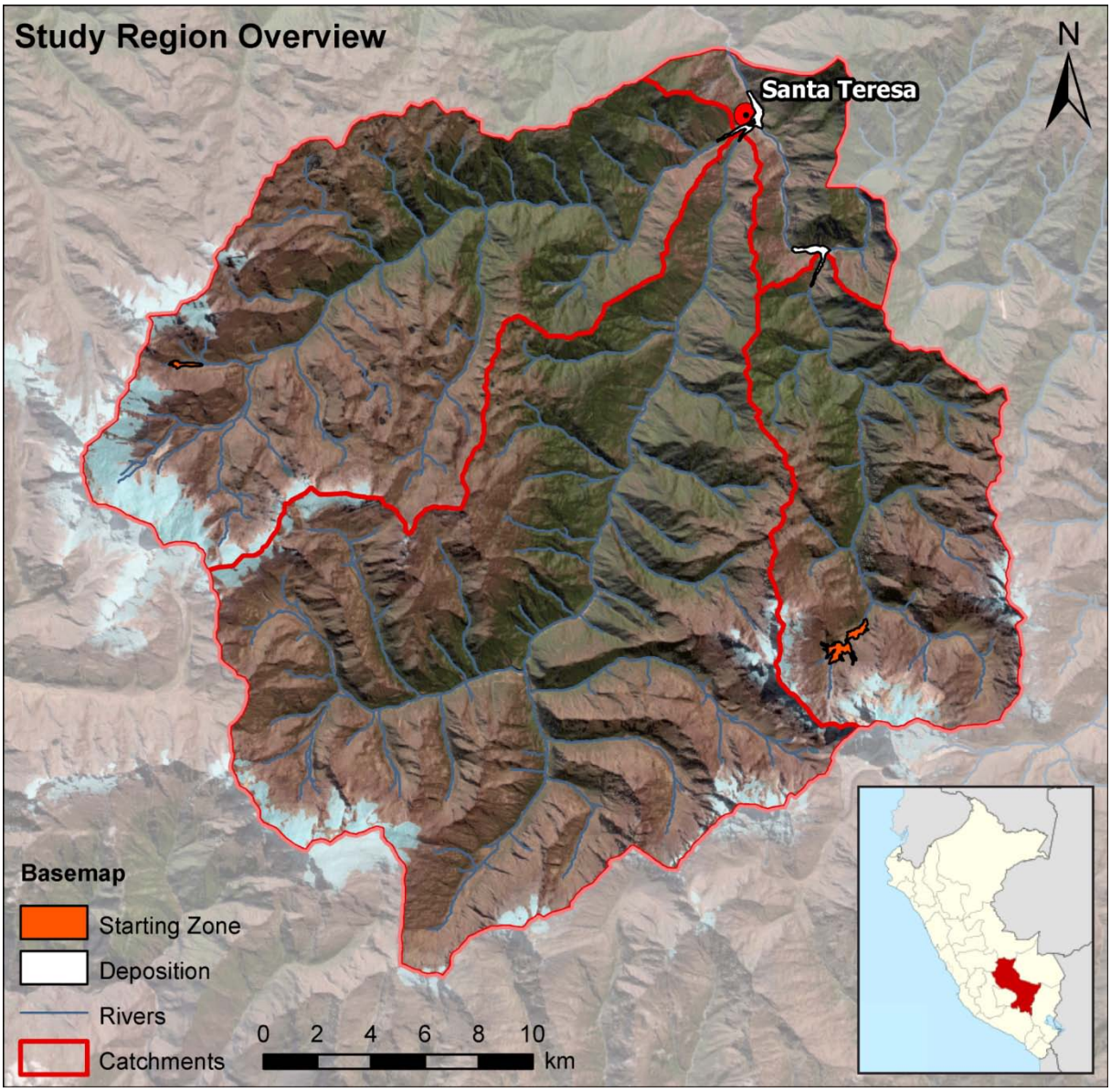

Figure 3.1: Study region; including starting zones (orange) and deposition zones (white) of the events in 1998.

Santa Teresa district lies in La Convención province in the Cusco region (red area in inset map) in Southern Peru, northwest of Machu Picchu. The area is characterized by complex process interactions, large size, remoteness and hard accessibility (Haeberli et al., 2012). Santa Teresa district is considered to be highly vulnerable due to climate variability, disaster risks, glacier recession, poverty and low human development (Carey, 2005; CARE & UZH, 2011; DesInventar, 2013), with Santa Teresa built in a location prone to mass movements due to limited favorable building space (Klimeš et al., 2007). Santa Teresa district extends over 1,340 km^2 and consists of six subcatchments with a total of 10,210 inhabitants (MAXIMIXE, n.d.). The study region covers 3 of these 6 catchments, all draining into Urubamba. Urubamba is not included in the thesis, as debris flows originating in this catchment can hardly damage Santa Teresa (Huggel et al., 2003b).

Fig. 3.2 shows the rebuilt village of Santa Teresa (top) as well as the destroyed remains of the old village (below). This picture impressively shows the destructive potential of the very large debris flows that happened in the study region.

Figure 3.2: Santa Teresa with Sacsara (top right), Salcantay (top left) and Urubamba (bottom). Source: Avalos, 2011.

The CCA DRR project launched an expedition in June 2012 to achieve an overview of the hazard potential in Salcantay valley for the scientific baseline and to analyze damages caused by the events in 1998 and a flood in 2010 (Haeberli et al., 2012). Later in 2012, a vulnerability analysis was conducted and participative risk maps for hazard detection developed. In August 2012, a second mission was sent to Santa Teresa in order to assess hazards, hydrology and adaptation measures (Huggel et al., 2012c). A third expedition in November 2012 aimed to study landslide scars, glacial and periglacial lakes and the deposits from the 1998 event. GPS measurements of landslides, lakes and further geomorphologic features were made (Giráldez et al., 2012).

3.1 Social Environment

Of slightly over 10,000 inhabitants, 70% are considered poor. 42% of children below 5 show signs of chronic malnutrition. 95% of the population does not have access to clean drinking water, 60% have no electricity and 29% do not have sanitation. The whole district is distinctly rural (MAXIMIXE, n.d.), which is reflected in its political organization: Communities have a mayor (as representative of the official political entity) as well as a president of the farmer community (as representative of the community) (Huggel et al., 2012c). The main economic activity is agriculture, especially coffee, passion fruit and coca leaves (Huggel et al., 2012c).The tourist sector is about to evolve due to the vicinity of Machu Picchu and the thermal baths close by (CARE & UZH, 2011).

Vulnerability of Santa Teresa to mass movements is very high, enhanced by the lacking confidence of locals in government or scientists (Carey, 2005) but also the poor emergency preparation and organization. Until now, no legal organization for watershed use exist (CARE & UZH, 2012), posing a large difficulty for efficient risk management. No fire brigade and no radio communication exists, and mobile phone connection often is limited (Giráldez et al., 2012; Huggel et al., 2012c). Despite high vulnerability to hazards, the social climate is very quiet, no urgent demands were identified (Huggel et al., 2012c). Vulnerability of communities depending on water for agriculture, energy production and drinking is increasing due to climate change (CARE & UZH, 2011). This is why the CCA DRR project can help in Santa Teresa area.

3.2 Basic Disposition

In this section, geomorphology, geology and hydrology are looked at for the study region. Basic disposition for specific starting zones is analyzed in Section 3.5.

3.2.1 Geomorphology

The study region is characterized by a complex topography with steep slopes, as shown in Table 3.1. As slopes over 15° (especially 40°) are critical (Takahashi, 2007a; Lehmann & Or, 2012), most of the study region is prone to debris flows. Slopes are often composed of loose sediments that can easily be mobilized or form a temporal dam (Frey et al., 2012). High sediment availability and low sediment stability characterize the study region (Carlotto et al., 1999). No data is available concerning soil cover, porosity, permeability, lithology or grain size distribution. Both 1998-event starting zones consist of highly unstable morainic sediment, with blocks, gravel and a non-compact, permeable sandy-silty matrix with unknown clay content (Carlotto et al., 1999). Debris originates from both continuous production (frost weathering, chemical weathering) and moraines, indicating potential for large flows (see Section 2.2.4.1).

Catchment	Ahobamba	Salcantay	Sacsara
Area (km^2)	129	372	228
Elevation (m a.s.l.)	Min: 1784 Max: 6231 Mean: 3875	Min: 1510 Max: 5792 Mean: 3792	Min: 1518 Max: 5858 Mean: 3804
Slope (°)	Mean: 33.4 Max: 73.9	Mean: 31.9 Max: 70.4	Mean: 29.1 Max: 66.8
Glaciers (km^2)	6.5	16.5	16.5
Lakes (km^2)	0.03	0.14	0.94
Vegetation (km^2)	29.8	84.0	60.1

Table 3.1: Characteristics of catchments in study region. Table modified after Frey et al., 2012.

3.2.2 Geology

A geological map for the area is provided by Carlotto et al. (1999) (see appendix). The higher part of the study region largely consists of Perm-Triassian intrusions. In the valleys, these are topped with large amounts of loose morainic deposits. The lower part of Ahobamba consists of Ordovician material from the San José group and the Sandia formation. A lot of fractures are visible. Salcantay consists of various Cambrian rocks, followed by Cambrian schists and finally Ordovician material from the San José group. The middle part of Sacsara consists of Cambrian schists, the lower of Ordovician material from the San José group. In Sacsara and Salcantay, several lateral displacements are identified. These are dangerous in terms of mass movements, as they allow for building a sliding surface for landslides, which can later transform into debris flows (Sassa et al., 2009). The area around Santa Teresa is nowadays filled with alluvial sediments from the 1998 debris flows. Before, fluvial depositions

were likely. In both starting zones, the underlying bedrock is Perm-Triassian intrusions, topped with large amounts of loose morainic deposits.
Additionally to geology with many displacements and fractures, the region of Cusco has shown significant seismic activity in the past. Earthquakes with a magnitude of 7.0 (Richter scale) are possible in the area (Avalos, 2011).

3.2.3 Hydrology

As seen in Fig. 3.1, three catchments influence Santa Teresa. Urubamba is much larger than the part shown in Fig. 3.1 and also influences Santa Teresa, but does not produce debris flows affecting Santa Teresa (CARE & UZH, 2012). No data on hydrological properties such as groundwater, infiltration rate, soil moisture, surface water flow, evaporation or permeability is available for the study region. All three catchments are mainly supplied with melt water from surrounding glaciers (e.g. from Nevado Salcantay). In summer, precipitation greatly increases runoff (Hermoza et al., 1998).

3.3 Variable Disposition

In this section, climate, vegetation and glaciology are looked at for the study region. Variable disposition for specific starting zones is analyzed in Section 3.5. Human activity in the area can be considered low (see Section 3.2) and was excluded from having influenced the triggering process of the 1998 debris flows through slope modification or land-use change.

3.3.1 Climate

Santa Teresa area shows two distinct seasons: In the wet season (October to March), more than 70% of annual precipitation is registered, the rest in the dry season (April to September) (Schauwecker et al., 2012). This is strongly reflected in runoff: Urubamba drains 30 m^3/s in dry season and 350 m^3/s in the wet season.
The study region is at the boarder of two climatic regimes, divided by the mountains of the Cordillera Vilcabamba. The Altiplano (to the south and east) has low precipitation, scarce vegetation and weak erosion. The Amazon basin (to the north and west) has high precipitation, dense vegetation, extremely steep slopes and high fluvial dynamics (Huggel et al., 2002). Santa Teresa's precipitation regime is influenced by the Amazon basin (Hermoza et al., 1998). In Machu Picchu, average daily maximum temperature from 1965 to 2006 is 21.1° on 2459 m a.s.l.; average annual precipitation is 965 mm (with 21% of days without data).

Conversation with locals resulted in astonishing agreement on (1) the weather being warmer in recent years and (2) the rain falling less regularly, but more heavily (Huggel et al., 2012c). Most climate models confirm this trend and predict an increase in precipitation during the wet season and a decrease during the dry season, making extreme weather phenomena more frequent and stronger in the future (Huggel et al., 2008). The Peruvian Andes experienced a temperature increase of 0.3°C/decade over the last few decades. Exact information is not available due to the limited climate monitoring network, but warming in the Andes is of similar magnitude than in the Arctic – future warming of 2.5 to 5°C is predicted by 2100 (Bradley et al., 2006).
Glacial and periglacial environments react sensitively to climate change (Huggel et al., 2004). Glaciers are expected to vanish near Santa Teresa in case of a temperature increase of 1.2°C (Huggel et al., 2002). Climate change leads to a rapid formation of potential new starting zones for mass movements (Gruber & Pike, 2008) and can lead to a shift of hazard sources – meaning that areas without historical events can now be endangered and that the historical knowledge base might not longer suffice. Events occurring for the first time or with exceptionally high volume can be a sign of a system change (Hug-

gel, 2004). Climate change increases the occurrence of mass movements in mountains due to larger debris amounts and slope destabilization due to permafrost degradation; rapid melting and refreezing of meltwater; and snowmelt (Gruber et al., 2004; Wieczorek & Glade, 2005; Clague, 2009; Huggel et al., 2004; Huggel et al., 2010; Huggel et al., 2012d).

In the years 1997 - 1999, an exceptionally strong negative phase of ENSO (El Niño-Southern Oscillation) was observed. During an El Niño phenomenon, the trade winds are weakened, causing the humidity to stay in the Amazon basin, where there is more rain – this means an increase in precipitation in the study region (Curtis et al., 2001).

3.3.2 Vegetation

Before the 1998 events, both Ahobamba and Sacsara showed typical "Ceja de Selva" vegetation (literally "rain forest eyebrow"), a type of mountain rain forest. Above 2,900 m (Sacsara) to 3,500 m (Ahobamba), arid mountain vegetation (called Ichu after the dominating grass) starts to take over (Carlotto et al., 1999). The debris flows eroded a lot of vegetation in their flow path, now there is only secondary vegetation where the debris flows passed through. The lack of vegetation on steep slopes adds to their instability (MAXIMIXE, n.d.).

3.3.3 Glaciology

Peru has the largest extension of tropical glaciers worldwide, with 70% of the total area (Carey, 2005; CARE & UZH, 2011). In the Vilcanota mountain range, where Santa Teresa is located, glacier cover was reduced from 221 km^2 to 116.4 km^2 from 1991 to 2011, which represents a loss of 48% (Suarez et al., 2013). Glaciers are found to be retreating faster than anticipated (Francou et al., 2004). Glacier retreat, together with Permafrost thaw, strongly influences sediment availability and stability. Small glaciers react sensitive to small changes in climate and thus are a good indicator (Portocarrero et al., 2010). All three catchments in the study region contain steep, fractured glaciers (Frey et al., 2012). The local population does no see glaciers as a threat, as they are "over there, up in the heights" (Huggel et al., 2012c).

Gruber (2012) developed a global permafrost model with a 1 km - resolution DEM and NCAR/NCEP reanalysis. As permafrost is a subsurface phenomenon, modeling proves difficult. The map resulting from this model does not necessarily represent ground truth but can be used as a reference for permafrost occurrence where no other data is available (Gruber, 2012).

Fig. 3.3 shows glaciological features in the study region, including the global model of Permafrost (PF) from Gruber (2012). Permafrost does only occur on the highest peaks in the study region with a lower limit of around 5,000 m in Peru. Both starting zones for the 1998 events are permafrost free (see also Huggel et al., 2012d).

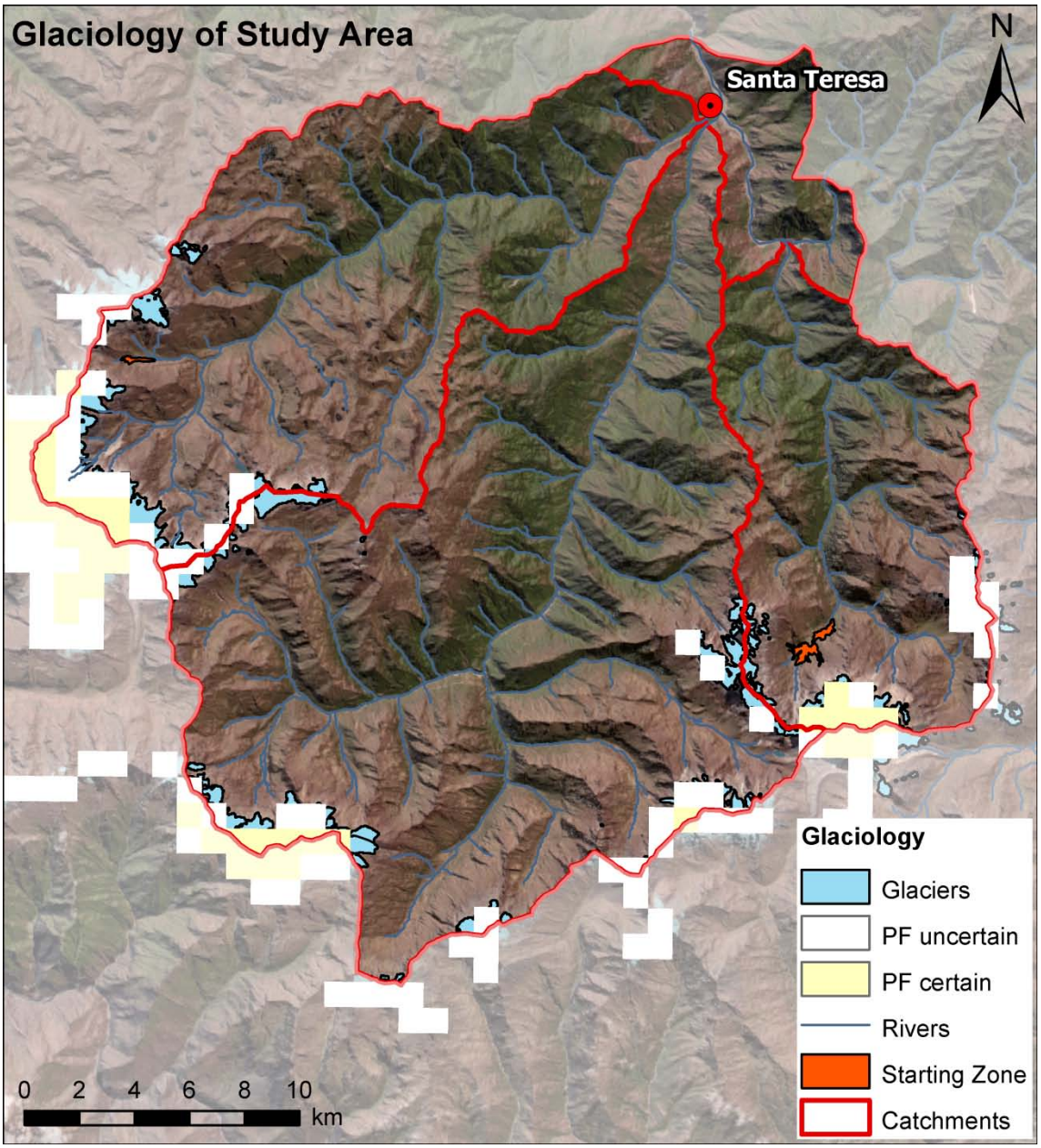

Figure 3.3: Glaciers (blue) and permafrost (PF) occurrence (white/yellow) in the study region.

3.4 Past Events

In the last decades, several debris flows were released around Santa Teresa (CARE & UZH, 2011). In 1998, two very large debris flows were triggered (Carlotto et al., 1999), which are described in this section. Both events were triggered in the rainy season (January and February) of the year 1998 from steep, loose talus slopes (Starting zone type 1, see Section 2.2.5.2). Event chronologies are mainly based on interviews with locals and some expedition reports, as no other data is available and is generally limited (Carlotto et al., 1999). Triggers are analyzed in Chapter 6. The 1998 debris flows were found to exhibit progressively increasing discharges and to last over a whole day (Huggel & Choquevilca n.d., Frey et al., 2012).

3.4.1 The Ahobamba Event in 1998

The starting zone of the Ahobamba debris flow is Quebrada Rayancancha between 3,950 and 4,250 m a.s.l. (Fig. 3.4, page 22) and starts below the glacier tongues. It is around one kilometer wide and long (Huggel et al., 2012d) in its largest extent (700,000 – 900,000 m^2 based on its overall extent) and up to 50 to 100 m deep (in average probably 10 - 30 m) (Carlotto et al., 1999), resulting in an already large starting volume of 7 – 27 mill. m^3 (Carlotto et al. (1999) state 12.5 - 25 mill. m^3). The starting zone was saturated by meltwater, precipitation and groundwater flow (Hermoza et al., 1998). Slopes are between 10° and over 40°, with an average of around 25°. Material was fine-grained, mainly silt and sand (Portocarrero, 2008).

On February 27th around 3 pm, a very large debris flow reached Urubamba valley. The starting time is unknown, leading to also unknown velocity. First, the saturated material slided slowly and destabilized moraines. These moraines held back the water momentarily and caused it to overtop, eroding morainic material. The flow accelerated when it reached an elevation drop of around 100 m. After, erosion took place along both valley sides. The erosion rates in Ahobamba were probably very large, the debris flow eroded nearly all erodible material on the bedrock, and the part between the starting zone and the confluence shows large erosion scars (Hermoza et al., 1998; Carlotto et al., 1999).
The Ahobamba event lasted for around three days (exact times are unknown), with up to 300 individual surges depositing at the confluence with Urubamba. A possible explanation for this surging behavior is that the first flow destabilized the valley sides, causing several landslides and many small temporal blockings of the river (Carlotto et al., 1999; Portocarrero, 2008). The flow regime was first laminar, but quickly changed to turbulent and erosive when the debris flow arrived in steeper slopes. During the Ahobamba debris flow, blocks were observed, but not larger than around two meters. Most of the material was fine-grained (sand, silt and clay) (C. Portocarrero, pers. communication).

The debris flow deposited at the confluence of Ahobamba and Urubamba (see Fig. 3.1) after 18 km distance and 2,470 m height drop, resulting in an overall slope of 0.14. It was estimated to reach a volume of 25 - 30 mill. m^3 (Hermoza et al., 1998; Carlotto et al., 1999). Estimations for deposit height vary between 30 m (DesInventar, 2013) and 74 m (Carlotto et al., 1999). 74 m are likely, as the water level of the dammed river was measured at the Machu Picchu power station (Central Hidroélectrico) (C. Portocarrero, pers. communication) and the number was confirmed by the responsible of the power station, Mario Ortiz. Event size was estimated taking into account the large starting zone, large erosion depths and flow heights (up to 40 m) and depositions (Carlotto et al., 1999) (Fig. 3.5, page 22). The first surges of the flow did exceed the final estimated deposition area (C. Portocarrero, pers. communication).

The structures in the front of Fig. 3.5 (page 22) are the remains of the power station, which was completely destroyed (Carlotto et al., 1999) and interrupted the production for three years (EGEMSA, 2011). Additionally, the debris flow destroyed several bridges, most of the railroad between the power station and Quillabamba and parts of Santa Teresa (Carlotto et al., 1999). This debris flow caused a lot of panic in Santa Teresa, as the population was relocated after the Sacsara event to the higher parts of Santa Teresa, where they could see the debris flow coming in from Urubamba valley (Carlotto et al., 1999). 51 people are listed missing (DesInventar, 2013).

The debris flow formed a temporal dam of the Urubamba river (Hermoza et al., 1998), damming approximately 30 mill. m^3 of water (DesInventar, 2013). In March 1998, the need for a fast drainage of the temporal lake was stressed by Hermoza et al. (1998). The lake was artificially drained four months after the event. This drainage caused some minor damages in communities downstream, but is of no

comparison to the Sacsara event or the first surges of the Ahobamba event (which also reached Santa Teresa) (C. Portocarrero, pers. communication). The runout of this drainage exceeded Quillabamba by far. The farthest effects were felt in Pongo de Mainique, around 200 km downstream from Santa Teresa (Carlotto et al., 1999). The total volume of the drained material, including water, is estimated to be around 50 mill. m^3.
The Ahobamba event is highly atypical, as no GLOF was observed and no ice or rock avalanche was incorporating debris (Hermoza et al., 1998). The trigger is yet unknown. Only the superficial scars of the starting zone are visible (C. Portocarrero, pers. communication). The Ahobamba event reached a debris flow magnitude of 8 (able to destroy cities), according to Jakob (2005b).

Figure 3.4: Rayancancha; the starting zone of the Ahobamba event. Source: Carlotto et al., 1999.

Figure 3.5: Machu Picchu power plant (front); Ahobamba depositions (back). Source: Carlotto et al. (1999).

3.4.2 The Sacsara Event in 1998

The starting zone of the Sacsara event is situated in morainic material near Nevado Chaupimayo on a height between 4,200 and 4,450 m (see Fig. 3.6, page 23). It is approximately between 100 and 300 m long, 100 m wide and 30 m deep. Slopes decrease from over 50° at the top to below 15° (Giráldez et al., 2012). The starting zone contains boulders, gravel and a sandy-silty matrix (Carlotto et al., 1999).

On January 13th 1998, a very large debris flow started from the top of Sacsara valley. Interviews with local witnesses suggest that there was intensive rain and high winds starting at 1 pm on January 13th, intensifying between 2 and 3 pm. At 4 pm, a loud noise comparable to a dynamite explosion was heard (Carlotto et al., 1999). Several small earthquakes were registered the days before the event – an earthquake of magnitude 6.1 (USGS, 2010) on January 10th was felt by locals. Around 6.20 pm, a first turbulent, watery surge passed Mukayoc (see Fig. 3.7, page 23), a zone with lower slopes situated 2 km downstream of the Sacsara starting zone. A second pulse passed within 10 minutes, a third between 7.30 and 8 pm, more between 9.15 and 10.15 pm. The last pulses passed around 5 am on January 14th. Minor pulses occurred every 10 to 15 minutes (Carlotto et al., 1999). The first pulses of the debris flow eroded lateral hillsides after the starting zone, producing landslides and increasing erodible material. In Mukayoc, a relatively flat zone, some material was deposited, mainly gravel and small boulders (Carlotto et al., 1999). After, the debris flow was channeled by the valley and continued to heavily erode lateral hillsides, continuously increasing the amount of debris (Carlotto et al., 1999).
The first surge reached the beginnings of Santa Teresa between 7.30 pm and 8.15 pm (Carlotto et al., 1999); resulting in a mean velocity of 3.5 - 6 m/s from Mukayoc to Santa Teresa (exact times are unknown due to contrasting time specifications of locals). Ground vibrations were felt and a power blackout was reported, together with a strong smell of excrements and loud noise (Carlotto et al., 1999). Other major pulses arrived around 8.30 pm, destroying a bridge at 10 pm. Many houses as well as the so-called peninsula separating the rivers Sacsara and Salcantay were flooded. At 11 pm, the train station was destroyed. This event lasted until 10 am on January 14th (Carlotto et al., 1999).

The Sacsara event stopped at the confluence with Urubamba after a distance of 29 km and a height drop of nearly 3,000 m (see Fig. 3.1), resulting in an overall slope of 0.10. The first surges of the flow however exceeded the estimated deposition area (C. Portocarrero, pers. communication). The Sacsara event caused the nearly total destruction of the communities of Yanatile and Andihuela, the road Yanatile-Santa Teresa including the bridge as well as the railroad and railway station (Carlotto et al., 1999; Huggel & Choquevilca, n.d.). Around 80% of the village of Santa Teresa was buried under the debris flow; only four houses were not completely destroyed. Hundreds of families lost their homes and needed government help. Five people died, 150 are listed missing. 340 houses and 90ha of agricultural land were destroyed, worth over 500,000$ (DesInventar, 2013).
The volume of the event is unknown, but estimated based on field reports to be 3 - 6 mill. m^3. Event duration was 16 - 18 hours. The Sacsara event reached a debris flow magnitude of 7 (can destroy parts of cities) according to Jakob (2005b). After these events, Santa Teresa was rebuilt in a zone with lower risk (CARE & UZH, 2011) (see Fig. 3.1).

Figure 3.6: Starting zone of 1998 event. Source: Giráldez et al., 2012.

Figure 3.7: First deposition zone Mukayoc. Source: Giráldez et al., 2012.

3.4.3 Other events

Mass movements are a common threat in Peru and are assessed in a variety of studies (for example Hermoza et al., 1998; Carlotto et al., 1999; Huggel et al., 2003b!; Hubbard et al., 2005; Vilímek et al., 2006; Klimeš et al., 2007; Valderrama & Vilca, 2010; Díaz, 2010; Klimeš et al., 2011; Frey et al., 2012; Worni et al., 2012). In Peru, over 9,000 natural disasters were recorded from 1970 to 2011 (DesInventar, 2013). In close vicinity to Santa Teresa, 26 debris flows were registered between 1946 and 2005, many of which caused damage to people and property (Klimeš et al., 2007). The main hazards in this area are slope instabilities due to landslides, rain or snowmelt (Huggel et al., 2003b; Frey et al., 2013). In addition, ice and rock avalanches, GLOFs, floods and earthquakes can cause significant damage to people and property (see Huggel, 2004 for an overview of literature). Also in the future, large mass movements are possible in the study region. Monitoring is recommended (Hermoza et al., 1998).
In Ahobamba valley, a GLOF in 1996 originating from Laguna Sisaypampa in Orcospampa river reached the main valley. It was caused by an ice avalanche hitting the lake, causing it to overtop (Hermoza et al., 1998). This event killed 5 people (CARE & UZH, 2013a). After the large event in February 1998, a second (12th of March, 1998) and a third (22nd of November, 1998) event, both smaller, incorporated material from the previous events but caused no major damage. The second event probably also originated from Rayancancha and added to the deposition in Urubamba valley (CARE & UZH, 2013a), the third event originated from Orcospampa (Carlotto et al., 1999).

In Sacsara, a smaller debris flow was triggered after the main event (CARE & UZH, 2011) and reached Santa Teresa around 4.30 pm on January 27th, overflowed deposits of the previous flow and destroyed previously spared parts. This debris flow was not registered in Mukayoc, as it is speculated to having either formed out of the material of the major debris flow on January 13th or being triggered by a reactivated landslide (Carlotto et al., 1999). A month previous to the main event, a small debris flow was triggered higher up in the valley, destroying one property. This debris flow was deposited in Mukayoc (Carlotto et al., 1999).

Also in other parts of Peru, glacial hazards are common. In the Cordillera Blanca, a glacier lake called Laguna 513 was hit by an ice avalanche in 2010, causing water to overtop the dam and forming an outburst flood (Carey et al., 2011, Worni et al., 2012, Schneider et al., 2014). This event was characterized by complex process interactions and was modeled by Schneider et al. (2014). In January 2010, strong rainfall affected Cusco region and caused large damages (CARE & UZH, 2011). A hyperconcentrated flow on January 24th originating from a pro-glacial lake destroyed parts of the village of Santa Teresa as well as the thermal baths. The original trigger factors are still unclear (Huggel & Salzmann, n.d.), but a possible source is a lake detected in 2008 but not found again in 2010 (Rohrer, 2012). Rainfall preceding the 2010 flood belongs to the highest monthly precipitation amounts ever recorded in the region (Frey et al., 2012).

3.5 Potential Hazard Sources

This section shows a hazard analysis for the study region (see Section 5.2.1). Areas most probable to trigger debris flows in the future are selected, in order to model potential debris flows. Not all potential starting zones are modeled, due to the large size of the study region and the large amount of potential starting zones. Potential volumes are based on basic and variable disposition as well as trigger analysis. In total, 7 starting zones were chosen, 3 in Ahobamba, 2 in Sacsara and 2 in Salcantay, totaling in 21 simulations. These zones reflect the range of possible volumes and events. Human activity can be considered low in all catchments and was neglected. Two (simplified) trigger conditions are distinguished: dam failure (here: GLOF) and slope instabilities (shallow and deep-seated). Both 1998 events were attributed to the second trigger.
Besides debris flow activity, Santa Teresa is threatened by Chilcapata hill (where Fig. 3.8 was taken), where the new town was built. This hill produced a landslide in 2010, causing significant damage. Currently, fractures indicating a large landslide can be seen (Giráldez et al., 2012). Most likely, the hill will continue to slowly slide without major effect. However, monitoring is strongly recommended (Huggel & Choquevilca, n.d)

Figure 3.8: View of Santa Teresa from Chilcapata hill. Source: Claudia Giráldez.

3.5.1 Ahobamba

Ahobamba valley origins from the confluence of Orcospampa river and Rayancancha, coming down from Nevado Salcantay (6264 m), and ends at the confluence with Urubamba at 1,800 m (Carlotto et al., 1999). Both Orcospampa river and Rayancancha are highly problematic zones, showing steep slopes and loose sediment. These zones have caused major events in the past – in 1996, 1998 and 2002 (Huggel et al., 2003b). Ahobamba is highly vulnerable and prone to local slope instabilities. These can temporally block the main river or increase the volume of an event (Huggel et al., 2003b).
Fig. 3.9 shows a slope map with potential starting zones indicated. Below 10°, danger of slope failure is low, above 15° high (Takahashi, 2007a) and above 40° very high (Lehmann & Or, 2012). Ahobamba shows very large areas of critical slope.

Laguna Sisaypampa (2) just north of Nevado Salcantay (Fig. 3.10) in Orcospampa river caused the GLOF in 1996 (Hermoza et al., 1998). Dam structure is weak and surrounding terrain steep, making Laguna Sisaypampa a potential threat (Huggel et al., 2003b). The lake is located at high elevation, surrounded by steep rock walls and glaciers. Some debris accumulation before the lake might slightly dampen the impact. The lake measures around 100 m x 300 m and has little freeboard. Lake volume could amount to 600,000 m^3. Debris amount is around 200 x 300 m, adding to another 1.8 mill. m^3 (with an estimated height of 30 m). Stability is low due to morainic material without vegetation similar to the 1998 starting zones. Permafrost thaw and glacier melt can influence this zone. This lake is considered a potential threat and is modeled in Chapter 8. Slopes surrounding this starting zone are over 25°, often over 40°. Potential maximum volume is 2.5 mill. m^3.

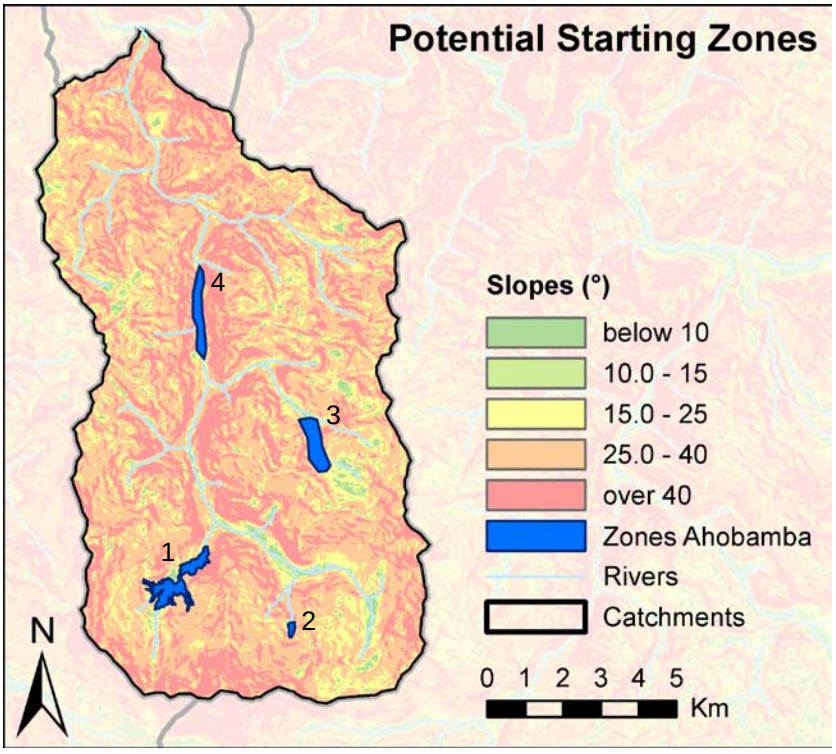

Figure 3.9: Slopes (from green to red) and potential starting zones (blue) in Ahobamba valley.

Figure 3.10: Lake Sisaypampa north of Nevado Salcantay. Source: César Portocarrero.

Quebrada Rayancancha (1) contains heavily fractured material. On the geological map, a lot of fractures are visible in Ahobamba (see Appendix). Still a lot of loose morainic material is present in the zone, together with steep and destabilized slopes (Carlotto et al., 1999). Past events laid the starting zone bare of vegetation, many landslide scars are visible and future events are possible. Debris amount

is around 1 km^2. With an estimated height of 10 m, this results in a potential volume of up to 10mill. m^3 material. Permafrost thaw and glacier melt only affects this area indirectly (see Section 3.4). This starting zone is not considered for scenario simulations, as the probable worst case already happened. Slope in Rayancancha is between 10° and over 40°, with an average of around 25°.
Manamayo (3), a side valley in the east of Ahobamba, contains a lot of morainic material similar to Rayancancha. Above the potential starting zone, steep glaciers and rock walls are present. Many small lakes, the largest being around 100 x 70 m, are detected in the area. Process chains could be very dangerous. The debris amount is estimated to be around 0.5 km^2. With a worst-case height of 40 m, this would give a potential maximum volume of 20 mill. m^3. This starting zone is considered a potential threat and is modeled in Chapter 8. Slope is between 10° (where the debris accumulation is) and over 40° (around it), with an average of around 30°, thus comparable to Rayancancha.
As Ahobamba shows many landslide scars, a scenario was built considering a landslide-triggered debris flow in any of the side valleys, accumulating at around 8 km upstream from the confluence with Urubamba (4). This corresponds to the lowest part of visible landslide scars on Google Earth. The total area with landslide scars adds up to 2 km^2 in the whole valley, most with steep slopes and bare of vegetation. No lakes of significant size were detected in Ahobamba. Permafrost thaw and glacier melt influences debris flow triggering only indirectly. Landslides accumulating in Ahobamba are considered a potential threat and are modeled in Chapter 8. Slope is below 15° in the valley, but above 25° and mostly even above 40° on lateral slopes. Potential maximum volume is 40 mill. m^3, based on 20m debris height.

3.5.2 Sacsara

The catchment of Sacsara river starts at the peaks of Chaupimayo and Sacsarayoc (5239 m and 5991 m) and flows into Urubamba at 1,400 m. An expedition was launched in October 2012 in order to investigate the hazard potential of Sacsara (Giráldez et al., 2012). Fig. 3.11 shows slopes and potential starting zones in Sacsara.

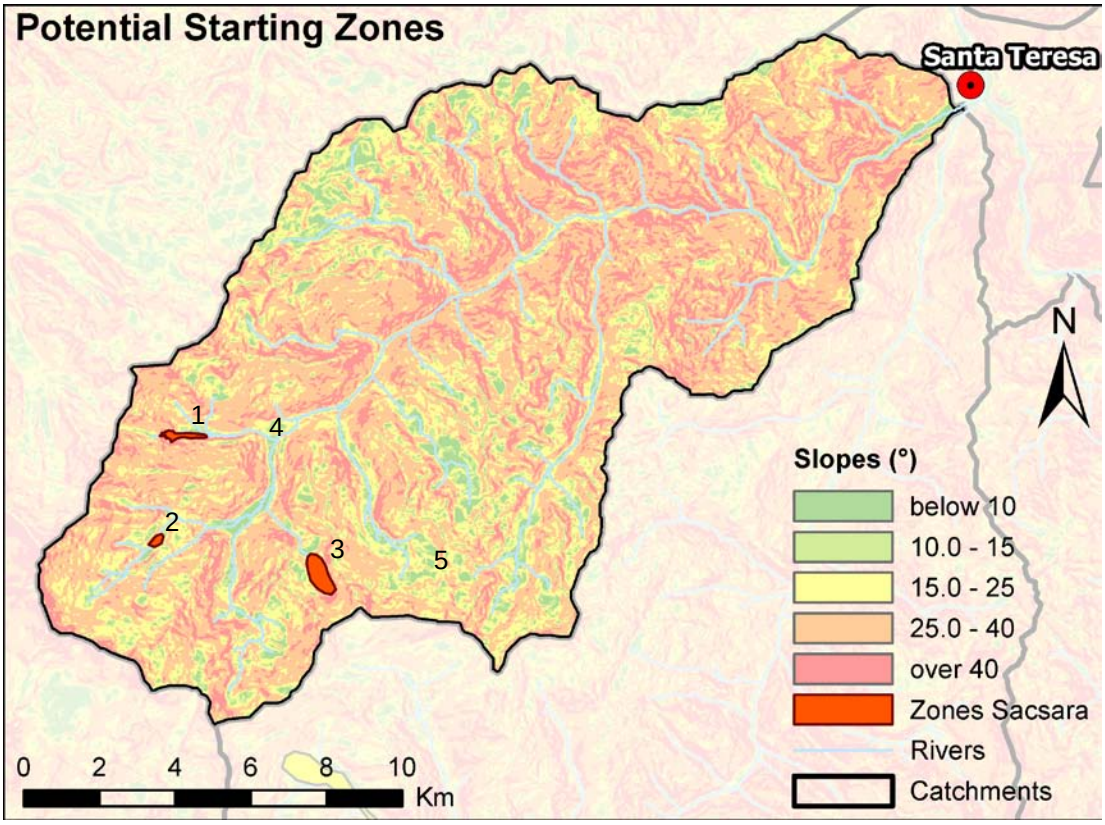

Figure 3.11: Slopes (from green to red) and potential starting zones (blue) in Sacsara valley.

During the expedition, deposits at the exit of the moraines of a debris-covered glacier were found, hinting at past floods originating from supra-glacial lakes (Giráldez et al., 2012). This debris-covered glacier (Fig. 3.12) is situated to the east of the starting zone of the 1998 event. The following processes were identified (Giráldez et al., 2012):

- supra-glacial lake formation.
- drainage channel formation.
- debuttressing (pressure release) on the inner walls of moraines.
- marginally stable hanging glaciers.

A lot of unstable morainic material covered with none or sparse vegetation is present, together with a retreating, heavily debris-covered glacier with detached dead-ice bodies and several ponds forming (2) (Giráldez et al., 2012). Frey et al. (2012) estimates the dead ice body area to be 15,000 m^2. The ponds around 450 m downstream are at the initial stage of lake formation and are expected to merge into one large lake, creating the potential for a GLOF or debris flow (Giráldez et al., 2012). The largest lake measures around 150 x 150 m, resulting in an estimated volume of 450,000 m^3. This starting zone is considered a potential threat and is modeled in Chapter 8. The slope of the glacier itself is below 15°, but around and above it slopes are over 25°. Potential maximum volume is 2.5 mill. m^3, based on the lake volume and the estimated debris amount in the area.

To the east of this starting zone, numerous lakes exist, most of which could trigger an outburst flood. The largest of them, Hanpi K'ocha 1 ((3), Fig. 3.13) was considered most dangerous, due to its small freeboard (1 - 5 m), lack of buffer zone and large volume of approx. 4.3 mill. m^3 (Giráldez et al., 2012). Steep glaciers and rock walls as well as a lot of loose material are present. Just below lake Hanpi K'ocha 1, another lake (Hanpi K'ocha 2) with an estimated volume of 400,000 m^3 is situated, also with little freeboard. This lake was included in the scenario. For these lakes, the area (530 x 270 m and 160 x 260 m) is measured and the depths (30 m and 10 m) estimated (Giráldez et al., 2012). Debris availability is high, another 5 mill. m^3 of debris as a worst-case seems realistic, resulting in a potential maximum volume of 10 mill. m^3. This lake is considered a potential threat and is modeled in Chapter 8. Slopes around the lake are very steep (over 25° and often over 40°). Hanpi K'ocha is taken as a representative for all the lakes in this subcatchment, as it has the largest hazard potential. The debris-covered lake is on the far side of the same subcatchment, covering the spatial range.

Figure 3.12: Supra-glacial lakes on debris-covered glacier. Source: Giráldez et al., 2012.

Figure 3.13: Lake Hanpi K'ocha 1. Source: Giráldez et al., 2012.

The starting zone of the 1998 event (1) was also investigated and showed little cohesion and many erosive traces (Giráldez et al., 2012). Slopes decrease from over 40° at the top to below 10° at the lowest part. This zone is still a potential threat, but was not modeled as a scenario, as future events are likely smaller than what happened. Mukayoc (4) also shows a lot of debris, but its slope is too low to

be a threat. The side valley Tambohauyco to the northeast of Sacsara (5) also contains many lakes and a lot of debris, together with sparse vegetation. However the terrain is not very steep and does not show large signs of instability. No expedition has been in this part yet.
Although numerous landslide scars were found (Giráldez et al., 2012), a landslide scenario was not made for Sacsara, as volumes are not expected to be larger compared to the event in 1998. However, monitoring of Sacsara is recommended.

3.5.3 Salcantay

Salcantay valley originates from Nevado Salcantay and Tucarhuay and flows into Urubamba river near Santa Teresa. Fig. 3.14 shows slopes and potential starting zones in Salcantay.

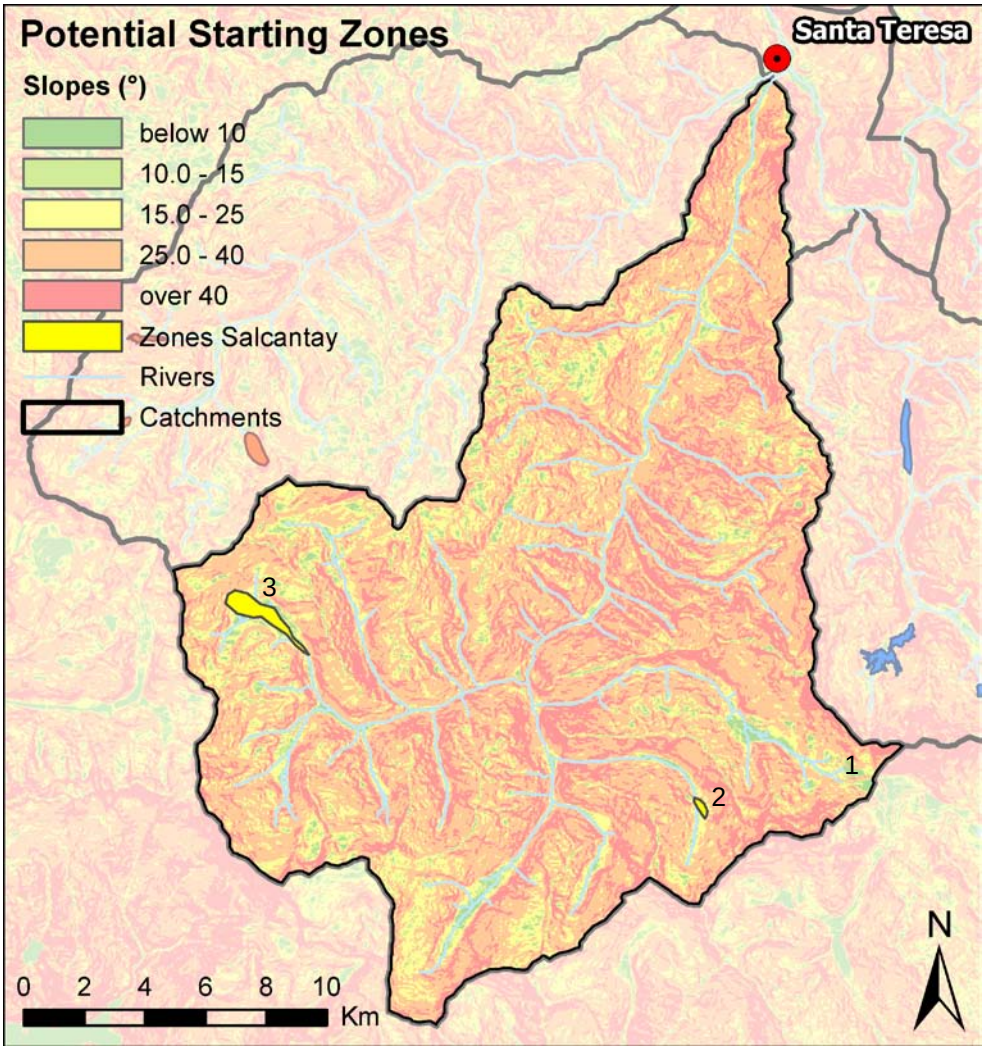

Figure 3.14: Slopes (from green to red) and potential starting zones (blue) in Salcantay valley.

Lake Salcantay (Salcantaycocha) (Fig. 3.15, page 29) south of Rayancancha in Ahobamba (1) has a volume of 1 - 2 mill. m^3 and active glaciers and a high rock wall close-by (Haeberli et al., 2012). An outburst is considered unlikely, due to its large freeboard (50 - 100 m) (Huggel et al., 2003b) and a talus would probably dampen a potential impact. Moraine dam stability seems to be high (Haeberli et al., 2012).

Figure 3.15: Salcantaycocha. Source: CARE & UZH, 2012 (left) and Google Earth (right).

To the northwest of Tucarhuay, a supra-glacial lake on a debris-covered glacier was detected with Google Earth in 2009 but did not grow much within two years (2, see Fig. 3.16). Characteristics are similar to the debris-covered glacier in Sacsara: A lot of debris, erosive traces and a dead-ice body with ponds forming are visible (Haeberli et al., 2012). Lake formation is still in an initial stage, with an area of 2000 - 2500 m^2 (Frey et al., 2012) and an estimated volume of 10,000 m^3 by the end of 2011. Due to the glacier below the lake, the situation is considered a potential threat and is modeled in Chapter 8. The slope on the glacier is below 15°, but around and above it between 15° and over 40°, with an average of around 30°. Potential maximum volume is 2 mill. m^3, based on the lake volume and the estimated glacier and debris volume close to the lake.

In Google Earth, large and deep erosion scars were found in Totora valley (3), a catchment draining into Salcantay in the southeast. The area appears similar to Rayancancha, with erosion scars and a lot of assumedly unstable available debris (around 1 km^2). This results in an estimated potential volume of 30 mill. m^3, based on a debris height of 30m. Slopes decrease from over 25° at the top and around the starting zone to below 10° at the bottom. No lakes of significant size were found. The starting zone is considered a potential threat and is modeled in Chapter 8.

Also in Salcantay, landslides (Fig. 3.17) form a high hazard potential (Haeberli et al., 2012) due to steep side slopes. This scenario was not modeled, as the magnitude of an event from landslide damming is not expected to exceed the volume modeled from Totora.

Figure 3.16: Debris-covered glacier in Salcantay valley. Source: Claudia Giráldez.

Figure 3.17: Landslide scars in Salcantay valley. Source: Claudia Giráldez.

4 Data

In this chapter, the various data sources and their uncertainties are discussed. This thesis is based mainly on remote sensing data. ASTER GDEM2 (Advanced Spaceborne Thermal Emission and Reflection Radiometer Global Digital Elevation Model Version 2) was used in combination with Landsat Thematic Mapper (TM5) and high-resolution imagery from Google Earth. All remote sensing data (including DEMs) was georeferenced with the projected coordinate system WGS (World Geodetic System) 1984 UTM (Universal Transverse Mercator), zone 18S, which covers the study region. From now on, error is defined as a known deviation of a value x from the true value x and uncertainty as the knowledge of value x having an error, but with unknown size, location or time (Andres, 2010).

4.1 Satellite Imagery

Satellite data is a remotely sensed. Remote sensing techniques collect information of objects from afar with electromagnetic energy (Rosenfeld, 1984). The best data acquisition techniques vary for electromagnetic, spatial and temporal scales and are divided into active (with their own source of energy) and passive techniques. Two sensor types exist: the framing sensor, portraying one area at a time, and the scanning sensor, acquiring data while the sensor sweeps over the surface (Rosenfeld, 1984).
Landsat imagery is very useful in visually detecting ground features, especially when combining multiple spectral bands (Rosenberg, 1984). Landsat TM has a resolution of 30 m (Pack, 2005). For this thesis, the Landsat TM5 scene "path 004/ row 069" with spectral bands 3, 2 and 1 is used, obtained on August 6th 2010. Landsat has the disadvantage of being a passive sensor. Active microwave sensors such as Radar (Radio Detection and Ranging) could also penetrate clouds, which would be useful in the wet tropics (Rosenberg, 1984). Radar data was not used within this thesis. Another active sensor, Lidar (Light Detection and Ranging, see Pack, 2005) neither was available.
As a spatial resolution of 30 m limits target feature details for complex topography as in the Andes, Google Earth imagery was additionally looked at. Google Earth was chosen as it is publicly accessible and has high resolution. Satellite data is available from 1.1.1970, the latest data used here is from 8.9.2003 (Santa Teresa); 30.6.2009 (Ahobamba and Salcantay); and 29.7.2011 (Sacsara). As Google Earth imagery data is not freely available, it cannot be used for quantitatively analyzing high-resolution satellite images (as proposed by Huggel, 2004).
Challenges in satellite imagery are that high resolution DEMs (Digital Elevation Models) are necessary for accurate interpretation, which in turn requires high user knowledge (Singhroy, 2009). Also, temporal and spatial resolution are inversely proportional (Huggel, 2004), limiting data availability.

4.2 DEMs

Modeling is based on ASTER GDEM2 and to a lesser extent on the DEM from the Shuttle Radar Topography Mission (SRTM). A DEM is a digital model representation of a part of the earth surface. Data source and data acquisition technique are crucial for DEM quality. DEMs can be generated from ground pictures, photogrammetric data, digitalized cartographic data, radar, laserscanning and sonar (Andres, 2010). The data structure of DEMs used in this thesis is raster.
DEM errors; a sort of input error; are one source of uncertainty for simulation models (Heuvelink, 1998). DEMs are the result of various modeling and processing steps (e.g. data acquisition technique and instrument). The errors from these steps propagate to the model results. Fisher & Tate (2006) distinguish three error sources: (1) data acquisition; (2) processing and interpolation of data; and (3) the relationship between modeled surface properties and representation in the model. DEM errors are divided into three types (Fisher and Tate, 2006):

1) Blunders and artifacts (unrealistic or missing values), mostly from device or digitalization errors (see Andres, 2010 for a literature overview).
2) Systematic errors, show a trend or dependency, can be the result of processing and acquisition techniques (Hebeler & Purves, 2009).
3) Random errors from various sources, without trend, only reducible with repeated measurements (Hebeler & Purves, 2009).

In DEMs, often only the vertical error (RMSE; Root Mean Square Error) is delivered with the data, which is a global estimation of DEM (Fisher & Tate, 2006). As topographic attributes are derived from a DEM, the DEM error is often more important than the errors from faulty algorithms. Higher resolution does not necessarily lead to a better DEM quality, as also the influence of DEM errors increases. With lower resolutions, algorithm errors are more important (Andres, 2010). Frey & Paul (2012) looked at topographic parameters for glaciers and found that coarser DEM resolution decreases maximum and increases minimum values of elevation. DEM errors are largest in terrain with strong topography like mountains and valleys (Chang & Tsai, 1991).
Better DEM resolution usually improves model results. Runout distance and lateral spreading decrease with rougher terrain; friction increases (Andres, 2010). Christen et al. (2008) recommend a resolution of 5 - 25 m for debris flow mapping; but large events can also be modeled with DEMs with lower resolutions than 25 m (Christen et al., 2010a). The largest uncertainties in DEMs occur when modeling maximum flow height in flat areas or on the boarder of debris flows (Heuvelink, 1998).

4.2.1 ASTER GDEM

The ASTER GDEM was generated from the ASTER instrument on board the Terra spacecraft launched 1999 (Frey & Paul, 2012). The ASTER instrument includes a nadir and backward visible and near infrared sensor (VNIR, 0.76 - 0.86 μm), separated by approximately 30° (Toutin, 2008) and an along-track stereoscopic capability; allowing for photogrammetric DEM generation. All scenes are acquired between 2000 and 2007, the exact date being unknown (Frey & Paul, 2012).
ASTER GDEM2 scene S014 W073 was used in this thesis. GDEM2 was strongly improved compared to GDEM1. Vertical accuracy is +- 0.2 m, with 17 m at a 95% confidence level and a RMSE of 8.7 m. Average elevation error is 7.4 m in mountainous areas, RMSE is 15.1 m (Tachikawa et al., 2011). Vertical uncertainty is highest in steep northern slopes, as they are turned away from the sensor (Huggel, 2004) and can also be caused due to distortions from clouds, snow or lakes (Toutin, 2002). Horizontal resolution is set to one arc-second (around 30 m); however actual resolution is 2.4 arc-seconds (72 m). Horizontal error is 0.13 arc-seconds to west and 0.19 arc-seconds to north. ASTER GDEM2 shows slightly more voids than GDEM1 but has significantly less artifacts (Tachikawa et al., 2011). In the vicinity of Santa Teresa village, a shift of around 1 Pixel (30 m) westwards compared to the deposit file georeferenced in RAMMS was found. This shift was corrected in this thesis.
Frey & Paul (2012) also found that artifact-related roughness in ASTER DEMs cancel out for larger phenomena, such as the large debris flows in Peru. ASTER DEMs can be used for first-order assessments in areas like Santa Teresa (Huggel, 2004) as done in this thesis. For detailed hazard analysis of events very close to infrastructure however, ASTER DEMs proved insufficient (Huggel, 2004).

4.2.2 SRTM DEM

The SRTM DEM was generated using the active system interferometric synthetic aperture radar (InSAR) technology and is the first near-global digital elevation model of a resolution of 3 arc seconds (approx. 90 m). All data was acquired by a space shuttle from February 11th to 22nd 2000, guaranteeing homogenous quality with an accuracy of +- 16 m absolute and +- 6 m relative vertical accuracy and less than 20 m horizontal accuracy (Rabus et al., 2003). In mountainous terrain, numerous data voids can occur in the SRTM3 version, but the Consultative Group on International Agricultural Research

(CGIAR) offers a void-filled version (SRTM3v4), where gaps were filled using interpolation and auxiliary DEMs (Frey & Paul, 2012). Scene S014 W073 from version SRTM3v4 was used for this thesis.

The SRTM DEM shows uncertainties in areas with dense vegetation, snow and ice, water and steep slopes over 30°, as was summarized by Andres (2010). SRTM is found suitable for assessing topographic parameters for glaciers in high mountain areas. Mean elevation differences are not larger than +- 7 m (Frey & Paul, 2012). In SRTM, concave features (e.g. valleys) have negative errors and convex features (e.g. ridges) have positive errors, meaning that valleys are “filled up” and mountains “eroded”. Maximum errors are -71 m and +94 m (Andres, 2010).

4.3 Climate Data

This section looks at data for precipitation and temperature analysis. Fig. 4.1 shows all available SENAMHI stations as well as used TRMM (Tropical Rainfall Measuring Mission) tiles. SENAMHI stations provide both precipitation and temperature data, TRMM tiles were used for precipitation only.

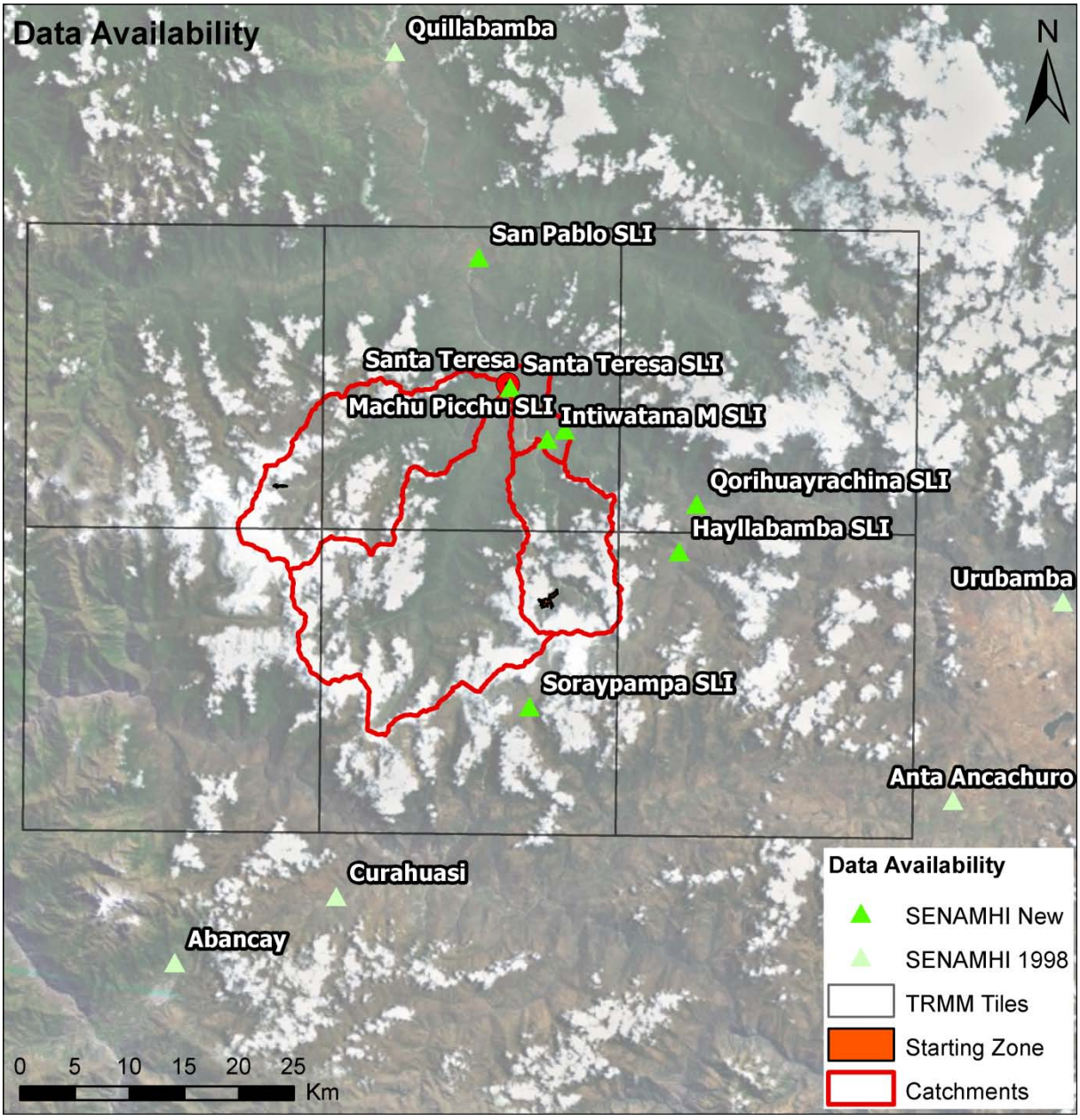

Figure 4.1: Study region with SENAMHI stations (1998 = containing data from 1998; new = newer stations) and TRMM tiles. Source of Basemap: ArcGIS.

4.3.1 SENAMHI

Meteorological stations from the Peruvian meteorological and hydrological agency (SENAMHI) were used for this thesis. Stations considered for this thesis were chosen according to their geographical location and their data availability (see also Raissig, 2011). Meteorological data was obtained from a data portal developed by Meteodat together with SENAMHI for the PACC-project (Programa de Adaptación al Cambio Climático). There, 97 stations from SENAMHI are available. Available data varies between several months and over 40 years, the oldest data used being from 1965, the latest from 2012. The data portal shows the following climatic variables (where available): maximum, minimum and mean daily temperature, temperatures, dew points and relative humidities at 7,13 and 19 o'clock local time, daily precipitation, relative humidity (daily), air pressure, wind velocity and wind direction. Older stations have a conventional Hellmann pluviometer which is still emptied manually, while newer stations (SLI) have automated measurements. The newer station either has a distrometer, measuring the impact and volume of raindrops; or a tipping bucket rain gauge. Metadata concerning acquisition techniques is missing, and acquisition techniques have changed over the operation time (M. Rohrer, pers. communication).
Table 4.1 below shows all stations containing data (daily maximum and minimum temperature, daily precipitation) for the years 1997 and 1998; situated less than 50 km from either the Sacsara or Ahobamba starting zone or Santa Teresa.

Table 4.1: Stations used for precipitation and temperature analysis of the 1998 events. Source: SENAMHI.

Station	Abancay	Anta Ancachuro	Curahuasi	Quillabamba	Urubamba
Coordinates	-13.6°/-72.9°	-13.5°/-72.2°	-13.6°/-72.7°	-12.9°/-72.7°	-13.3°/-72.1°
Start Measurements	01.04.1964	01.06.1964	01.12.1963	01.05.1964	01.11.1963
End Measurements	30.11.2012	31.01.2013	28.02.2013	28.02.2013	31.01.2013
Elevation	2750m	3340m	2763m	990m	2863m

As no station with data from 1998 lies within the TRMM grid, stations without data in 1998 are used to compare SENAMHI and TRMM precipitation. Table 4.2 shows these 8 stations, containing data about daily maximum and minimum temperature as well as daily precipitation and wind speed (m/s); situated less than 20 km from either the Sacsara or Ahobamba starting zone or Santa Teresa. These stations were only used for a quality check of SENAMHI stations and a precipitation comparison with TRMM tiles.

Table 4.2: Stations used for quality check and precipitation comparison. "Start" and "End" refers to measurements taken. Source: SENAMHI

Station	Coordinates	Start	End	Elevation (m)
Hayllabamba SLI	-13.3°/-72.4°	18.10.2010	06.05.2013	3020
Intiwatana M SLI	-13.2°/-72.6°	18.10.2010	05.05.2013	1808
Machu Picchu SLI	-13.2°/-72.5°	14.10.2010	06.05.2013	2459
Machu Picchu	-13.2°/-72.5°	01.05.1964	31.01.2013	2459
Qorihuayrachina SLI	-13.2°/-72.4°	01.02.2011	06.05.2013	2508
Santa Teresa SLI	-13.1°/-72.6°	18.10.2010	06.05.2013	1520
San Pablo SLI	-13.0°/-72.6°	01.02.2011	06.05.2013	3491
Soraypampa SLI	-13.4°/-72.6°	21.10.2011	06.05.2013	3868

Hourly values are available from 35 stations from SENAMHI Peru, including the stations in Table 4.2 (except for Machu Picchu). SENAMHI data is reported in PET (Peru time; UTC-5 (UTC: Coordinated Universal Time). Machu Picchu (manual) and Machu Picchu SLI (automatic) are at the same location. Distance of all used stations to the starting zones for the 1998 events are given in Table 4.3 (page 34).

Table 4.3: Distance of SENAMHI stations to starting zones.

Sacsara		**Ahobamba**	
Station Name	Distance (km)	Station Name	Distance (km)
Santa Teresa SLI	23	Soraypampa SLI	9
Intiwatana M SLI	25	Hayllabamba SLI	13
Machu Picchu (SLI)	27	Intiwatana M SLI	15
San Pablo SLI	28	Machu Picchu (SLI)	16
Soraypampa SLI	30	Qorihuayrachina SLI	17
Hayllabamba SLI	37	Santa Teresa SLI	20
Curahuasi	37	San Pablo SLI	32
Qorihuayrachina SLI	38	Curahuasi	32
Quillabamba	41	Anta Ancachuro	41
Abancay	44	Abancay	47
Anta Ancachuro	68	Urubamba	47
Urubamba	73	Quillabamba	52

Only few meteorological stations exist in the study region. In total, 13 stations at 12 locations (Machu Picchu and Machu Picchu SLI are counted separately) are available within 75 km around the starting zones and Santa Teresa, 5 of which contain data from 1997 and 1998.
Limited station availability and their large distance to the starting zones (especially for stations with data for 1997 and 1998) are a considerable source of uncertainty. Also, stations often are on other elevations or even across the Cordillera Vilcabamba, e.g. Curahuasi. In addition, many days do not contain data due to various reasons, including defect measurement devices or hindered access to the station. It is not possible to give a quantitative statement concerning data quality of SENAMHI stations, as no such metadata is recorded (M. Rohrer, pers. communication). For example, a daily precipitation of 0 mm can mean “no data” instead of “0 mm precipitation”, as is the case in Pacaymayo station (0.6 mm yearly precipitation in 2012). A measurement period as mentioned in Table 4.3 above does not guarantee continuous data availability. Missing data is given for each graph individually in Chapter 6.

4.3.2 TRMM TMPA

In addition to SENAMHI stations, data from the TRMM Product 3B42 Version 6 is used. This product aims to produce TRMM-adjusted merged infrared (IR) precipitation and root-mean square precipitation-error estimates (NASA, 2013b). The data is provided on a 0.25° x 0.25° grid (roughly 25 km x 25 km in Central Peru) with three-hourly intervals using Multi-satellite Precipitation Analysis (TMPA) (Scheel et al., 2011). TMPA combines precipitation estimates from four passive microwave sensors, flying on a variety of platforms. They are calibrated with a combined instrument product of the TRMM Precipitation Radar (PR) and TRMM Microwave Imager (TMI), one of the microwave sensors and merged to a high-quality microwave product. If data for this product is lacking for a certain time or location, IR data (“variable rain rate” (VAR)) calibrated with this product is used. The final product consists of microwave and IR data (Scheel et al., 2011). As follows, TRMM constitutes the TRMM mission and TMPA the resulting data product. TMPA data was also obtained via the Meteodat portal.
Table 4.4 shows the TRMM tiles used for precipitation analysis. Note that TMPA data is stored in UTC, whereas Peru lies in the time zone UTC-5 (PET). This means that all data is two 3-hour intervals shifted. Analysis of an event starting in Peru at 3 pm would have to include TMPA data of 9 pm.

Table 4.4: TRMM tiles used for precipitation analysis.

TRMM tile	W72P875x S13P125	W72P625x S13P125	W72P375x S13P125	W72P875x S13P375	W72P625x S13P375	W72P375x S13P375
Name	Sacsara	Santa Teresa	Santa Teresa East	Between Sacsara & Ahobamba	Ahobamba	Ahobamba East

A main advantage of TMPA data is its availability: From January 1st 1998 to February 28th 2013, there is daily data coverage of 99.996%. Only September 16th 1998, 06.00 and January 9th 2001, 15.00 have no data. However, TMPA data products are a merged and interpolated product and are not necessarily directly based on satellite measurements for a given time period (Scheel et al., 2011). Between the 3-hour intervals, no data is available – the 3-hour interval is simply filled with the following value, assuming this value to be the best estimate for the whole interval and that this error will cancel out over longer periods of time.
Uncertainties arising from this procedure are especially large when looking at short time periods in regions with high temporal precipitation variability (Scheel et al., 2011). Ground stations for calibration are unknown. Available microwave satellites varied significantly over time. Also the aggregation process, changes in satellite configurations and physical constraints of the satellite sensors as well as the processing algorithms add uncertainty (Scheel et al., 2011). Remote sensing precipitation measurements further have uncertainties as they are indirect measurements, have limited resolution and do not implement of orogaphic effects or measure wind speed (Wieczorek et al., 2003). TMPA uncertainties are higher in the wet season (when the debris flows in Santa Teresa occurred), due to higher precipitation amounts (Scheel et al., 2011). Microwaves are scattered on land, especially over cold surfaces. Also the relief has a strong effect (Scheel et al., 2011). TMPA relative errors can be three times higher than the actual precipitation measured (NASA, 2013a). In spite of these uncertainties, TMPA can help complement data from field measurements (Wieczorek et al., 2003), especially when field data is as limited as in Santa Teresa due to difficult access.

4.4 Further Data Sources

Various field trips were carried out in recent years (see Chapter 3) in order to visually assess hazard potential in terms of lake and moraine stability, slope stability and potential GLOFs in Santa Teresa area (CARE & UZH, 2011 and 2012; Haeberli et al., 2012; Huggel & Schneider, 2012; Huggel et al., 2012c). Assessment was qualitatively and based on expert knowledge, which can be subjective. Input parameters are based on these expert reports. Quantitative data about the study region is rare. No quantitative information on soil properties (soil cover, porosity, permeability and grain size distribution), vegetation, lithology or hydrology (runoff, groundwater, infiltration rate, soil moisture, surface water flow and evaporation) is available.

Several photographs from reports about the events (Hermoza et al., 1998; Carlotto et al., 1999) are available. A topographic map used for the names of rivers and towns was made for Vilcabamba by the Peruvian geographical institute (IGN; Instituto Geográfico Nacional) in the scale of 1:100,000. Frey et al. (2012) provide a scientific baseline for the study region. A geological map is provided by Carlotto et al. (1999). Some video material is provided by Panamericana Televisión.
The event database DesInventar (Disaster Inventory System) listed hazards events from 1970 to 2011. There, climatically induced natural events are stored (DesInventar, 2013). INDECI, another event database, did not start to collect data until 2001 (Raissig, 2011).
Earthquake data was used from USGS (United States Geological Survey, 2010), where an earthquake archive is available. Literature considered in this thesis contains papers, books and reports of varying kind and quality, with material from 1932 to 2014.

5 Methods

This chapter summarizes the workflow (part 1 to 3, shown in Fig. 5.1) and the methodology chosen in order to obtain the results shown in Chapters 6 to 8.

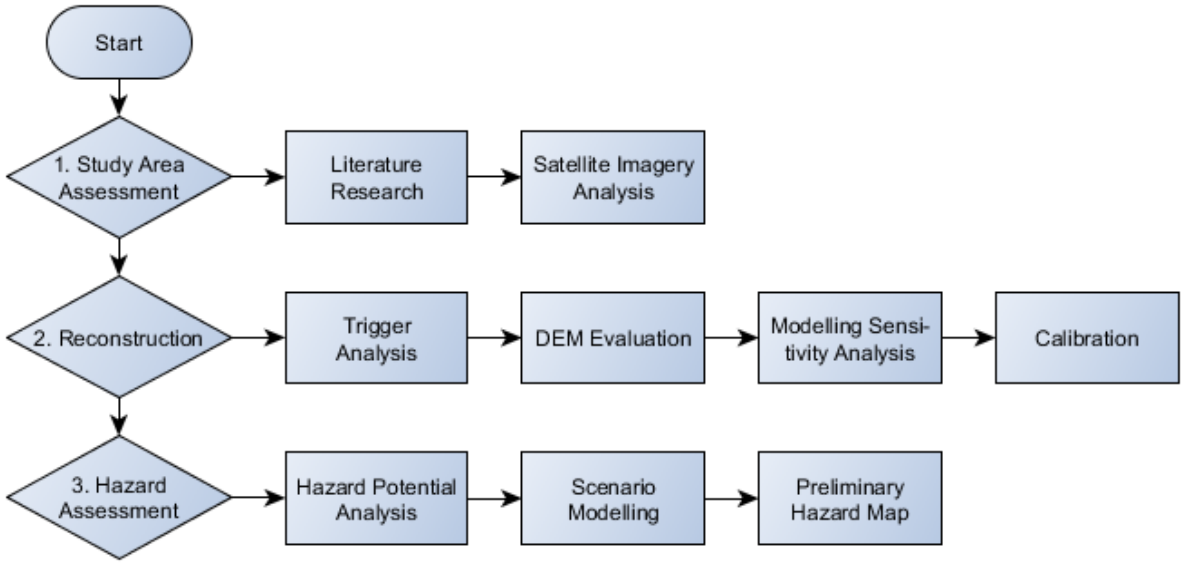

Figure 5.1: Work flow diagram.

In part 1, the background of the topic and conditions of the study region are assessed (goal 1, see Chapters 2 and 3). The reconstruction part aims to find out what happened in 1998 (goals 2 and 3, see Chapters 6 and 7). The third part corresponds to goals 4 and 5 and assesses what can potentially happen in the future (Chapter 8). This procedure is loosely based on similar works by Scheuner (2007) and Stricker (2010). This thesis builds on various field work conducted within the CCA DRR project.

5.1 Study Region Assessment

This section corresponds to goal 1 of this thesis. An overview of the topic (Chapter 2 “Background”) and the study region in terms of environmental and social conditions (Chapter 3 “Study Region”) was achieved, based on a thorough literature study as well as visual analysis of satellite imagery of the study region. As no detailed information concerning soil, hydrology and vegetation is available (see Chapter 4), these aspects were assessed qualitatively. Geology was evaluated by Carlotto et al. (1999). Climate analysis was described in more detail in Section 3.3.1. Slope was assessed with ASTER GDEM2.
Satellite imagery served as a basis for delineating the starting zones of the 1998 events (Section 3.4) as well as potential starting zones (Section 3.5). Deposition areas are qualitatively estimated based on pictures, videos, Google Earth and Landsat satellite data. Their delineation is conservative and aimed to correspond to the area where the debris flow certainly formed deposits. Geomorphology, vegetation and glaciology of the study region were assessed visually with Google Earth.

5.2 Reconstruction

This section corresponds to goals 2 and 3 of this thesis aimed to assess what happened in 1998, namely to find triggers of the 1998 debris flows and reconstruct them with RAMMS, based on the overview obtained in Chapters 2 and 3 (Chapter 6). DEMs were evaluated (Section 7.1) and a model sensitivity analysis was carried out for model input parameters (Section 7.2). Last, the 1998 debris flow events of

Ahobamba and Sacsara were calibrated (Section 7.3). Modeling was done with RAMMS developed by the Swiss Federal Institute for Snow and Avalanche Research (SLF) in Davos (see Section 5.2.2) and ArcGIS (version 10) from ESRI. Systematic modeling based on remote sensing is considered a useful first-order approach to assess glacial and periglacial hazards and their interactions (Huggel et al., 2004).

5.2.1 Trigger Analysis

This section shows the procedure for examining precipitation, temperature and earthquakes. Surface runoff and groundwater upwelling would be other interesting factors. However, as runoff and groundwater data is not available for Ahobamba or Sacsara, runoff and groundwater cannot be used for trigger analysis due to high precipitation variability in mountainous terrain and different precipitation regimes. Data from different climate reanalysis projects (GPCP, CMAP, MERRA, NCEP-NCAR, ERA-40, JRA-25 and JRA-55) was looked at, but found not to be useful for this thesis. For mountainous terrain, a resolution of 60 x 60 km or lower is too limited (Huggel et al., 2008); and their correlation in South America is low (Bosilovich et al., 2008). For more information, see also Rienecker et al. (2011) and Adler et al. (2003). A precipitation map from CARE Peru first was considered but discarded due to unknown temporal resolution. A separate landslide analysis was not done, as triggers for landslides and debris flows are very similar (see Section 2.2.3.4). The question why the debris flows were triggered at the actual location and not somewhere else was not addressed within this thesis; only why they were triggered. Human activity is low upstream the tributary rivers of Urubamba and can be excluded from being a triggering factor for both debris flows.

5.2.1.1 Precipitation

Pre-event precipitation was analyzed based on SENAMHI and TMPA data, as is an important factor when considering debris flow triggers (Zimmermann et al. 1997). Data availability from SENAMHI stations and TMPA defined the temporal extent and temporal resolution of precipitation comparison:

- January 1st to February 28th 1998 for SENAMHI stations containing data of 1998;
- January 1st to 7th 2012 for SENAMHI stations without data of 1998;
- January and February 1998 and the year 1999 for TMPA data.
- The year 2012 for comparison of SENAMHI and TMPA data.

Before the trigger analysis, SENAMHI stations were quality checked. SENAMHI station sensitivity was tested for stations closest to the Sacsara and Ahobamba starting zones (30 km distance from starting zone or less; daily precipitation; January 2012) as well as stations with data from 1998 (daily precipitation; January and February 1998). After the quality check, pre-event precipitation (1-day, 3-day, 1-/2-/3- and 4-week) for stations with data from 1998 (daily precipitation; January and February 1998) was analyzed. A weighted average of 1998 stations based on their difference to Machu Picchu was discarded, as uncertainties for Machu Picchu are too large to reflect starting zone conditions.

TMPA precipitation data was used as an additional source. First, TMPA data was quality-checked for all six TRMM tiles for January 7th to 13th 1998 (daily precipitation) and the year 1999 (monthly precipitation; better data availability in 1999). Then, TMPA and SENAMHI data were compared. Last, TMPA data was added to pre-event precipitation analysis. The Precipitation Radar (PR) instrument from the TRMM was discarded due to poor availability of data in the necessary time interval. No interpolation of SENAMHI and TMPA data was made, as TMPA is already a merged product and has low accuracy for short-term precipitation.

A rainfall threshold for Peru was considered not feasible due to low data availability (concerning precipitation data and historic events) and temporal resolution (See Stricker, 2010 or Guzzetti et al., 2007a). Rainfall thresholds are only statistical measures to average uncertainty over larger periods of time and space. They can not be used to predict single events like Ahobamba and Sacsara (M. Rohrer, pers. communication). The actual triggering of a debris flow depends on many interacting factors, for example lithological, morphological, vegetation and soil conditions or different climatic regimes (Guzzetti et al., 2007a). Also precipitation pattern matters - a daily precipitation amount of 10 mm can be a trigger for a debris flow when it falls within 10 minutes, but probably not when it falls within 24 hours continuously (M. Rohrer, pers. communication).

5.2.1.2 Temperature

Temperature was analyzed with SENAMHI data, which is the only available data source, except climate reanalysis (see above). Only stations with data of 1998 were used. Monthly temperature was analyzed for December 1997 as well as for January and February 1998. Maximum temperature was analyzed as snowmelt is suspected to be a trigger for the 1998 events. Minimum temperature could have played a role at higher elevations, causing erosion from freeze-thaw cycles. The degree-day factor concept is not applicable for this thesis, as snow cover, amount and distribution as well as surface properties are unknown (M. Rohrer, pers. communication).

5.2.1.3 Earthquakes

Earthquake activity was investigated with the earthquake archive of the USGS (2010). A further method to gain insights to what happened during the 1998 events is to look at seismic data recordings during the event, as was done in Schneider et al. (2010). However, this analysis is very complex and would exceed the extent of this thesis.

5.2.2 RAMMS

RAMMS is a dynamic flow model developed in 2005 at the SLF in Davos, Switzerland. It is designed to replace one-dimensional numerical models such as AVAL-1D and to overcome their limitations (Christen et al., 2008). RAMMS was first created for avalanches and later complemented with a module for debris flows, which was also used for landslides. An additional module for rockfalls is currently under development (Christen et al., 2012). All modules are linked by a common user interface aimed to facilitate visualization of results and planning of mitigation measures for the corresponding processes (Christen et al., 2012). Simulations were made with snow avalanches (Christen et al., 2008), debris flows (Scheuner, 2007) and rock- and ice avalanches (Schneider et al., 2010). The RAMMS debris flow module can be used to calculate impact pressures and flow heights. Although RAMMS was developed for avalanches, several authors state that debris flows have similar flow properties (Iverson & Denslinger, 2001).

5.2.2.1 Mathematical Model

RAMMS debris flow uses an advanced second order numerical scheme to solve depth-averaged equations of granular flow motion in two dimensions, using a finite volume scheme (Christen et al., 2008):

$$\delta_t H + \delta_x (HU_x) + \delta_y (HU_y) = 0 \tag{5.1}$$

$$\delta_t (HU_y) + \delta_x (HU_x{}^2 + g_z \frac{H^2}{2}) + \delta_y (HU_x U_y) = S_{gx} - S_{fx} \tag{5.2}$$

$$\delta_t (HU_y) + \delta_y (HU_y{}^2 + g_z \frac{H^2}{2}) + \delta_x (HU_x U_y) = S_{gy} - S_{fy} \tag{5.3}$$

Where *H* is the flow height, *U* the mean velocity, g_z the gravitational acceleration, S_g the gravitational acceleration of the flowing mass and S_f the frictional resistance (see below). *X* and *y* indicate the quantities in the x and y directions. The second order scheme improves unrealistic lateral spreading on open slopes (Christen et al., 2008). In the avalanche model, the mass balance (Eq. 5.1) equals the snow entrainment rate (when above 0) or snow deposition rate (when below 0). However as in the debris flow module entrainment is not considered (Christen et al., 2012), it is set to zero. For more information about model equations, see Christen et al. (2008, 2010a, 2012). RAMMS uses a single-phase Voellmy fluid friction relation (Christen et al., 2008):

Frictional resistance $S_f = \mu\rho gh\cos\alpha + \frac{\rho g u^2}{\xi}$ (5.4)

Where μ (mu) is the Coulomb-friction coefficient (proportional to the normal stress at the flow bottom (Voellmy, 1955)), ρ is density, *g* is the gravitational acceleration, *h* is flow height perpendicular to the surface, α is slope, ξ (xi) is the velocity-squared dependent turbulent viscous friction and *u* is velocity. This division allows for modeling of flow behavior when the flow is going fast in the acceleration zone (ξ dominates) or when it is close to stopping in the deposition zone (μ dominates) (Christen et al., 2010a). The Voellmy model approximates velocity and deposit distribution very well. A main advantage of the Voellmy model is its simplicity, requiring only two empirical parameters (Ayotte & Hungr, 2000).

Turbulent friction ξ quantifies the velocity-dependent loss of kinetic energy created by inter-particle friction and thus highly influences mass velocity (Scheuner, 2007). It depends on the surface geometry and thus is not constant for the whole flow (Salm et al., 1990). Dry friction μ depends on material properties like density and water content as well as the pressure perpendicular to the surface. The higher the water content, the lower is μ. Also high pressure due to flow height can lower μ (Scheuner, 2007).

5.2.2.2 Input Data

Three input quantities have to be specified (Christen et al., 2008): (1) DEM; (2) Release zone area or hydrograph and (3); Friction parameters. The choice of the DEM has a large influence on simulation results (Christen et al., 2010b; Schneider et al., 2008). DEMs with low spatial resolution (25 m and more) can miss important terrain features, DEMs with high spatial resolution (5 m and less) lead to long computation times and sometimes to wrong results (Christen et al., 2008). Higher resolution increases DEM roughness, which leads to a smaller runout distance and less lateral spreading (Andres, 2010). For very large processes like in Peru, a DEM resolution of 30 m might still be suitable (Christen et al., 2010b). DEMs are evaluated in Section 7.1.

The release zone can either be defined with a block release polygon shapefile and a corresponding height, or a so-called input hydrograph with volume, maximum discharge and the time of maximum discharge specified (Christen et al., 2012). For large channelized debris flows, a hydrograph is the better choice, as they provide more realistic input conditions. Discharge can be estimated using empirical relations. Also, simulation time can be strongly reduced by placing a hydrograph just above the area of interest (WSL, 2013). For a comparison, see Section 7.2.7.

Choosing correct model parameters probably is the most difficult and uncertain part of modeling. More parameters lead to more uncertainty; less parameters are a stronger simplification (Christen et al., 2012). For the sensitivity of modeling input parameters, see Section 7.2.

5.2.2.3 Output Data

Output data is a visualization of all numerical calculations (Christen et al., 2008), including flow and deposition height, velocity, pressure, momentum and maximum values. Also, 2D and 3D maps and animations, profile and single point graphs of a state variable, XY-plots (e.g. the time evolution of flow height) can be created. Extensive logfiles report various processes (Christen et al., 2012). Flowing mass reports with the total amount of material moving at any time are defined, which is useful for determining the stopping of the flow. The output is written in user-specified dump intervals (Christen et al., 2008).

RAMMS results are displayed in grid cells. However the resolution of the model results are generated by RAMMS and are not necessarily the same as the DEM used (Christen et al., 2010a). Finally, results can also be exported into a GIS (Geographic Information System) or Google Earth. Also import from GIS or Google Earth is possible. (Christen et al., 2012). Georeferenced maps and photographs can be superimposed for better visualization (Christen et al., 2008).

5.2.3 Modeling Sensitivity Analysis

Due to lack of information on rheological parameters for such large events, an alternative approach was chosen similar to Pirulli & Sorbino (2008): Rheological parameters were found in literature and combined with the results of the study region analysis in Chapter 3. Rheological parameters were evaluated in a strongly qualitative way, similar to Schneider et al. (2014). Results can be seen in Section 7.2. As model parameters have considerable uncertainty (Ghilardi et al., 2003), they are tested for sensitivity and calibrated with the 1998 events.

The area of interest is based on the deposition Shapefiles estimated with Google Earth and is a square Shapefile containing the deposition area. The following three methods were applied:

1) Flow height and velocity profiles: A profile line was drawn according to the path of the maximum flow height from all simulations (red line in Fig. 5.2, page 41), starting at the highest point of the estimated depositions of the 1998 events and ending at the lowest. Then, it was converted to a 3D feature showing flow height or flow velocity at a certain location along the deposition. All flow height and velocity profiles in this thesis are based on this profile line.
2) Simulation Performance Index (SPI): This index is the ratio of all cells in the investigated area correctly modeled (cells affected in both simulation and deposit) and the total amount of cells in the observed deposit file. This is only one of many possibilities to quantify the overlap of simulations and depositions. Cells correctly modeled to not be affected were discarded, as the correct simulation of cells affected by the debris flow is more important than the correct simulation of cells not affected. The SPI does not consider simulation errors: False negative (a cell is simulated not to be affected but was) is more dangerous than false positive (a cell is simulated to be affected but was not), as it can give a false sense of security.
3) 2D Illustration: The outline of the simulation extents is plotted. First, all the simulation extents are overlaid; second, the two extreme values are shown individually. A pixel count was not made, as most simulations exceed the area of interest.

Table 5.1 (page 41) shows parameters influencing simulation results in RAMMS, their priority for sensitivity analysis and the applied method. 1 has highest priority, 5 lowest. X means that priority is unimportant.

Table 5.1: Parameters tested for sensitivity

Sensitivity Analysis & Calibration		
Parameter	**Priority**	**Method**
Dry-Coulomb friction coefficient μ	1	Flow height profile, SPI
Turbulent friction coefficient ξ	2	Flow velocity profile
Input Volume	3	2D Illustration
Input Velocity	4	Qualitative
Input Discharge	5	Flow height profile
Input t1 (and t2)	5	Qualitative
Release zone type and position	x	Qualitative
Stop/ End time	x	Qualitative
Lamda	x	Qualitative
H Cutoff	x	Qualitative
Numerical scheme	x	Qualitative

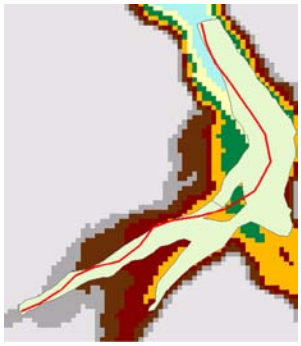

Figure 5.2: Path of maximum flow height (red line) and depositions of the Sacsara event (light green).

μ has a very large influence on simulation results and thus has to be evaluated first, before the other friction parameter ξ. Next, input volume, velocity, discharge and t1 are evaluated. Other aspects tested are the release zone type and position, the stop condition (or end time criterion), Lamda, h cutoff and the numerical scheme. Friction parameters were simulated with a hydrograph placed at the lowest point of the starting zone of Sacsara. Volume, velocity, discharge and t1 were simulated from a hydrograph 8 km upstream of Santa Teresa in Sacsara valley to reduce computational time. All parameters were tested with a 30 m DEM resampled (with bilinear interpolation) from ASTER GDEM2 with sinks filled in GIS. Discharge is the only parameter where the nearest neighbor-interpolated 30 m DEM from ASTER GDEM2 is used, without the sinks being filled.

Less sensitive parameters were evaluated qualitatively. Cross-relations of parameters were not tested for sensitivity within this thesis (e.g. if ξ varies differently with differing μ). Calculation domains in RAMMS were chosen iteratively in order to reduce computation time. Sensitivity analysis was only carried out for Sacsara to reduce computational time. For Ahobamba, an iterative approach was taken to find the best fit simulations (see Section 5.2.4). Modeling sensitivity analysis results are presented in Section 7.2.

5.2.4 Calibration

For scenario simulation in RAMMS, calibration with historical events is recommended, as model parameters are often poorly constrained and can have significant uncertainty (Ghilardi et al., 2003; Hegg & Rhyner, 2007; Christen et al., 2010b; Andres, 2010). Calibration is based on trigger analysis, sensitivity analysis and study region preconditions (basic and variable disposition). The main goal of modeling the 1998 events is to find realistic values for input parameters; in order to use similar values for scenario simulations (see Section 5.3). Calculation domains in RAMMS were chosen iteratively in order to reduce computation time. Friction parameters were estimated based on sensitivity analysis and depending on overall slope, water content and grain size in a qualitative way, comparable to Christen et al. (2010b).

Calibration was made iteratively and was based on a trial-and-error approach (see also Ayotte & Hungr, 2000). Criteria for the calibration of input parameters were:

1) Stop Criterion: Simulations were stopped when less than 10% than the maximum momentum moved or when they were flowing for over 30,000 seconds (see also discussion in Chapter 9).

2) Deposits: RAMMS modeling results were visually compared to estimated depositions of the events. This part is based on the SPI and 2D illustrations from the sensitivity analysis in Section 7.2. Depositions for the Sacsara and Ahobamba events are derived from Google Earth, pictures and videos of the events and Landsat TM5 (Section 3.5).
3) Flow height and velocity: Finding realistic values is based on flow height and velocity profiles from the sensitivity analysis of Section 7.2 as well as field reports.

Calibration of input parameter aims to find a "best-fit" simulation for both the Ahobamba and the Sacsara debris flows. However, due to limited data availability concerning input parameters; deposition areas; flow heights and velocities, large uncertainties persist. A quantification of uncertainty or reliability is not possible. The best known characteristics are deposition area for the Sacsara event and deposition height in Urubamba valley for Ahobamba. Two calibration procedures were considered:

1) Input calibration: Input parameters (based on all data and total volume) were calibrated.
2) Runout calibration: Runout was iteratively tested: volume was reduced until simulated and estimated runout corresponded. Then, the number of surges was calculated for the whole event based on the volume with the best runout and the estimated total volume. Volume was left as large as possible (considering above criteria), in order to account for the worst-case. The first surges of the flows could and did exceed the estimated deposition areas (C. Portocarrero, pers. communication).

The second approach was chosen, as based on input parameter calibration, runout proved much too large and deposition height too low, as in reality the total volume would not flow in one surge but in many smaller ones, resulting in the same volume being distributed in a smaller area. For more information on the calibration process, see Sections 7.3 and 9.3. The Ahobamba event produced a dam break in the main valley around four months later, going down as hyperconcentrated flow or a debris flood. This dam break was simulated separately. Calibration results were visualized using 2D-illustration.

5.3 Hazard Assessment

This chapter corresponds to goals 4 and 5 of this thesis, which aim to find out what hazards could affect Santa Teresa in the future. A hazard is defined as the magnitude of an event multiplied by its probability of occurrence (Fell, 1994). Assuming a constant physical system, magnitude and frequency are inversely proportional (Huggel, 2004). Debris flow magnitude can be given in volume, peak discharge or area covered (Jakob, 2005a). Raetzo et al. (2002) developed guidelines for debris flow hazard assessment in Switzerland and identified three steps for hazard assessment (complemented with Wrachien, 2006):

1) Hazard identification, based on field work, maps and event registers (see Section 3.5).
2) Hazard assessment and scenario building, including the assessment of intensity, probability, residual danger and the creation of hazard maps (see Chapter 8). Hazard assessment is based on sensitivity analysis (Section 7.2) and calibration (Section 7.3).
3) Risk management and land-use planning (see outlook in Chapter 10), including mitigation solutions (active and passive (Lorenzini & Mazza, 2004)) and a monitoring system.

The hazard assessment done in this thesis cannot be treated as a full-scale hazard assessment, as data is too limited as yet (see Chapter 4). This thesis should merely give a first order assessment of potential hazards in the study region.

5.3.1 Hazard Potential Analysis

Based on Section 3.5, 7 starting zones were chosen; 3 in Ahobamba, 2 in Sacsara and 2 in Salcantay. These zones are aimed to cover the area of the subcatchment and reflect the range of possible processes and volumes, with volumes varying from 100,000 m^3 to 10 mill. m^3. In each subcatchment, the most probable starting zones were manually selected. ASTER GDEM2 was used to analyze slopes; field reports, high-resolution images as well as expert knowledge (C. Giráldez, C. Huggel and H. Frey) were used to evaluate starting zone locations and potential volumes. The starting zones of the 1998 events were neglected, as the calibration simulations can be taken into account as the worst-case scenario from these zones. No automatic starting zone classification (as done by Huggel et al., 2004) was done, as no high-resolution imagery of the study region is freely available.

5.3.2 Scenario Modeling

Scenarios are plausible outcomes of the future, however small the probability of their occurrence (Wright & Cairns, 2011). By neglecting the probability of events, critical uncertainties can be taken into account, making scenarios a useful tool for decision-making (Wright & Cairns, 2011) and hazard assessment. Scenarios should include extreme outcomes, to set the broadness of possible hazards (Wright & Cairns, 2011). Scenarios provided in this thesis evaluate a broad variety of potential hazards for Santa Teresa area. Scenarios of possible future hazards were modeled with RAMMS based on basic and variable disposition as well as the hazard potential analysis provided in Section 3.5. Scenarios were simulated using ASTER GDEM2 from the potential starting zones defined in Section 3.5. Scenarios were evaluated in two ways:

1) How plausible/realistic are simulation outputs? Criteria for analysis are the same as for the calibration: Stop criterion, runout as well as flow height and velocity. Scenario simulation outputs were compared to the results of the calibration with 1998 events.
2) Hazard assessment: How are communities in the study region and Santa Teresa affected?

The usual procedure for scenario planning is to look at a magnitude-frequency curve of events in the study region (Hungr, 2005). However, no historical record large enough exists for debris flows. This is why for every potential starting zone in Section 3.5, a “small”, “medium” and a “large” scenario was designed to roughly correspond to return periods of 30, 100 and 300 years as proposed by Raetzo et al. (2002). A qualitative probability is possible as it is no necessary input for scenario modeling (Wright & Cairns, 2011). Triggers were not explicitly taken into account. Climate change is taken into account only qualitatively. As the database for past climate is limited, it does not make sense to try to quantify climate change impacts on debris flow magnitude and frequency in Santa Teresa.

Scenario modeling was made with the bilinear interpolated ASTER GDEM2 with 30 m resolution and filled sinks. All input parameters are based on sensitivity analysis – only the following depend on the starting zone and were selected as follows:

1) μ was chosen according to the overall slope from the highest point in the starting zone to the confluence with Urubamba. μ is decreased when the potential debris flow is suspected to be muddy based on the material in the starting zone (-10%). This choice showed good results in the event calibration. For GLOFs, μ was reduced from the overall slope by -20%.
2) The largest single surge volume and not the total event volume was considered (see Chapter 7). Potential volumes are based on hazard potential analysis, basic and variable disposition, trigger analysis (see Section 9.2) and present lakes. When lakes are present, volumes correspond to partial and full lake outbreaks with negligible sediment incorporation and a full outbreak with sediment incorporation 3 times larger than water input. GLOFs are assumed to go down in one single surge. Without a lake, the largest single surge volume from Ahobamba and

Sacsara (1 mill. m^3) is taken as a basis. “Small” scenarios use this volume divided by 2, “medium” scenarios use the same volume and “large” scenarios used this volume multiplied by 3, in order to account for the worst case. Differences between small, medium and large scenarios are a factor of 2 - 3 (see also Schneider et al., 2014). The largest single surge volume was left as large as possible, in order to account for the worst-case.

3) Discharge: The discharge formula of Costa & Schuster (1988) was taken for all scenario simulations (see Section 9.3).

Scenarios were visualized using 2D-illustration, with flow heights below 0.1 m discarded. No intensity categorization (as made in Raetzo et al., 2002) was implemented, as such large debris flows were considered to have high intensity in their path. Flow height profiles were made for each valley.

5.3.3 Preliminary Hazard Map

Two types of hazard maps can be distinguished (Hürlimann et al., 2008): (1) preliminary hazard maps, based on empirical relationships or flow direction algorithms; and (2) final hazard maps, generated with dynamic flow modeling (see Section 2.3). Hazard maps are a passive mitigation solution and lay the foundations for risk management, land-use planning and various active measures, helping to avoid damage caused by mass movements Hazard maps are widely used in geomorphology and should be easy to interpret for users (Fleisher, 1984; Lorenzini & Mazza, 2004). They usually contain three degrees of danger (red, blue and yellow) and the assessment of intensity, probability and residual danger (Raetzo et al., 2002). Intensity is defined as potential impact energy of the flow onto obstacles (Hürlimann et al., 2008) but is typically expressed as flow or deposit height (C. Huggel, pers. communication). It is qualitatively given in three levels: high, medium and low, with decreasing danger of injury and building damage. Schneider et al. (2014) adapted this concept for debris flows, where no low intensity exists. Flow heights and velocities below 1 m and 1 m/s are medium intensity, anything above high intensity.

The preliminary hazard map done in Section 8.4 is based on all scenario simulations (Section 8.1 - 8.3) and was made in order to show how Santa Teresa could be affected by future debris flows. It is no final hazard map and does not contain any intensity classification as described above, as calibration of rheological parameters proved difficult due to limited information on deposits and flow behavior (see also discussion in Section 9.4). Probability classification for the preliminary hazard map is shown in Section 8.4. No hazard map was made for communities in the study regions.

6 Trigger Analysis

This chapter evaluates possible trigger mechanisms and processes as defined in goal 2. Discussion of this chapter is provided in Section 9.2. The most common triggers based on the list in Section 2.2.3.3 are considered: moisture addition through precipitation (Section 6.1); temperature and snowmelt (Section 6.2); and earthquakes (Section 6.3). Volcanic eruptions, pyroclastic flows or floods incorporating sediments were excluded as there is no field evidence. GLOFs and other dam failures are not considered in this chapter, as this process could be excluded from triggering the 1998 debris flows (Huggel et al., 2003b). Shallow and deep-seated slope instabilities are not separately discussed, as they have the same triggering events as debris flows.

6.1 Precipitation

6.1.1 Plausibility of SENAMHI Station Data

SENAMHI data availability is limited due to low spatial coverage (in terms of amount, distance or location, see Chapter 4) and not quality-checked. Here, quality of stations with a distance of less than 30 km from a starting zone was analyzed for daily precipitation for January 2012 (see Fig. 6.1 and 6.2 below). Days without data are not shown in the figures.

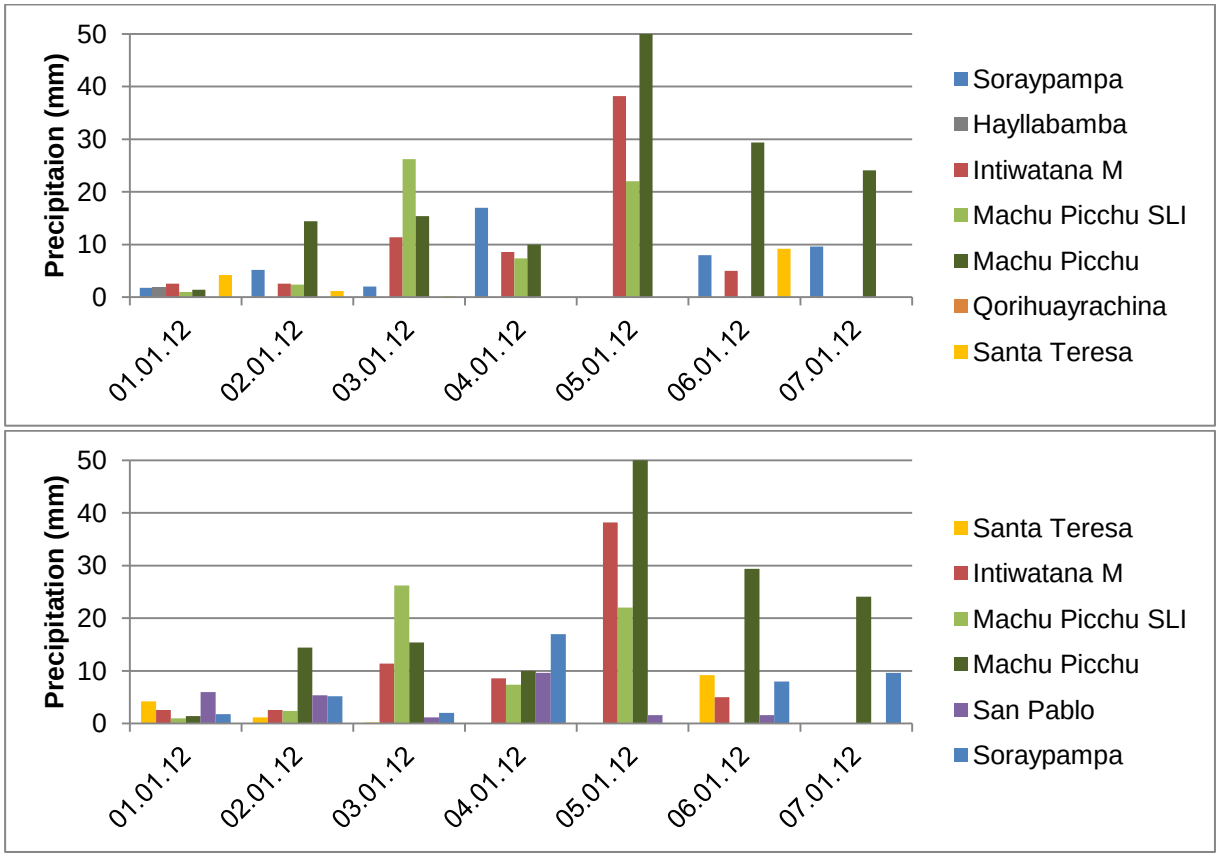

Figure 6.1 and 6.2: Daily precipitation near Ahobamba (top) and Sacsara (bottom) starting zone from January 1st to 7th 2012 from SENAMHI stations. Stations are listed according to their distance to the starting zones.

In January 2012, data was missing from variable days, 6 (Santa Teresa); 5 (Intiwatana M), 19 (Machu Picchu SLI), 0 (Machu Picchu), 7 (San Pablo), 8 (Soraypampa), 13 (Hayllabamba) and 3 (Qorihuayrachina). Intiwatana has conspicuously low precipitation (probably “no data” was reported as “0 precipitation”) and Machu Picchu SLI and Qorihuayrachina have too little data. Soraypampa at the southern side of the Nevado Salcantay shows slightly different precipitation patterns (see 13. -

17.1.2012) and was discarded for Sacsara; but not for Ahobamba due to its vicinity (9 km to starting zone). Stations taken into account for further analysis are San Pablo, Santa Teresa and Machu Picchu for Sacsara and Hayllabamba, Santa Teresa, Machu Picchu and Soraypampa for Ahobamba. Spatial plausibility of SENAMHI data is limited – as seen in Fig. 6.1 and 6.2 above, daily precipitation peaks can vary strongly, even for stations close to each other (Santa Teresa and Machu Picchu) or at the same location (Machu Picchu and Machu Picchu SLI). Differences between Machu Picchu stations can be explained by different acquisition techniques (see Section 4.3.1). The manual Machu Picchu station shows large outliers, maybe due to measurement errors. Differences in daily precipitation between stations with data from 1998 are even larger, due to their larger distance to each other.

Relative humidity was compared to precipitation in Machu Picchu and Quillabamba in Fig. 6.3, in order to test stations for internal plausibility. October 1st to 7th 2012 is chosen due to good data availability (only 3 values for relative humidity in total missing).

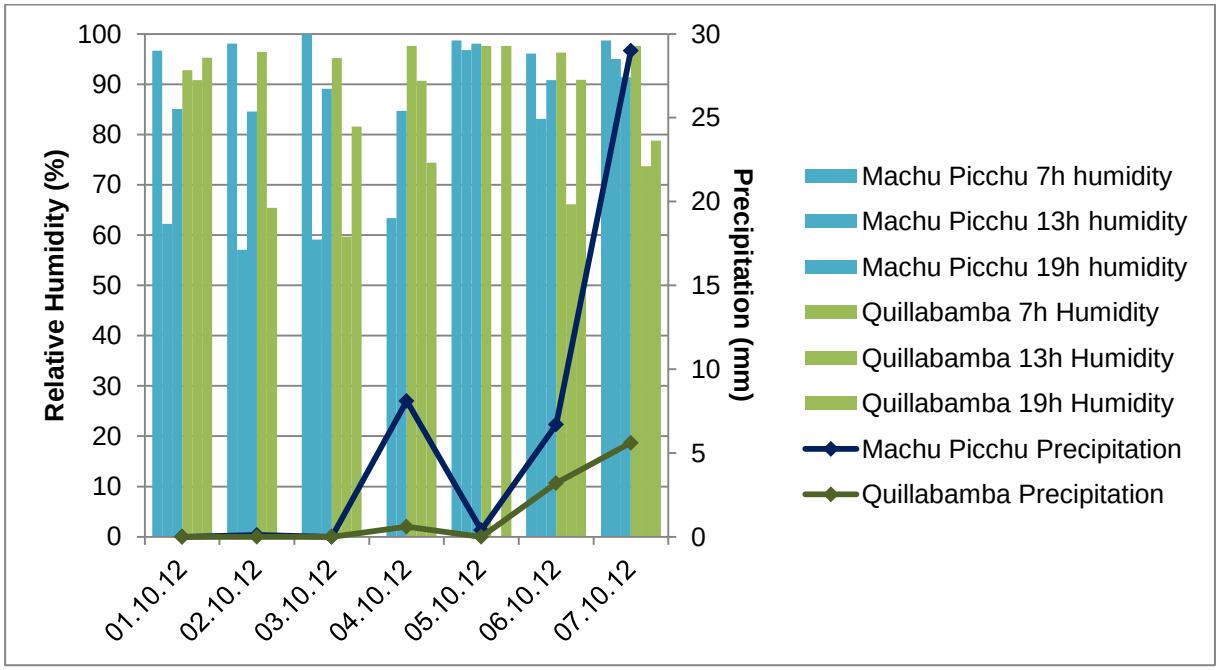

Figure 6.3: Relative humidity (7, 13 and 19 hours) and precipitation for Machu Picchu and Quillabamba.

Fig. 6.3 shows that internal plausibility of stations is limited, as in both stations one day without rain shows high humidity and in Machu Picchu, one day with rain has low humidity.

Comparison of monthly precipitation between SENAMHI stations containing data from 1998 and Machu Picchu showed that Quillabamba has the least differences (Table 6.1). Monthly precipitation shows good correlation for Quillabamba, but lower correlation for other stations with data from 1998. Comparison was made with Machu Picchu as it showed reasonable results for both starting zones and had high data availability for the years analyzed. Quillabamba is the only SENAMHI station with data for 1998 not located in the drier Altiplano.

Table 6.1: Sum of squared differences in precipitation compared to Machu Picchu for 1999 - 2003. Months without data are excluded.

	Abancay	Anta Ancachuro	Curahuasi	Quillabamba	Urubamba
Total Error	2,145,075	1,857,333	2,600,848	1,394,287	3,284,786

6.1.2 Plausibility of TMPA Data

TRMM TMPA data was analyzed additionally to SENAMHI station precipitation data. TMPA quality was tested for daily precipitation from January 7th to 13th 1998 (Fig. 6.4) and monthly precipitation in the year 1999 (Fig. 6.5), as not all data for 1998 was available (see Chapter 4).

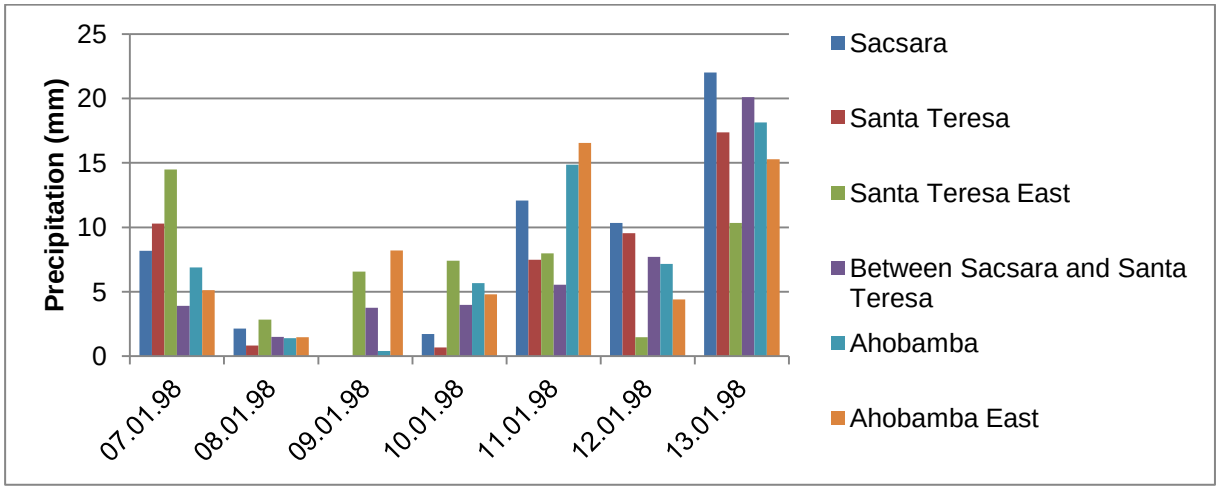

Figure 6.4: TMPA daily precipitation from January 7th to 13th 1998 (one week prior to the Sacsara event).

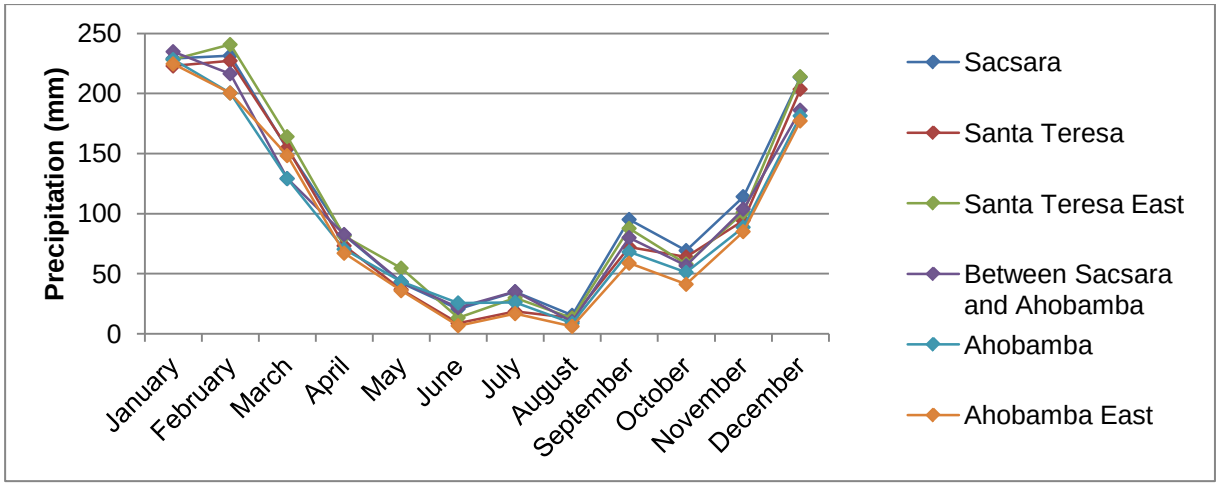

Figure 6.5: TMPA monthly precipitation in 1999.

TMPA data shows good spatial correlation: precipitation events are consistent, although their magnitude varies for different grid cells. Correlation for monthly precipitation is very good. The correlation for weekly aggregated TMPA precipitation data is intermediate between daily and monthly (graph not shown), with a correlation coefficient of around 0.8 (Scheel et al., 2011). Weeks with higher and lower precipitation are consistent in all starting zones, but precipitation amounts vary. TMPA is spatially plausible; cells have values similar to each other.

6.1.3 Comparison of TMPA and SENAMHI

Here, daily precipitation was compared for all TRMM tiles and all SENAMHI stations averaged for January 2012 (Fig. 6.6). Stations with data from 1998 were not compared, as they are outside the TRMM tiles evaluated.

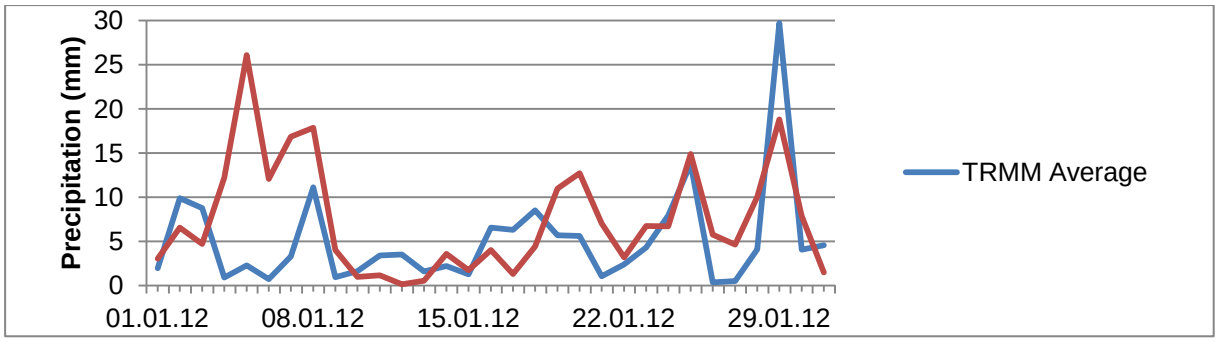

Figure 6.6: Comparison of daily precipitation for January 2012.

Close SENAMHI stations (less than 30 km distance; in brackets are days without data) considered are Soraypampa (8), Hayllabamba (13), Machu Picchu (0), San Pablo (4) and Santa Teresa (6). Points without data are not taken into account for the SENAMHI average. This comparison was not made on a weekly or monthly basis, due to low data availability of SENAMHI stations. It can be expected however that correlation would improve, as TMPA shows good correlation on a monthly basis (see above or Scheel et al. (2011)).

6.1.4 Pre-Event Precipitation

In this section, pre-event precipitation (1-day, 3-day, 1-/2-/3- and 4-week) is analyzed for all 5 SENAMHI stations with data in 1998 (Abancay, Anta Ancachuro, Curahuasi, Quillabamba and Urubamba) and all used TRMM tiles (between W72P375xS13P125 and W72P875xS13P375) (see Chapter 4). Daily precipitation in January and February 1998 is shown in Fig. 6.7 and 6.8 for SENAMHI stations and Fig. 6.9 and 6.10 (page 49) for TMPA. Data for all days was available.

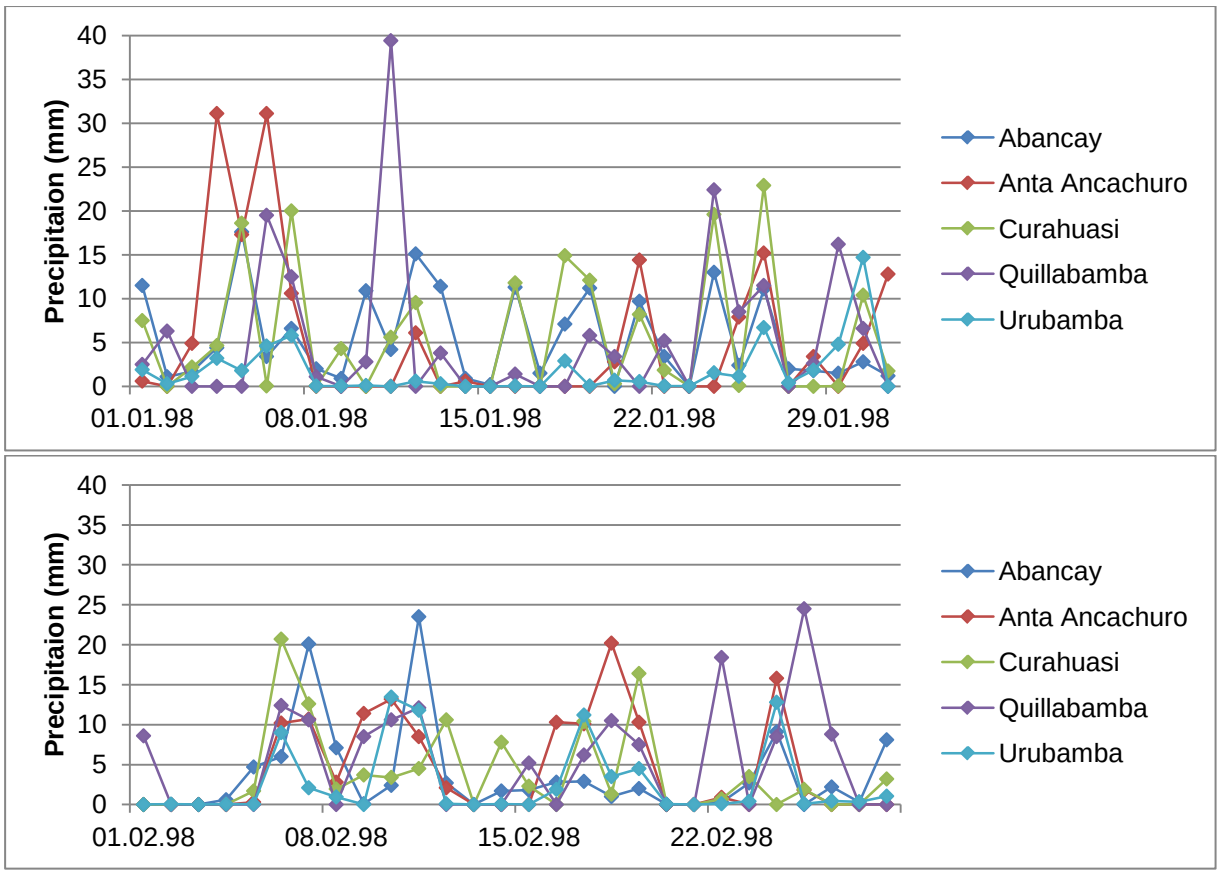

Figure 6.7 and 6.8: Daily precipitation in January (top) and February (bottom) 1998 from SENAMHI stations.

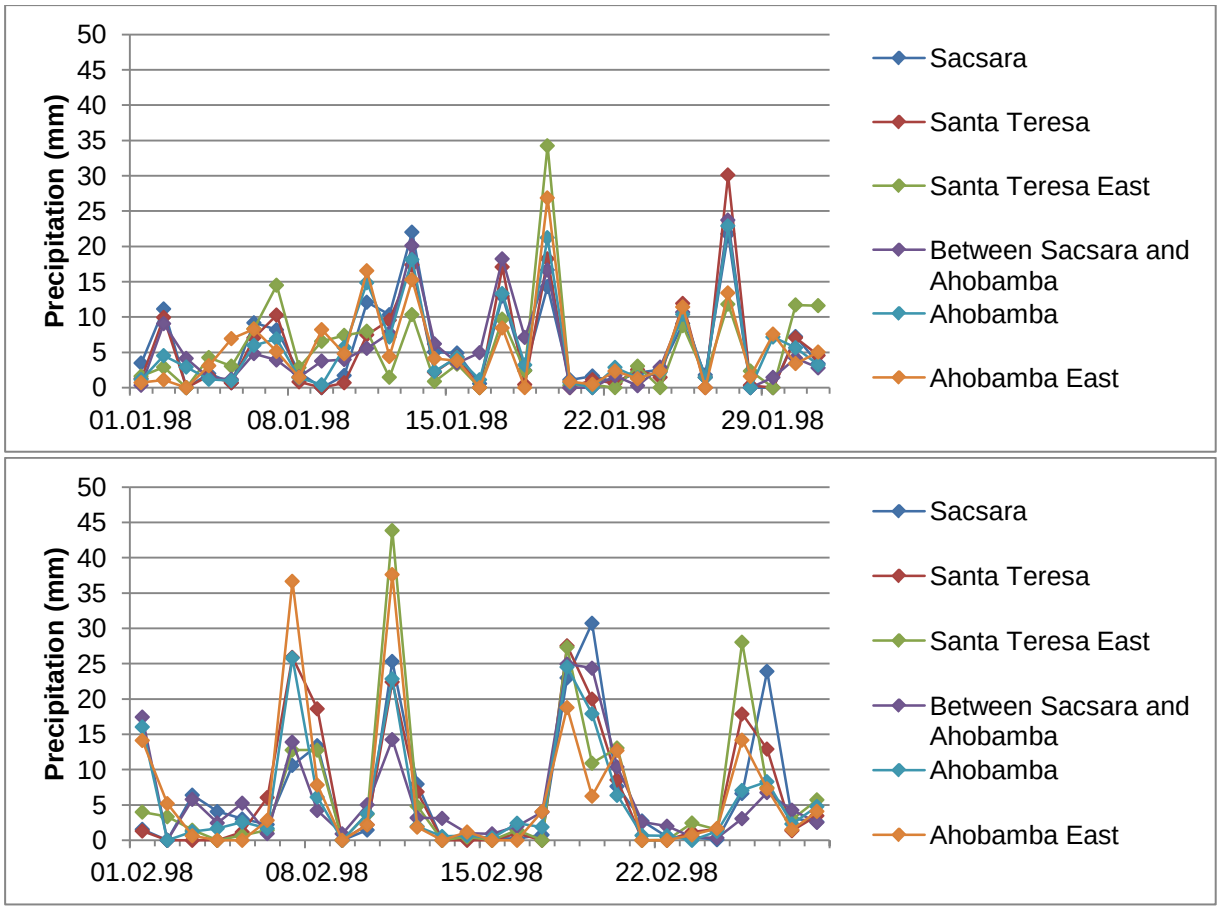

Figure 6.9 and 6.10: Daily precipitation in January (top) and February (bottom) 1998 from TMPA data.

In both January and February, several days showed high precipitation amounts. Peaks are higher in SENAMHI stations for January and for TMPA data in February. Abancay and Curahuasi show similar patterns (except for 8. - 15.2.), as do Urubamba and Anta Ancachuro (except for 4. - 6. and 31st of January and February 18th), probably due to their relative closeness. Quillabamba has a wetter climate, probably due to its location closer to the amazon (Peaks of January 3rd to 5th; January 10th; February 22nd and 25th, see also Section 3.3.1). Although spatial plausibility is limited, closer stations also show closer results. Differences in results seem plausible when considering the large distance between stations. TMPA data shows less variation between tiles.

Subdaily precipitation from TMPA data is shown for Ahobamba (Fig. 6.11, page 50) from February 24th 1 am to February 27th 4 pm Peru time and for Sacsara (Fig. 6.12, page 50) from January 10th 1 am to January 13th 4 pm Peru time; these are three days prior to the event including the event day (Ahobamba reached Urubamba valley on the 27th at 3pm; Sacsara was reported to start on the 13th at 3 pm). Note that SENAMHI data is reported in PET time and TMPA in UTC. This means that a day of SENAMHI data roughly corresponds to the sum of subdaily TMPA data from 6 am to 3 am UTC (1 am to 10 pm PET).

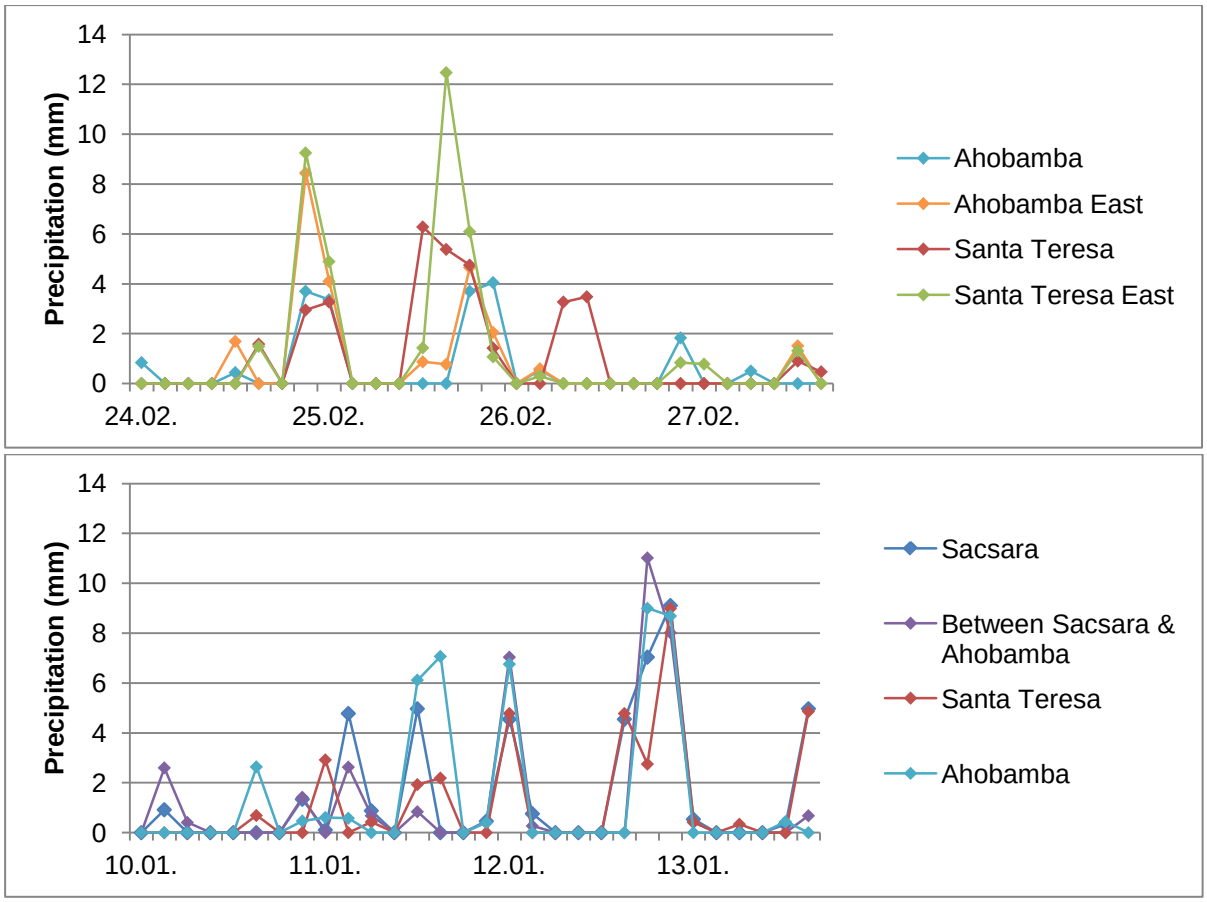

Figure 6.11 and 6.12: Subdaily TMPA precipitation (3-hour intervals) before the debris flows of Ahobamba (top) and Sacsara (bottom) in 1998 for TRMM tiles closest to the starting zones.

As shown in Fig. 6.11 for the Ahobamba scene, where the starting zone is, some precipitation was registered in the nights between 24th and 25th and 25th and 26th. However, on the event day, no significant precipitation amounts were registered. For Sacsara, precipitation was registered nearly continuously for four days, with several peaks visible in all relevant TRMM tiles. In the night between the 12th and 13th, the largest peak was registered.

Tables 6.2 and 6.3 (page 51) show the pre-event precipitation from SENAMHI stations and TMPA data for Sacsara and Ahobamba. Note that the “3d Sum” is the Sum of the day with the event as well as the previous three days, while “Week Sum” (and 2/3/4 week) is the sum of one week, including the event day (7 days in total). A weighted pre-event precipitation was considered but discarded, as spatial variability is very large (see Fig. 6.1; 6.2; 6.7 - 6.10).

Table 6.2: Pre-event precipitation amounts prior to the Sacsara event. The climatic average daily precipitation is taken from 1965 to 2012 with only days containing data included. Yellow means above (wet season) average, orange means above 3 times the (wet season) average.

Sacsara									
	TMPA				SENAMHI				
Name	Sacsara	Between Sacsara & Ahobamba	Santa Teresa	Aho-bamba	Abancay	Anta Anca-churo	Cura-huasi	Quilla-bamba	Uru-bamba
Climatic	3.9	4.1	3.0	3.7	1.9	2.4	1.7	3.3	1.3
Climatic (wet)	5.4	5.2	4.9	4.9	3.8	4.8	3.7	5.1	2.6
10.01.1998	2.3	4.4	0.7	3.1	10.9	0.0	0.0	2.8	0.1
11.01.1998	13.5	9.0	8.2	17.9	4.2	0.0	5.6	39.4	0.0
12.01.1998	26.0	26.4	21.3	24.5	15.1	6.1	9.6	0.0	0.6
13.01.1998	10.9	7.3	7.8	2.7	11.4	0.0	0.0	3.8	0.3
3d Sum	50.4	42.6	37.3	45.1	41.6	6.1	15.2	46.0	1.0
Week Sum	56.1	51.2	39.4	54.2	51.1	16.7	39.5	59.6	6.9
2 Week Sum	88.0	73.8	69.0	73.6	90.8	103.0	73.5	87.9	19.9
3 Week Sum	no data	no data	no data	no data	105.7	259.9	113.7	106.3	51.4
4 Week Sum	no data	no data	no data	no data	164.8	347.3	176.3	151.4	76.8

Table 6.3: Pre-event precipitation amounts prior to the Ahobamba event. The climatic average daily precipitation is taken from 1965 to 2012 with only days containing data included. Yellow means above (wet season) average, orange means above 3 times the (wet season) average.

Ahobamba									
	TMPA				SENAMHI				
Name	Aho-bamba	Aho-bamba East	Santa Teresa	Santa Teresa East	Abancay	Anta Anca-churo	Cura-huasi	Quilla-bamba	Uru-bamba
Climatic	3.7	2.7	3.0	3.2	1.9	2.4	1.7	3.3	1.3
Climatic (wet)	4.9	4.4	4.9	4.8	3.8	4.8	3.7	5.1	2.6
24.02.1998	5.0	10.1	4.5	10.7	9.1	15.8	0.0	8.5	12.8
25.02.1998	11.1	12.4	21.1	26.0	0.0	1.8	1.9	24.5	0.1
26.02.1998	2.4	0.6	6.8	1.1	2.2	0.0	0.0	8.8	0.5
27.02.1998	1.7	1.5	2.7	2.1	0.3	0.0	0.0	0.0	0.4
3d Sum	20.2	24.7	35.1	39.9	11.6	17.6	1.9	41.8	13.7
Week Sum	20.8	25.4	36.2	42.4	14.6	18.5	6.1	60.2	14.2
2 Week Sum	75.0	67.3	93.2	95.2	26.8	69.4	44.3	89.6	35.4
3 Week Sum	115.2	126.0	155.7	162.8	82.7	118.1	81.1	131.4	63.8
4 Week Sum	161.3	179.1	179.0	188.3	95.2	141.4	105.2	152.4	73.0

TMPA only contains data for 13 days prior to the Sacsara event, as TMPA started collecting data on January 1st 1998. The longer the timeframe, the closer are precipitation amounts for TMPA and SENAMHI measurements.

TMPA has higher precipitation amounts registered prior to the Ahobamba event, but not on the day of the event. For Sacsara, TMPA shows 3-day precipitation amounts comparable to Quillabamba and Abancay. Total monthly precipitation values for January and February 1998 were not out of norm. In 1999, more precipitation fell without large debris flow activity (DesInventar, 2013).

Antecedent to the Sacsara event, average 3-day precipitation was exceeded only in Abancay and Quillabamba. In Curahuasi, precipitation was average and in Anta Ancachuro and Urubamba even below average. In Quillabamba, a high peak of 39.4 mm two days before the event is visible, while in Abancay, it rained continuously for 4 days. Considering the 4-week sum, Anta Ancachuro has much more precipitation than on average; Abancay and Curahuasi also higher than average; Quillabamba and Urubamba exactly average. TMPA data shows high precipitation amounts prior to the Sacsara event.
Antecedent to the Ahobamba event, 3-day precipitation was about average for Abancay, Anta Ancachuro, Curahuasi and Urubamba. Only Quillabamba showed higher than average 3-day precipitation, with a peak two days before the event (24.5 mm). Considering 4-week precipitation sums, all stations measured average precipitation amounts. TMPA data shows high values 3 and 4 days prior to the event, but also low preciptiation on the event day.
Note that on the day of the Ahobamba event, no precipitation amounts above average were registered; but precipitation amounts above average were registered on the day of the Sacsara event for 3 out of 4 TRMM tiles and one SENAMHI station. Also, actual amounts were larger for Sacsara, with 7 (compared to 5 for Ahobamba) tiles or stations showing daily precipitation amounts higher than 3 times the wet season climatic average. Generally, TRMM tiles show more precipitation than SENAMHI stations. No significant trend concerning elevation dependency of precipitation was found.

Long-term precipitation analysis from SENAMHI stations showed that in 1998, monthly, seasonal and annual precipitation amounts prior to the events were average. However, Fig. 6.13 below shows that precipitation from August to December 1997 was wetter than average (1965 – 2012, shown are 1996-2002). Total precipitation from September 1997 to February 1998 is 500 mm (Abancay), 900 mm (Anta Ancachuro), 520 mm (Curahuasi), 790 mm (Quillabamba) and 310 mm (Urubamba). Long-term pre-event precipitation comparison was not possible for TRMM, as the data series does not start until January 1998.

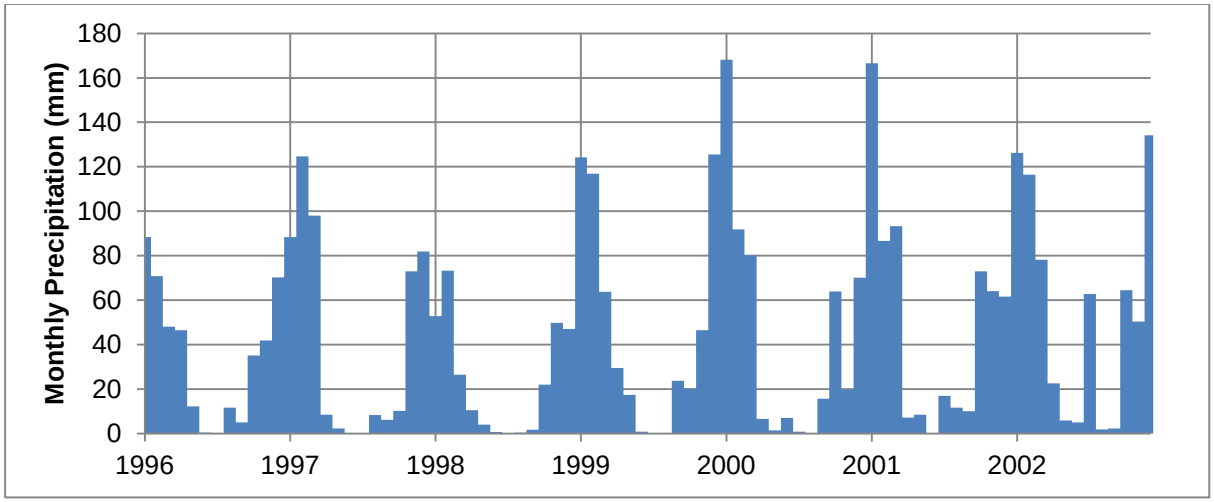

Figure 6.13: Monthly precipitation in Quillabamba from 1996 to 2002. Source: SENAMHI.

6.1.5 Thresholds

As stated in Chapter 5, no rainfall threshold was made for Santa Teresa. Maximum daily precipitation values for 2012 are between 22 mm (Hayllabamba) and 51 mm (Machu Picchu) for all new stations. Out of these daily precipitation amounts, it is possible that 5 mm (Hayllabamba) to 25 mm (Santa Teresa) can fall within one hour and possibly even less. Hourly precipitation amounts can be close to the total daily precipitation.

A pre-event precipitation analysis of four smaller events (mentioned in Section 3.4.3) near Santa Teresa showed that except for the GLOF in 1996, pre-event precipitation was high. Only one event (November 1998) also showed high precipitation amount on the day of the event. It would be interesting to undertake a specific rainfall threshold analysis for the Santa Teresa region with new available data.

6.2 Temperature

Temperate can be used as a proxy for the snowmelt rate. As mentioned in Section 2.2.3.4, snowmelt can influence soil saturation, pore pressure and thus soil stability. In order to assess if temperature played an important role in the Ahobamba and Sacsara events, monthly temperatures were analyzed for December 1997 to February 1998 (Fig. 6.15 -6.17). Daily temperatures are not shown here, as they were not found to be higher shortly before the events than at other days. Over a longer time, differences get averaged, which is why long-term temperatures were assessed.

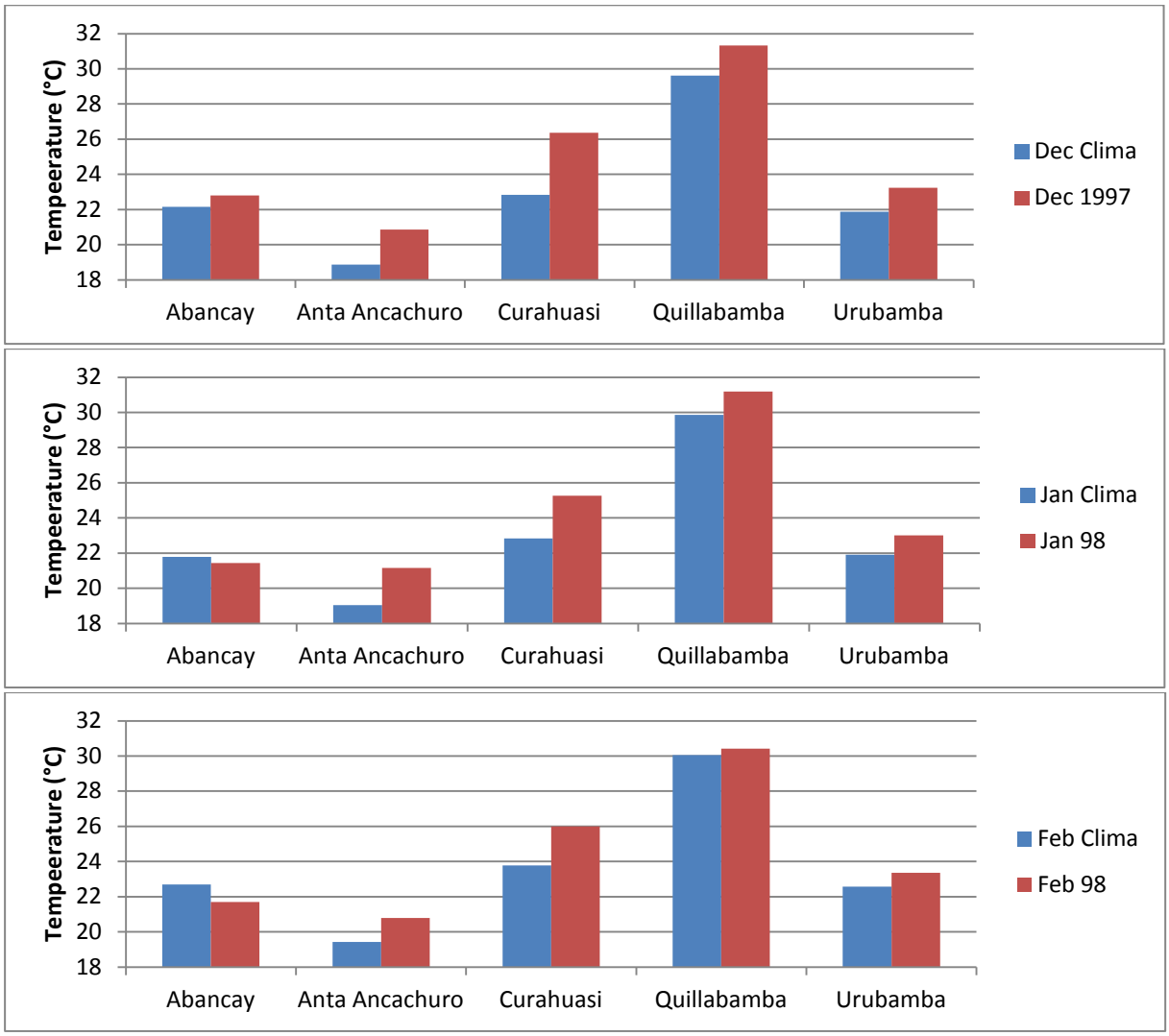

Figure 6.15, 6.16 and 6.17: Monthly maximum temperature in December 1997 (top); January 1998 (middle) and February 1998 (bottom). The climatic average is given in blue, the corresponding temperature in 1997/ 1998 in red. Note that the temperature axis starts at 18°C.

Except in Abancay (January and February 1998), temperature is always warmer than average. Analysis of the highest recorded monthly temperatures from 1965 to 2010 showed that January 1998 was the warmest on record for Quillabamba and February 1998 the warmest on record for Urubamba. Additionally, December 1997 was the 5th-warmest on record for both Urubamba and Quillabamba. Also in other stations, temperatures close to the current record were measured.

6.3 Earthquakes

On January 9th at 23.54.24 local time (06.54.24 UTC+2), a 6.1 earthquake was registered in a depth of only 16.9 km at location 11.988°S 72.030°W (USGS; 2010), which is around 150 km from the Sacsara starting zone. This earthquake was felt by the population (CARE & UZH, 2013a). Two smaller aftershakes were registered in the morning of January 10th, but probably did not influence Santa Teresa region much, due to their lower magnitude and rather large distance.
Another earthquake was registered on January 13th at 12:01:36 (three hours prior to the event) with a magnitude of 5.3 at location 14.098°S 73.468°W, around 130 km from the Sacsara starting zone, in a depth of 94.3 km. No reports claim that this earthquake was felt by the population; however it could have further destabilized the morainic material, especially in combination with the intense rains starting around this time.

In connection with the Ahobamba event, no significant earthquake activity (earthquakes larger than magnitude 2.0) was found prior to the Ahobamba event near the study region. However, the earthquakes in January probably did also destabilize morainic material in the Ahobamba starting zone.

7 Modeling of 1998 Debris Flows

In this chapter, modeling results are presented. First, DEMs were evaluated (Section 7.1); then, sensitivity analysis was carried out for various parameters (Section 7.2); last, calibration for the Sacsara and Ahobamba events was made (Section 7.3).

7.1 DEM Evaluation

As DEM properties such as resolution or acquisition technique influence simulation results (see Chapter 4), ASTER GDEM2 was evaluated and compared to SRTM3x4 from CGIAR. DEM evaluation is recommended for low resolution DEMs (Andres, 2010). In order to ensure comparability, DEMs were reprojected to the projected coordinate system WGS 1984 UTM, zone 18S with bilinear interpolation (to 30 m resolution for ASTER and 90 m resolution for SRTM). Then, DEM scenes were clipped to the study region and artificial sinks in the DEMs were filled. Bilinear interpolation was chosen as it is preferable to nearest neighbor, which decreases runout due to higher roughness (D. Schneider, pers. communication). Resampling of ASTER to a resolution of 10 m proved impractical due to very long calculation times and limited increase of simulation quality. A comparison of the available DEM and a DEM after a modeled debris flow is of limited use, as the available DEMs were already made after the events.

DEMs were tested for artifacts and DEM shifts (compared to a basemap provided in ArcGIS and to each other). DEM shifts were removed when found. Then, height differences (including the minimum and maximum values) were analyzed using hillshade, contour lines, the minimum and maximum heights and direct subtraction. The main focus of analysis are the close surroundings of Santa Teresa. This procedure was adapted from Frey & Paul (2012).

Both ASTER GDEM2 and SRTM showed a shift westwards of 30 m compared to the Google Earth-referenced deposition file near Santa Teresa. This shift was corrected in shifting the deposition areas one pixel (30 m) to the west for the SPI. The shift is only relevant when quantitatively comparing with depositions (SPI). For flow height or velocity, the shift was not corrected for, as the simulations maximum flow depth corresponds well to the lowest part of the DEM. For 2D-illustration, the shift was only discussed but not corrected. This shift of one pixel is not consistent in the whole ASTER GDEM2 scene but varies. Some parts of the GDEM do not correspond to the Basemap, e.g. in terms of the lowest flow path. This discrepancy is partly because of DEM errors and maybe also due to Basemap map errors.

Fig. 7.1 (page 56) shows a comparison between two differently resampled ASTER GDEM2 DEMs. Height differences are mostly small but can be as large as 10 m. Another comparison of two ASTER GDEMs (30.7 m resolution) showed that filled sinks reduce runout and velocity. This is counterintuitive and shows the large influence of DEMs on model results.

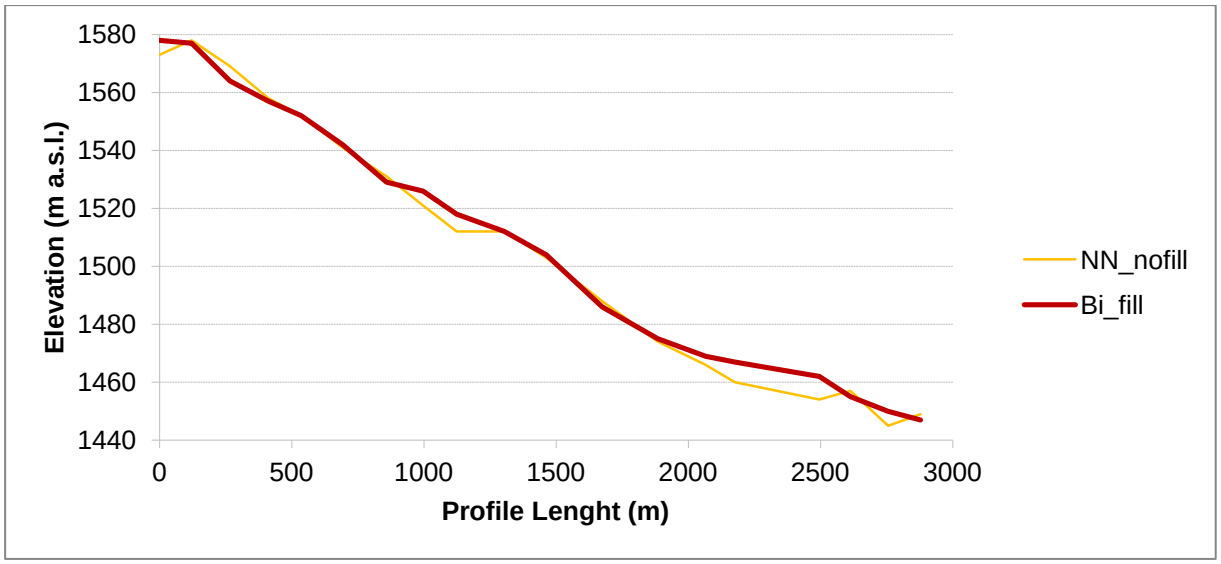

Figure 7.1: Comparison of ASTER GDEM2 resampled to 30 m resolution with nearest neighbor interpolation and without filled sinks (NN_nofill; used for discharge sensitivity analysis) and an ASTER GDEM2 resampled to 30 m with bilinear interpolation and filled sinks (Bi_fill; used for all other simulations).

Fig. 7.2 shows height differences between ASTER GDEM2 and SRTM. The vast majority of pixels have a height difference less than 50 m. The very large differences of over 100 m in height difference occur in very steep areas (e.g. mountain peaks) and were found to not affect simulations. ASTER GDEM2 shows minimum and maximum heights of 1,423 m and 6,230 m, SRTM minimum and maximum heights of 1,422 m and 5,837 m for the area of interest. This shows the large influence of DEMs on the extremes. High peaks show larger differences than the flatter, lower parts.
Direct subtraction shows the patterns of the valleys and the mountains, as in all concave and convex features, differences occur. The very large differences mentioned above do not show this pattern, they might also be the result of a faulty interpolation of missing values in SRTM. Analysis of contour lines showed that although differences between the two DEMs exist, they agree well on the relatively high and low areas. This means that SRTM and ASTER are of comparable quality.
The hillshade illustration shows various small artifacts for ASTER, especially lines crossing in a north-south-direction probably caused by the image processing of single images. SRTM does not show these lines, but there are various artifacts in SRTM owned to the interpolation of data voids, for example “blurred” areas in hillshade and flat areas on top of mountains (see Fig. 7.3). It seems that for Santa Teresa area, ASTER GDEM2 is of higher quality. This makes it more suitable, together with its higher resolution, to model debris flows in the area.

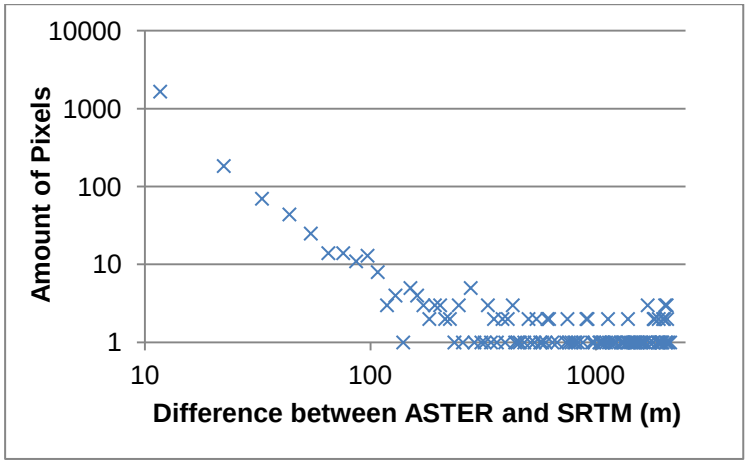

Figure 7.2: Amount of Pixels (blue x) for DEM height differences on a logarithmic scale.

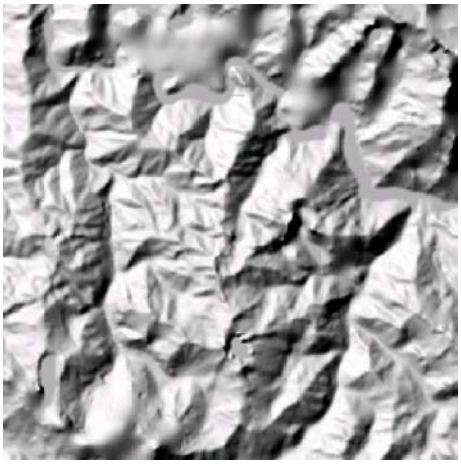

Figure 7.3: Hillshade of the SRTM DEM used for this thesis.

7.2 Modeling Sensitivity Analysis

In this section, input parameters mentioned in Section 5.2.3 are tested on their sensitivity to model results. Two simulation runs with exactly the same parameters showed the same results. This means that for the same input, always the same output results. Very high volumes (e.g. 50 mill. m^3) caused unrealistic overflow on opposite hills, which was corrected by RAMMS automatically after further calculation steps. Sensitivity analysis is only shown for Sacsara, as parameters will change similarly for Ahobamba. Sensitivity analysis was made with the bilinear interpolated ASTER GDEM2 with 30 m resolution and filled sinks (except for discharge). Fig. 7.4 by Scheuner (2007) gives an overview of values for the friction parameters ξ and μ.

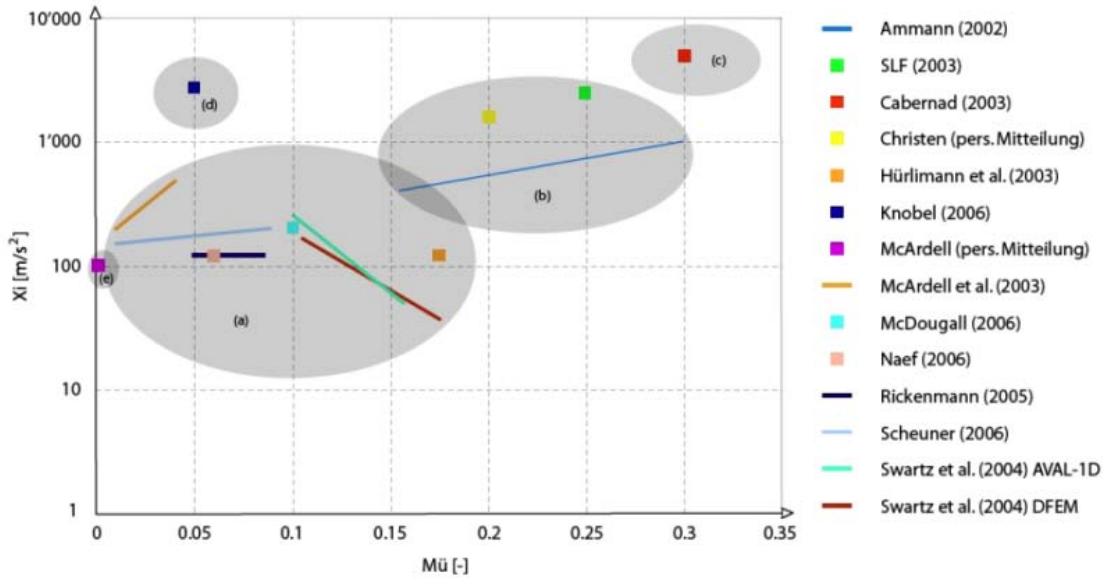

Figure 7.4: Range of values for ξ and μ for various mass movements: (a) debris flows, (b) snow avalanches, (c) rockfalls, (d) ice avalanches, (e) floods. Source: Scheuner (2007).

7.2.1 Dry-Coulomb friction coefficient μ

The dry-Coulomb friction coefficient μ is the basal friction (D. Schneider, pers. communication) and dominates when the flow is about to stop (Christen et al., 2010a). It depends on density, water content and pressure perpendicular to the surface. For high water content (Scheuner, 2007) and fine-grained flows (Rickenmann, 2005), μ is lower. μ is defined as the ratio between drop height H and maximum horizontal runout distance L (H/L = tangent of slope), which is also called the angle of reach (Schneider, 2011) or the overall slope (see Section 2.2.2.3) (Bartelt et al., 2013). L starts at the highest point of the starting zone and ends at the lowest point of the deposition zone. This gives a value of 0.104 (0.1) for Sacsara and 0.135 (0.14) for Ahobamba from the starting zones to the confluence with Urubamba. As large events have a larger runout distance (Rickenmann, 2005), the overall slope (and thus μ) is reduced (Schneider, 2011).

Fig. 7.4 from Scheuner (2007) gives values for μ for debris flows of 0.01 - 0.2. For the debris flow resulting from the Kolka-Karmadon ice avalanche, μ was found to be 0.08 (Schneider, 2011). Armento et al. (2008) have found μ values of 0.12 - 0.21; Sosio et al. (2008) of 0.05 - 0.2; Pirulli & Sorbino (2008) of 0.01 - 0.12. Rickenmann (2005) found a lower boundary of 0.07 in Canada.

Simulations for the sensitivity analysis of μ were started from the lowest point of the starting zone Sacsara with a hydrograph. μ sensitivity was tested for μ values of 0.05 - 0.15 in 0.01 steps in Sacsara (Simulations 0003 - 0013) based on above values in literature. Taking strictly the overall slope, μ for Sacsara would be 0.1 (0.104). With lower μ, (1) the moving momentum and thus calculation time decreases strongly; (2) velocity increases; (3) flow height increases and (4); runout increases. μ is a highly sensitive parameter (see also Walser, 2013). From the Sacsara starting zone to Santa Teresa, a debris flow simulation took 2,000 s (μ 0.02) and 18,000 s (μ 0.14) to reach Santa Teresa. Fig. 7.5 shows the Simulation Performance Index. μ values of 0.09 or 0.1 both show best results.

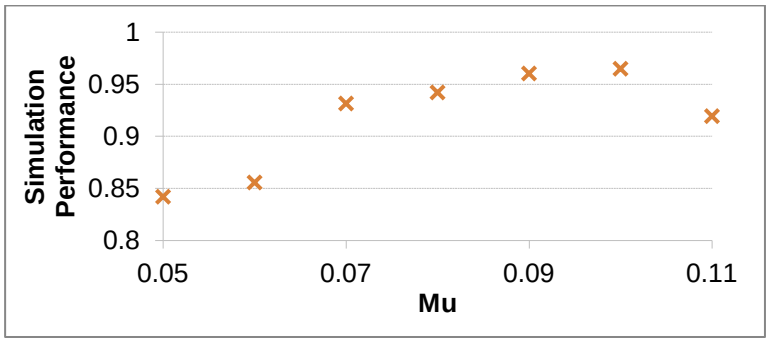

Figure 7.5: The simulation performance index (SPI) for different values of μ. This index is the ratio of all cells in the investigated area correctly modeled (cells affected in both simulation and deposit) and the total amount of cells in the observed deposit file (see Section 5.2.3).

A tradeoff between the ratio of cells correctly simulated to be unaffected and the cells wrongly simulated as affected (false positive) and the SPI exists. Simulations with high SPI have less cells correctly simulated to be unaffected and more false positive. However as the correctly simulated affected areas are more important, SPI was chosen.

Fig. 7.6 shows μ sensitivity on flow height along the profile line at the deposition zone. With lower μ, flow height variation increases and flow height shows larger extremes. For further sensitivity analysis, a μ of 0.09 (bold) was chosen.

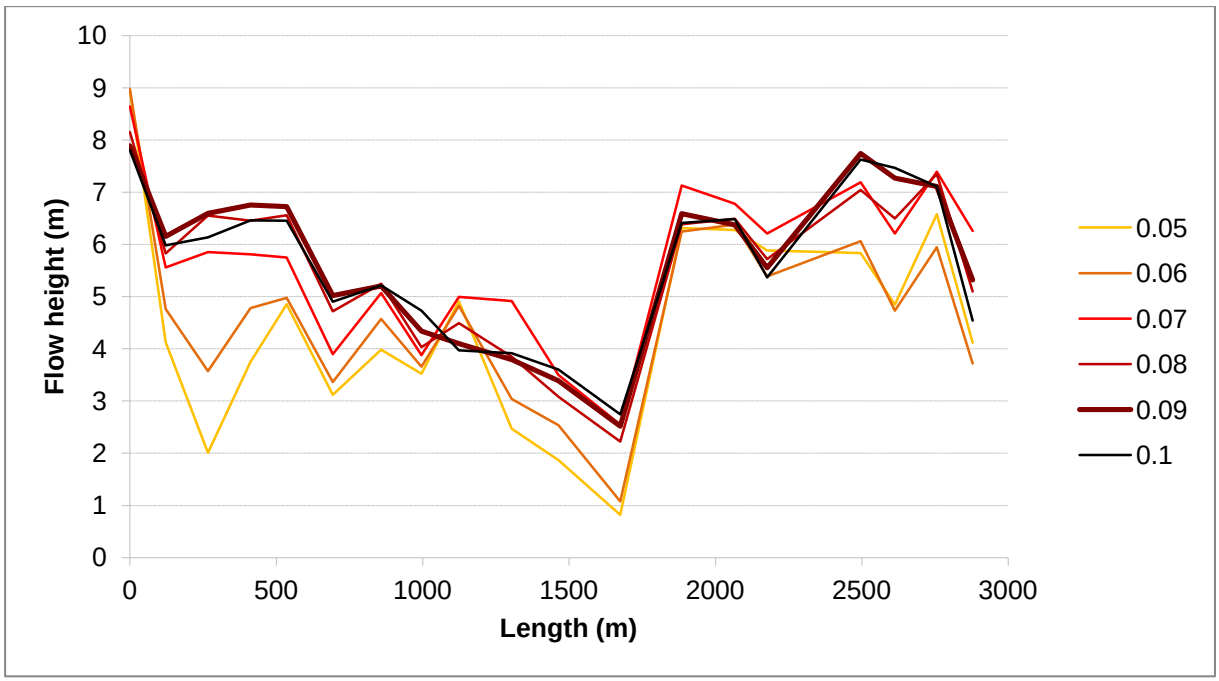

Figure 7.6: Flow heights in the deposition zone near Santa Teresa for varying μ.

7.2.2 Turbulent friction coefficient ξ

The turbulent friction coefficient ξ dominates in the acceleration zone, when the debris flow is going fast (Christen et al., 2010a). It depends on the surface geometry and thus is not constant for the whole flow (Salm et al., 1990). ξ is an inverse parameter: the higher it is, the lower are turbulent effects (Ayotte & Hungr, 2000), which means friction is reduced and velocity increased. As the moving momentum consists of mass * velocity, flow velocity is larger with larger ξ and runout increases (Scheuner, 2007). Turbulent friction is also called internal friction, internal shear, internal or granular temperature and random kinetic energy. Granular temperature is the movement of single grains and corresponds to shear rate (slope of the velocity curve, with max velocity = shear rate 0 and 0 velocity = shear rate infinity). It is not calculated internally, as RAMMS works depth-averaged (D. Schneider, pers. communication).

Fig. 7.4 from Scheuner (2007) gives values for ξ for debris flows of 20 - 1000. For large events, the largest value of ξ is most realistic, as geometry gets less important (Salm et al., 1990). For ξ, an extreme value of 3000 was found by Christen et al. (2010b) for an avalanche. Also Schneider (pers. Communication) says that values of ξ over 1000 are well possible for very large debris flows. Armento et al. (2008) recommend a ξ value of 100 - 500, Sosio et al. (2008) of 200 - 500 and Pirulli & Sorbino (2008) of 100 - 1000.

Simulations for the sensitivity analysis of ξ were started from the lowest point of the starting zone Sacsara with a hydrograph. ξ sensitivity was tested for ξ values of 500 to 3000 in steps of 500 (and steps of 250 from 500 to 1500) (Simulations 0014 - 0022). All simulations were made with a μ of 0.09. In ξ sensitivity analysis, it was found that ξ has low sensitivity and nearly no influence on runout, flow height and velocity. With lower ξ calculation time increases slightly and velocity decreases. Influence on velocity can be larger in the flow path than in the deposition zone. Velocity is rather small in the middle of the debris flow path and larger at the boarder of the flow. ξ of 1500 was used for further sensitivity tests, calibration and scenario simulations.

7.2.3 Input Volume

As event magnitude strongly influences the friction parameters (Ayotte & Hungr, 2000), volume sensitivity was tested for Sacsara for 5 to 10 mill. m^3 (with 1 mill. - steps) from a hydrograph positioned 8 km upstream from Santa Teresa (Simulations 0023 - 0028). All simulations were made with a μ of 0.09 and ξ of 1500. Discharge was estimated based on Costa & Schuster's (1988) formula with a dam height of 25 m. Tested volumes proved too large for the largest single surge volume but rather reflect the total volume of the Sacsara event (3 - 6 mill. m^3). Volume sensitivity is visualized with 2D-illustration.

Input volume shows large sensitivity for comparatively small changes. With higher volume; (1) moving momentum and calculation time increases slightly; (2) average and maximum velocity increases slightly; (3) flow height increases and (4); runout increases. Fig. 7.7 below shows the covered area for volumes of 5 - 10 mill. cubic meters. The white area in the middle is the mapped deposition area. The blue marked area is the volume chosen for further simulations (8 mill. m^3).

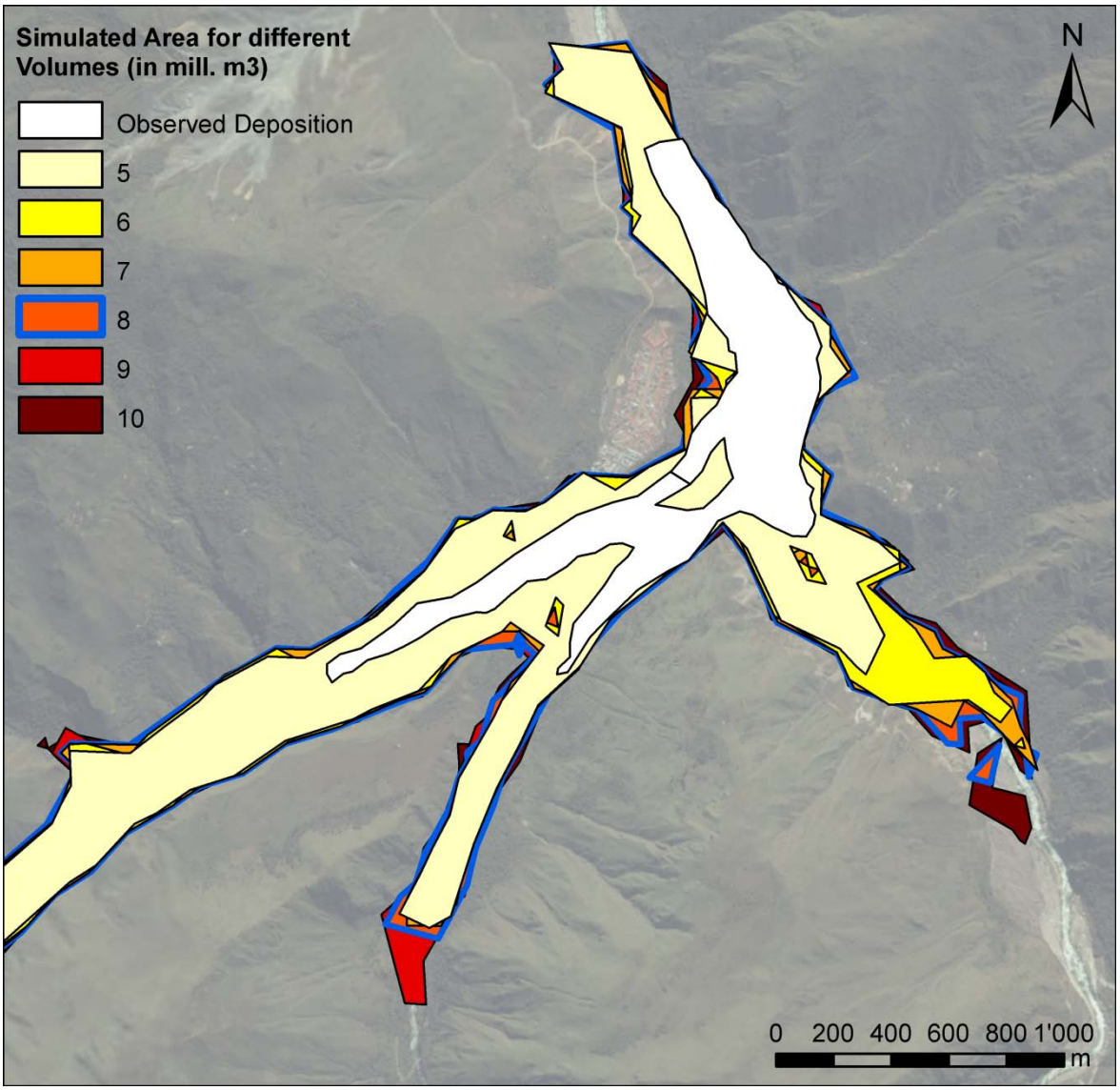

Figure 7.7: Varying debris flow volumes of the Sacsara event (yellow to red) compared to depositions (white).

Extreme values are shown in Fig. 7.8 and 7.9 (page 61). Flow heights of 0.5/5/10/15 m are shown for Sacsara (all below 0.5 not shown). Flow height strongly increases when comparing a volume of 5 and of 10 mill. m^3. It seems that a volume of 10 mill. m^3 is overestimated.

0023: 5 mill. m^3 0028: 10 mill. m^3

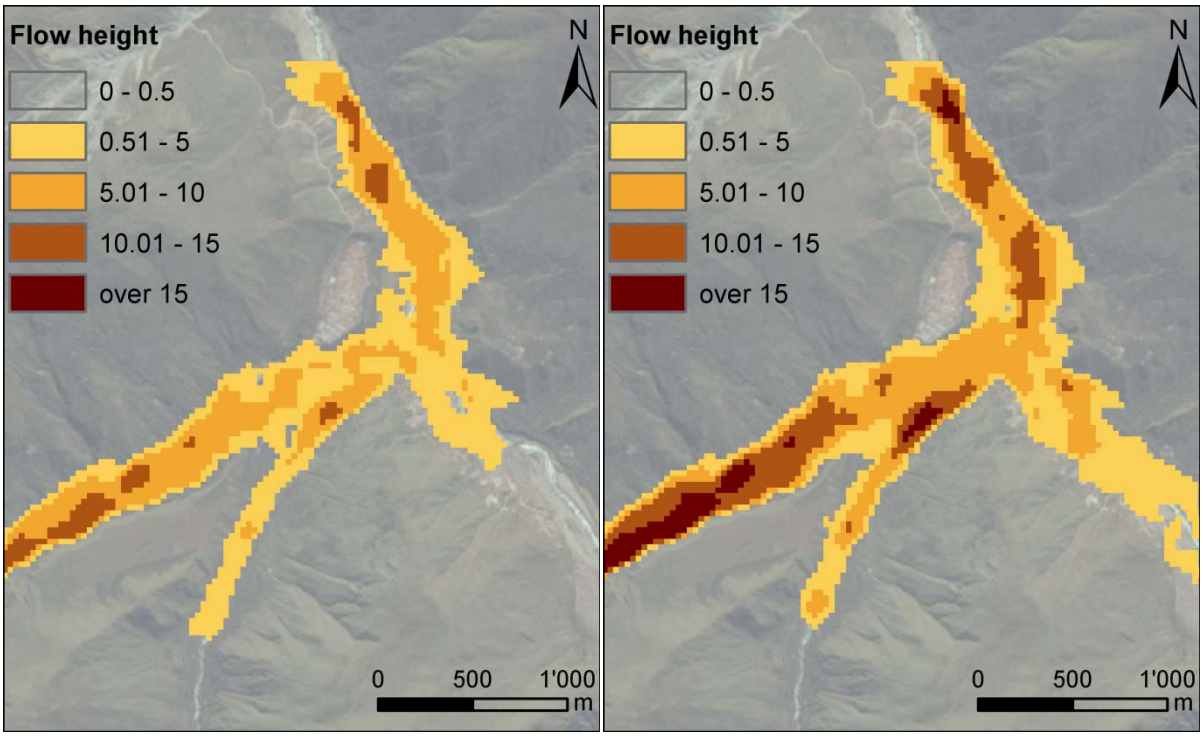

Figure 7.8 and 7.9: Flow heights for a volume of 5 mill. m^3 (left) and 10 mill. m^3 (right).

As input volume of the Ahobamba event is uncertain, volumes from 10 to 50 mill. m^3 were tested. These simulations were started 8 km upstream, as it was assumed that the main erosion took place further upstream and that the whole volume passes through the 8km hydrograph. For the Ahobamba event, a total event volume of 25 mill. m^3 seems realistic.

7.2.4 Input Velocity

Velocity increases with increasing volume and discharge (Rickenmann, 2005). Velocity formula (2.4) by Rickenmann (1999) gives a flow velocity of 18.6 m/s for Sacsara and 28.5 m/s for Ahobamba. As the dependency of velocity on slope and discharge can be assumed to be nonlinear, flow velocities lower than those calculated with Rickenmanns (1999) formula seem reasonable. Velocity was tested for 3, 5, 10, 15 and 20 m/s (Simulations 0029 - 0033). Velocity influence on flow height, calculation time and runout was found to be low. Input velocity cancels out during simulation with RAMMS (see also Walser, 2013 and Schneider, 2010). A starting velocity of 15 m/s proved reasonable for both Sacsara and Ahobamba.

7.2.5 Input Discharge

Three discharge formulas were compared in simulations 237, 238, 241 in Fig. 7.10 (page 62): 2,500 m^3/s (Evans, 1986), 7,500 m^3/s (Costa & Schuster, 1988), 38,000 m^3/s (Rickenmann, 1999). As Costa & Schuster's (1988) formula showed best results, discharges of 3,750 m^3/s, 5,625 m^3/s, 9,375 m^3/s and 11,250 m^3/s (Costa & Schuster +- 25% and +- 50%) were compared in simulations 245 - 249 in Fig. 7.11 (page 62). For potential energy in Costa & Schuster's (1988) formula, a dam height of 25 m was assumed based on estimations in the starting zones. All simulations were made with a μ of 0.09 and ξ of 1500 and a volume of 8 mill. m^3. Illustration was made with a flow height profile. Calculated discharges are always rounded to 100 m^3/s.

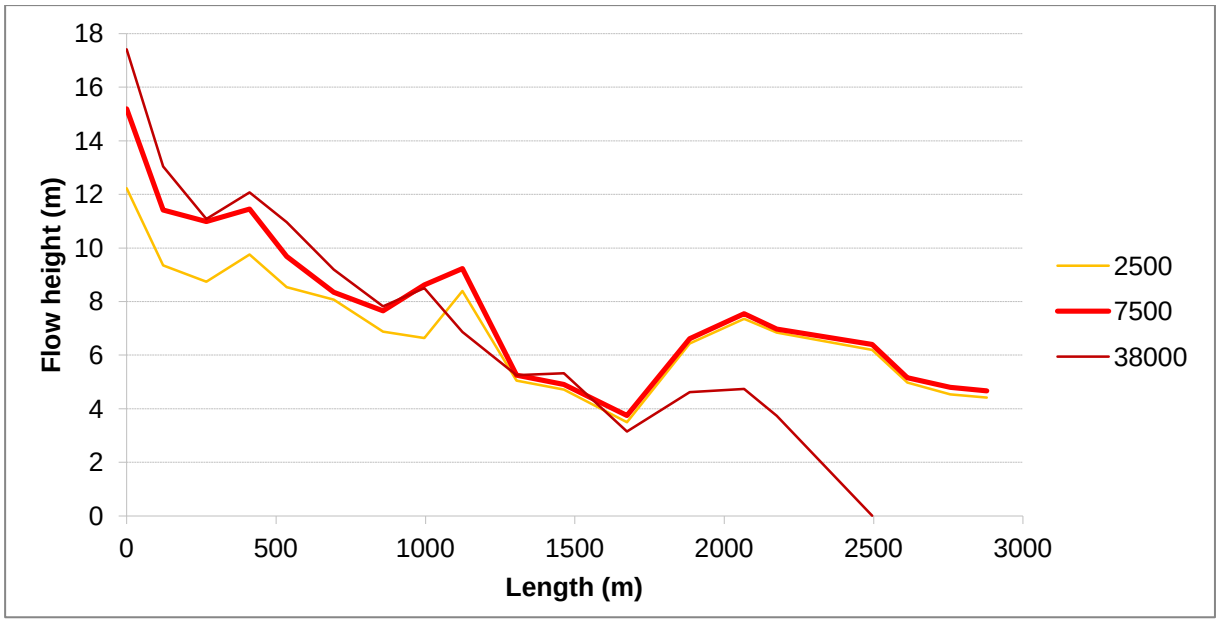

Figure 7.10: Discharge sensitivity on flow heights in the deposition zone near Santa Teresa.

These three simulations were started from the hydrograph at the starting zone and had an additional mu/xi area (μ 0.2, ξ 500) added in order to stop the debris flow in Santa Teresa. Note that the debris flow simulated with Rickenmanns (1999) formula stops before the end of the deposition zone.

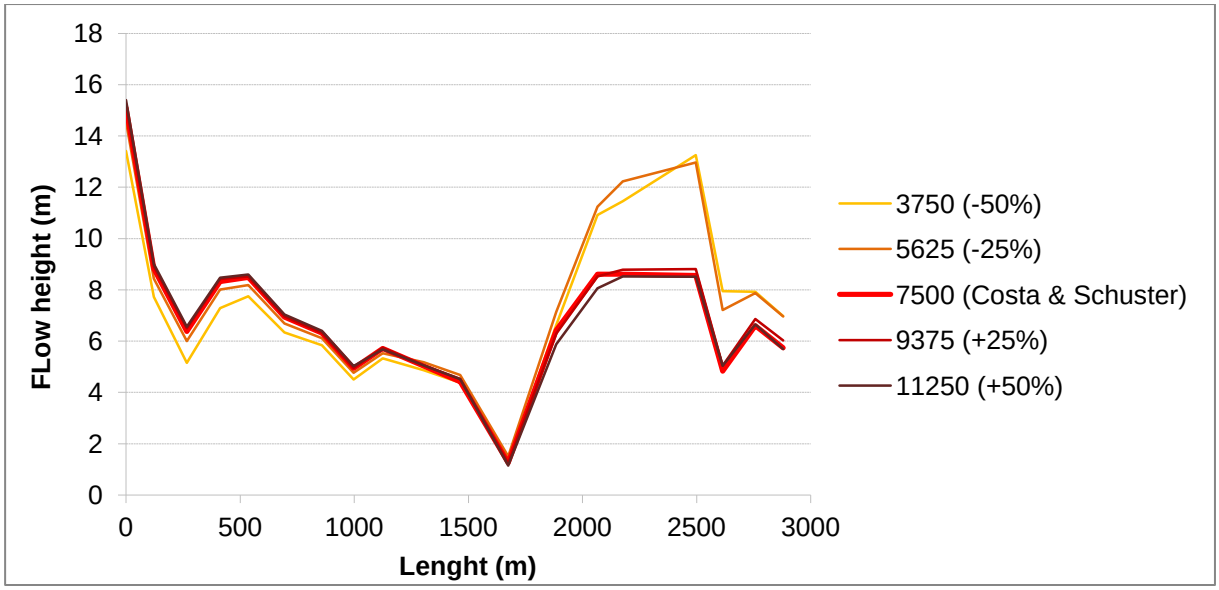

Figure 7.11: Discharge sensitivity on flow heights in the deposition zone near Santa Teresa, based on the formula from Costa & Schuster (1988).

These simulations were started from the hydrograph 8 km upstream from Santa Teresa. No additional mu/xi area was added. Sensitivity analysis shows that discharge was rather low (a discharge as proposed by Rickenmann (1999) stopping too early), which is supported by Jakob (2005a), who states that muddy debris flows have lower discharge. Input discharge shows a large sensitivity on comparatively small changes. With lower discharge; (1) calculation time increases strongly; (2) velocity stays the same; (3) flow height decreases at the beginning of the hydrograph (but not so much downstream) and (4); runout increases strongly. Sensitivity of discharge in Ahobamba is assumed to be equivalent to Sacsara. For Ahobamba, a simulation started from the top with a discharge according to Costa & Schuster (1988) with 25 m dam height gave good results. Costa & Schuster's (1998) formula gave best results and was used for calibration, hazard assessment and further sensitivity analysis.

7.2.6 Input t1

Input t1 is the time needed until the maximum discharge is reached at the hydrograph position. It was tested in RAMMS for values of 60 s, 120 s, 180 s, 240 s and 300 s (Simulations 0034 – 0038). For Sacsara, 180 s and for Ahobamba 300 s are considered reasonable input t1. Sensitivity on flow height, velocity, calculation time and runout has proven to be very low.

7.2.7 Release Zone Type and Position

In RAMMS, block and hydrograph can be chosen as input release zone file. Hydrograph is more realistic (WSL, 2013), which is why all simulations in this thesis are made with a hydrograph release file. Calculation time can be strongly reduced with hydrographs (WSL, 2013). A main shortcoming is that more input parameters need to be specified, which results in higher uncertainty.

Hydrograph position was tested for sensitivity because a lot of computation time can be reduced when the hydrograph is placed close to the area of interest. Compared to a hydrograph placed at the starting zone, a hydrograph 8 km upstream from Santa Teresa shows similar results, when the hydrograph at 8 km is based on the hydrograph measured at 8 km from the simulation from the top. Smaller variations in hydrograph position show very low sensitivity on simulation results. Hydrograph width corresponds to the width of the debris flow. In order to reduce computational time, a hydrograph approximately 8 km upstream from Santa Teresa was used for a variety of simulations. As with this procedure, runout information gets lost (as the debris flow travels much farther compared to a hydrograph at the starting zone); some simulations were also made from the starting zone.

7.2.8 Stop Criterion

The stop criterion has a large influence on simulation results. A stop criterion of 10% means that the simulation stops when 10% or less of the total mass is in movement (Stricker, 2010). This value is on the upper boarder for realistic stopping, but as the events are very large, 10% are sufficient (M. Christen; D. Schneider, pers. communications). This was confirmed by an analysis of the mass momentum plot in RAMMS. The stop criterion was set to be 10% for all simulations.

The end time condition defines where RAMMS stops the simulation. With an end time condition of 15,000 s, a debris flow from Sacsara or Ahobamba should realistically reach Santa Teresa (corresponding to an average velocity of around 2 m/s). Rickenmanns (1999) velocity formula (2.4) gives a distinctly higher flow velocity of 18.6 m/s. End time was set to 15,000 s for sensitivity analysis, but to 30,000 s for calibration and scenario simulations.

7.2.9 Lamda, H Cutoff and Numerical Scheme

Lamda is the active-passive earth pressure coefficient and can be used to account for the internal energy dissipation of debris flows. H cutoff eliminates unrealistic very small flow heights. The second order numerical scheme is preferable over the first order, as it gives more accurate results (Bartelt et al., 2013). For this thesis, always the second order scheme is used and Lamda and h cutoff are kept constantly at default values from RAMMS, as recommended by Bartelt et al. (2013).

7.3 Calibration

The goal of this section is to find the largest single surge of the events, calibrated based on runout (see Section 5.2.4). As the exact runout distance is unknown, a criterion was that the flow at least reached Urubamba and then continued to flow for a couple of kilometers. Calibration focused on the stop criterion, deposits and flow height and velocity. Input parameters are based on sensitivity analysis (see Section 7.2). The hydrograph position is at the starting zone. Calibration was made with the bilinear interpolated ASTER GDEM2 with 30 m resolution and filled sinks. In calibration scenarios, no intensity categorization (as made in Raetzo et al., 2002) was implemented, as such large debris flows can be considered high intensity in their path (see Sections 9.3 and 9.4 for more information).

7.3.1 Ahobamba

Fig. 7.12 (page 65) shows simulation "Ahobamba 0064", representing the estimated largest single surge of the Ahobamba event. μ was selected based on the overall slope from the highest point in the starting zone to the confluence with Urubamba, which was decreased by 10% as the debris flow was muddy (C. Portocarrero, pers. communication). This results in a μ of 0.12. Volume was 1 mill. m^3, t1 120 s. No DEM shift is visible here; largest flow heights correspond well to depositions. Dam height for Costa & Schuster's (1988) discharge formula was 10 m, resulting in a discharge of 2,600 m^3/s. Input parameters were considered realistic by M. Christen (pers. communication).

The simulation stopped after 30,000 s, with still 14% of its mass moving. This means that runout would be even larger, but due to the low slope around Santa Teresa, the surge can be expected to stop soon after. Runout is reasonable, as Santa Teresa was affected by the first surges of the Ahobamba event (C. Portocarrero, pers. communication). Modeled flow heights and velocities for the largest single surge are realistic. Simulation of the total debris flow volume contained in one surge only proved unreasonable, as runout was consistently too large and deposition height in Urubamba consistently too low. No outflow was detected in the flow path.

The simulation fits well to depositions, except for (1) the counter slope, where the actual surge does not flow up the hill as much as depositions suggests and (2) the east of the deposit, just after the confluence with the main valley (see Section 9.3).

Modeled flow height is much too low for the whole event, as only the largest single surge was modeled. Flow height is 8 - 14 m (average 10 m) just after the height drop after the starting zone and 2 - 8 m (average 3 m) in the valley after that, decreasing to 2 - 4 m (3 m in average) at the confluence. After, flow height is 2 - 5 m (3 m), before decreasing to 1 - 3 m (1.5 m) when the valley broadens around 3 km upstream of Santa Teresa. As a deposition height of 74 m was reported from the Hídroelectrica and 2 - 4 m (3 m) was simulated, 18 - 37 similar surges (with 1 mill. m^3) are needed to reach this height (see discussion).

Flow velocity was modeled to be around 3 - 12 m/s (on average 6 - 8 m/s) for the whole valley section until close to the confluence with Urubamba, with higher velocity at the beginning (due to the large height drop and the input velocity of 15 m/s) and lower towards the confluence (due to flatter slopes). At the confluence, velocity decreases below 5 m/s (around 3 m/s in average, towards the end even 1 m/s). Note that from the starting zone to the confluence, 33 - 35 calculation steps at 300 s each are necessary in the simulation. This would result in a velocity of only 1.6 - 1.8 m/s over the whole distance (the distance is 17 - 18 km depending on the exact path of the river and flow), as opposed to simulated velocities being around 7 m/s (see Section 9.3).

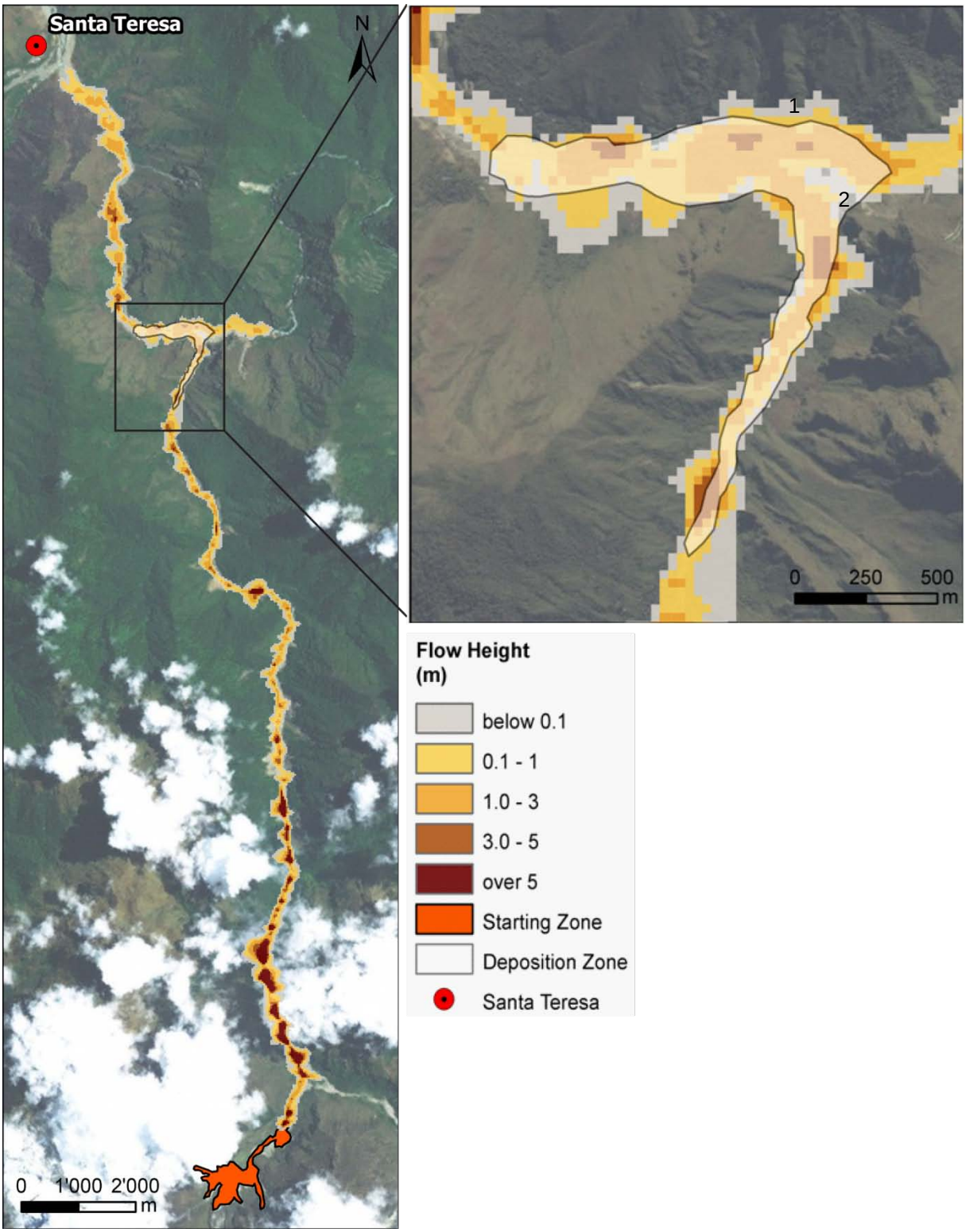

Figure 7.12: 2D illustration of the Ahobamba event.

After the first surges, the debris flow started damming Urubamba. This temporal damming was artificially drained around four months later, flowing downstream as hyperconcentrated flow or debris flood (see Fig. 7.13, page 66).

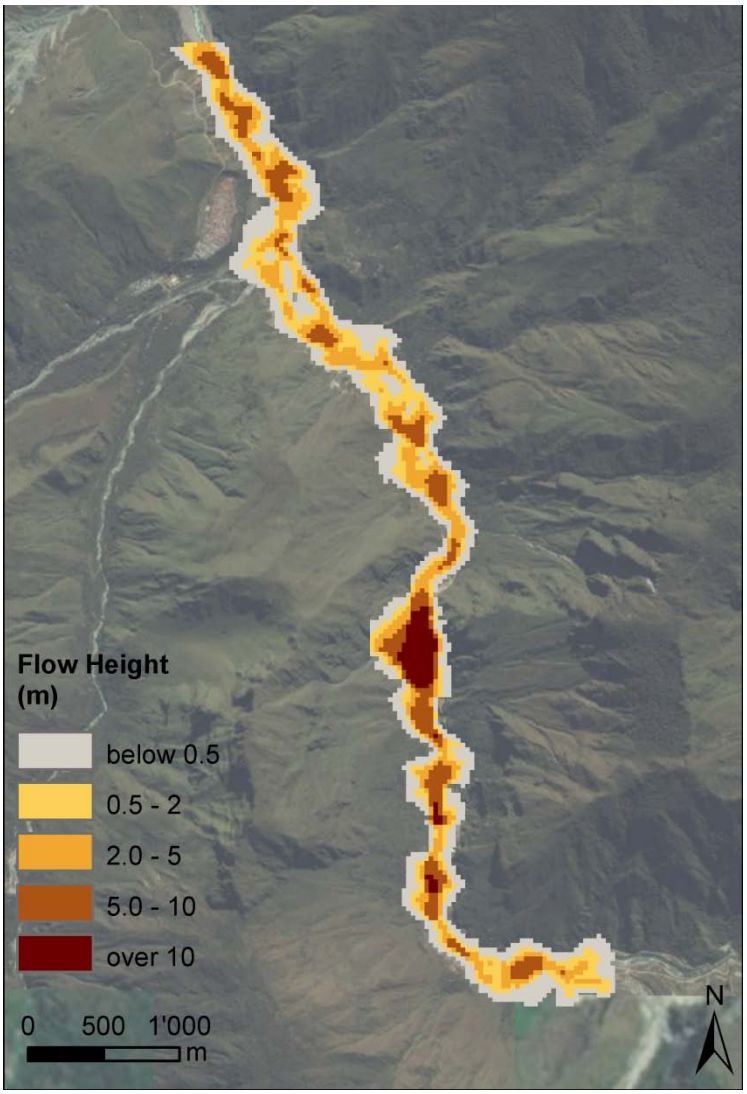

Figure 7.13: 2D illustration of hyperconcentrated flow artificially triggered after the Ahobamba event.

Simulation "Ahobamba 0066" shows this hyperconcentrated flow/ debris flood, modeled with Costa & Schuster's (1988) discharge formula designed for dam breaks. A dam height of only 0.1 m was chosen, as it the dam was drained artificially and supposedly over along period of time. This resulted in a discharge of 1,900 m^3/s for a total volume of debris and water of around 50 mill. m^3 (25 mill. m^3 debris reported, as much water estimated as well). This gives a time of 14h 30min until the dam was drained. In reality, this was probably even longer. For the dam break, ξ of 1000, μ of 0.02 and t1 of 300 s was taken. A μ that low is realistic for hyperconcentrated flows (see Section 7.2.1).

The simulation stopped after 30,000 s, with still 54% of the mass moving. It is likely that runout extended much farther, which is confirmed by reports (see Section 3.4). Due to very large runout, no comparison with depositions can be made. No outflow during the flow path was detected.
Maximum flow height was 4 - 12 m (average 5 - 6 m), with a maximum of 23 m and still 6 m at Santa Teresa. This height seems too high (see Section 9.3). Maximum flow velocity was 8 - 20 m/s (average 10 m/s), which seems realistic for a dam break/hyperconcentrated flow/debris flood. Velocity was larger at the start (due to the input velocity of 15 m/s but also the steeper slope) and lower towards Santa Teresa.

7.3.2 Sacsara

Fig. 7.14 shows simulation "Sacsara 0047", representing the estimated largest single surge of the Sacsara event. μ was selected based on the overall slope from the highest point in the starting zone to the confluence with Urubamba, which was decreased by 10% as the debris flow was muddy. This results in a μ of 0.09. Volume was 500,000 m^3; t1 120 s. Dam height for Costa & Schuster's (1988) discharge formula was 10 m, resulting in a discharge of 1,900 m^3/s.

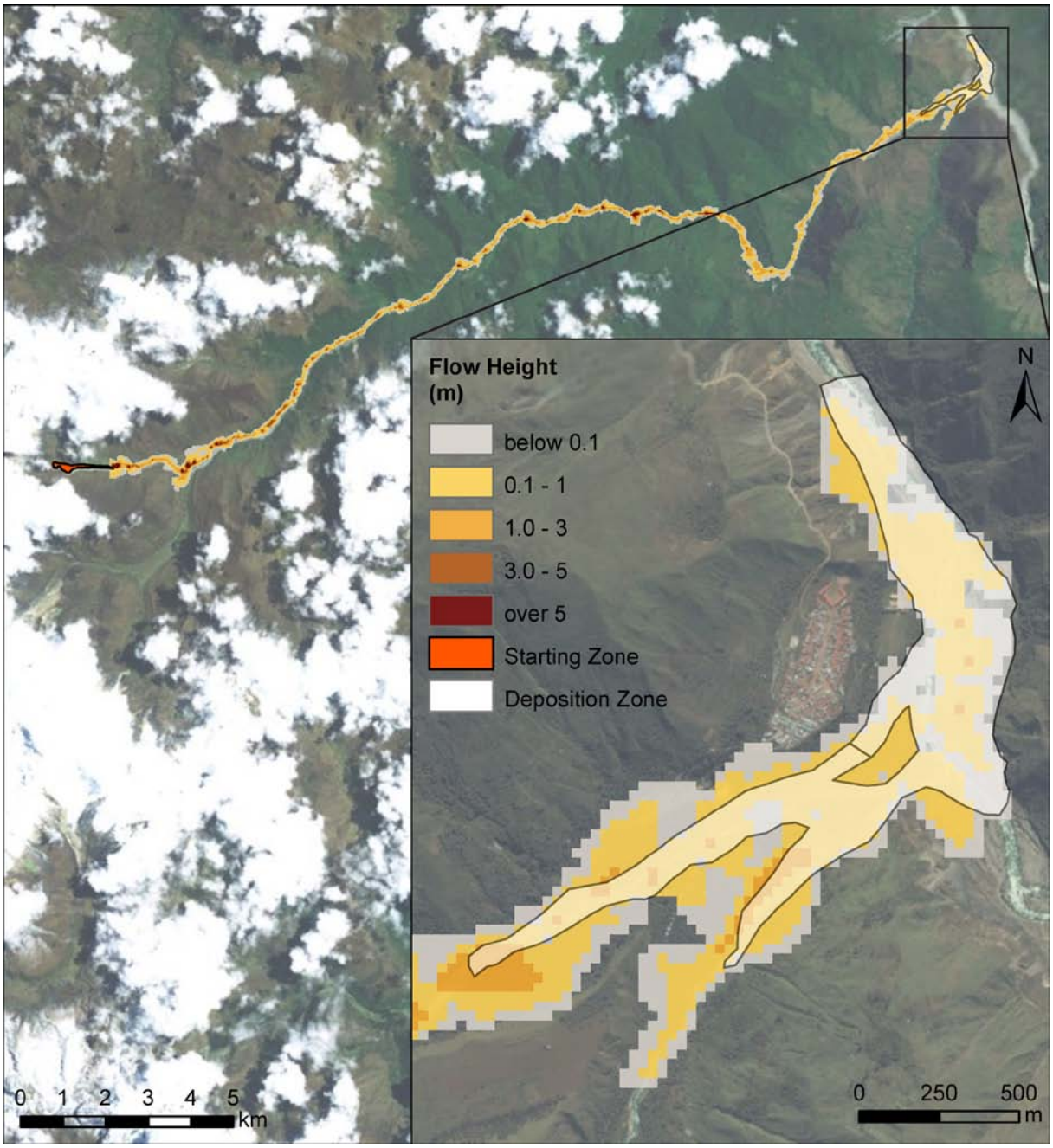

Figure 7.14: 2D illustration of the Sacsara event.

The simulation stopped after 22500 s, with less than 10% of the mass moving. The simulation corresponds well to the deposition file, except for a DEM shift of 1 pixel westward around Santa Teresa and rather large spreading. Some differences in extent are also visible in Urubamba valley. Spreading is too large south of Santa Teresa and too low north of it (most of the flow north of Santa Teresa in Urubamba valley is below 0.1 m and can be discarded). Another difference is that the debris flow does not split in two forks directly southeast from Santa Teresa. No outflow on the flow path was detected.

Flow height is again too low (around 0.5 m - 1 m at Santa Teresa). Based on videos and images, total flow height is an estimated 2 - 5 m, needing 2 - 10 similar surges to reach this height (this corresponds well with reports, where 5 major surges reported) (see discussion).

Flow velocity is fast at the beginning (due to 15 m/s input velocity and steep terrain), then very slow in Mukayoc, the first deposition zone (1 - 2 m/s), only to accelerate again to 4 - 10 m/s (7 - 8 m/s on average) in the valley until 8 km upstream of Santa Teresa. There, the slope slowly flattens, the valley broadens, and the debris flow has to flow around two tight curves. These curves slow down the flow to around 5 m/s. The flow spreads exactly where the old village of Yanatile was, where the valley is broader. This is realistic, as Yanatile got destroyed in the 1998 event. 2 km upstream from Santa Teresa, the valley gets flatter and broader again, which decreases velocity to 2 - 3 m/s until Santa Teresa. Modeled average velocity from Mukayoc to Santa Teresa is comparable to the 6 m/s mentioned in reports. On videos, flow velocity of near Santa Teresa seems larger than 2 - 3 m/s. From Mukayoc to Santa Teresa, 45 - 50 calculation steps at 300 s each are necessary in the simulation. This would result in a velocity of only 1.8 - 2.2 m/s based on an estimated distance of 27 - 30 km (depending on the exact path of the river and flow), as opposed to velocities simulated being around 7 m/s.

7.3.3 Comparison to SRTM

In this section, calibration simulations from above are compared for ASTER GDEM2 and SRTM DEM, in order to test DEM influence on model results. All input parameters except the used DEM were kept constant.

With the SRTM DEM, the Ahobamba event stopped after 17400 s with less than 10% of the mass moving (ASTER: 30,000 s and 14%). Runout is lower than for ASTER, as it stayed for about 12000 s (calculation steps) at nearly the same location, just after the confluence with Urubamba. Flow velocity is 7 - 25 m/s (12 m/s on average) in Ahobamba (ASTER: 3 - 12 m/s; on average 6 - 8 m/s). Flow height is 1 - 7 m (2 m on average) in the valley (ASTER: 8 - 15 m; on average 10 m). At the confluence it is 1.5 - 2.5 m (2 m on average) as compared to 2 - 4 m (3 m) in ASTER.

The Sacsara event stopped after 13800 s with less than 10% of the mass moving in the SRTM DEM (ASTER: 22500 s and 10%). Runout is larger than for ASTER. Flow velocity is 5 - 20 m/s (average 10 m/s) as opposed to 4 - 10 m/s (7 - 8 average) in ASTER. Flow height is between 0.3 m and 2 m with 0.5 - 1.5 m near Santa Teresa, which is comparable to ASTER (0.5 - 1 m at Santa Teresa).

Runout increases with lower resolution; except in Ahobamba, but there artifacts in the SRTM DEM distort results. Simulations with lower resolution (SRTM DEM) stop earlier (13800 s as compared to 22500 s).

Fig. 7.15 shows large differences in flow height between ASTER GDEM2 and the SRTM DEM for the Sacsara event. No pattern is discernible. ASTER S0047 is the calibration simulation with ASTER GDEM2 for Sacsara, SRTM S001 it's counterpart in the SRTM DEM.

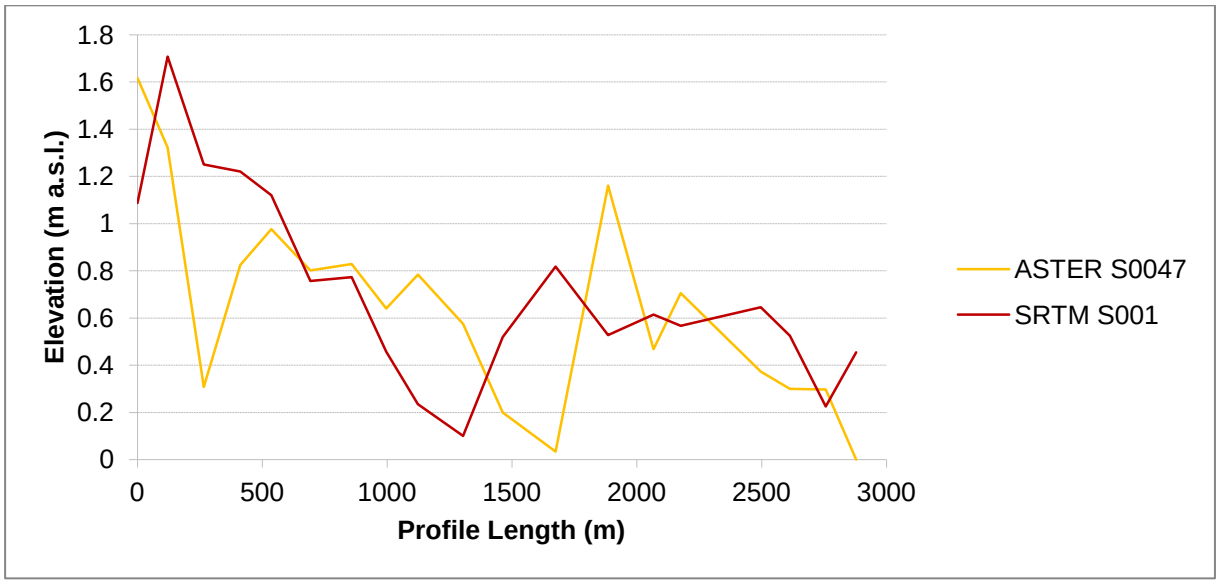

Figure 7.15: Flow heights in the deposition zone near Santa Teresa for varying DEMs.

Fig. 7.16 shows flow velocity differences between ASTER GDEM2 and the SRTM DEM for the Sacsara event. Velocity is much smaller for higher resolution (30 m in ASTER compared to 90 m in SRTM). Differences are very large, due to different flow paths.

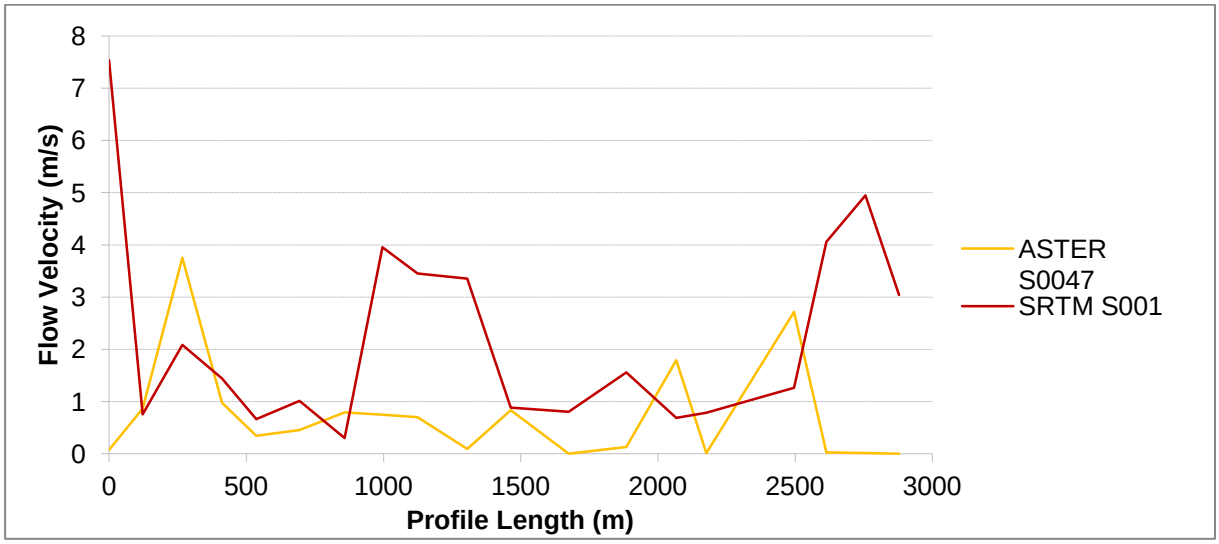

Figure 7.16: Flow velocities in the deposition zone near Santa Teresa for varying DEMs.

8 Scenario Modeling

Scenario modeling was made with the bilinear interpolated ASTER GDEM2 with 30 m resolution and filled sinks. μ, volume and discharge depend on the starting zone and were selected as indicated in Section 5.3. Other input parameters are based on the sensitivity analysis and were chosen as follows: ξ of 1000; 15 m/s input velocity; t1 varying between 60 s and 300 s depending on volume; Lamda and h cutoff constant; second numerical scheme; stop criterion 10% of moving mass; 30,000 s simulation end time and a hydrograph starting zone at the lower boarder of the starting zone. Scenarios are based on the fact that the largest single surge volume is of higher importance than the total volume of the events.

Table 8.1: Comparison of scenarios most similar to the 1998 events (Aho means Ahobamba, Sacs means Sacsara and Salc means Salcantay). Only the scenario with comparable volume to past events (out of three scenarios made per starting zone) was directly compared with calibration results (Table 8.1) – smaller or larger scenarios were used for hazard assessment only.

Scenario Comparison									
Event	**Aho 1998**	**Sacs 1998**	**Aho Sisay-pampa**	**Aho Land-slide**	**Aho Mana-mayo**	**Sacs Debris Glacier**	**Sacs Hanpi K'ocha**	**Salc Glacier Lake**	**Salc Totora**
Simulation	0064	0047	A002	A020	A023	Sac002	Sac011	Sal009	Sal018
Scenario	-	-	Medium	Medium	Medium	Medium	Small	Large	Large
Volume (mill. m^3)	1	0.5	1	1	1	1	1	2	3
Stop	14% 30,000s	10% 22,500s	11% 30,000s	10% 18,000s	14% 30,000s	10% 20,700s	10% 28,200s	20% 30,000s	10% 26,700s
Flow Height (m)	2-4 (3)	0.5-1 (0.7)	2-4 (3)	3-7 (5)	2.5-4 (3)	0.5-2 (1)	0.5-2.5 (1)	0.5-2 (1)	1.5-5 (3)
Flow Velo-city (m/s)	3-12 (7)	4-10 (7)	5-13 (7)	7-20 (12)	5-15 (8.5)	5-12 (7)	4-12 (6.5)	3-12 (6)	4-17 (7.5)

The volumes in Table 8.1 correspond to the largest single surge volume, not the total volume. Stop means either the end time condition (in seconds) or the amount of mass still moving (in %). Flow height was estimated at the deposition zones (at the confluence with Urubamba), flow velocity in the valley path. In brackets, average values are given.

For Salcantay, the medium scenarios (the most similar to 1998) did not reach Santa Teresa as calculation time was too short. Thus, the large scenarios were taken for comparison. Flow heights and velocities generally are comparable for all scenario simulations with the 1998 events. However, A020 showed much higher flow heights and velocities. In Salcantay, average and maximum velocities are lower than for Ahobamba and Sacsara. Volumes were simulated from 100,000 m^3 to 10 mill. m^3, with corresponding discharges of 500 - 10,900 m^3/s. μ varies between 0.07 and 0.15. An overview of all scenario simulations is given in Fig. 8.1 (page 71).

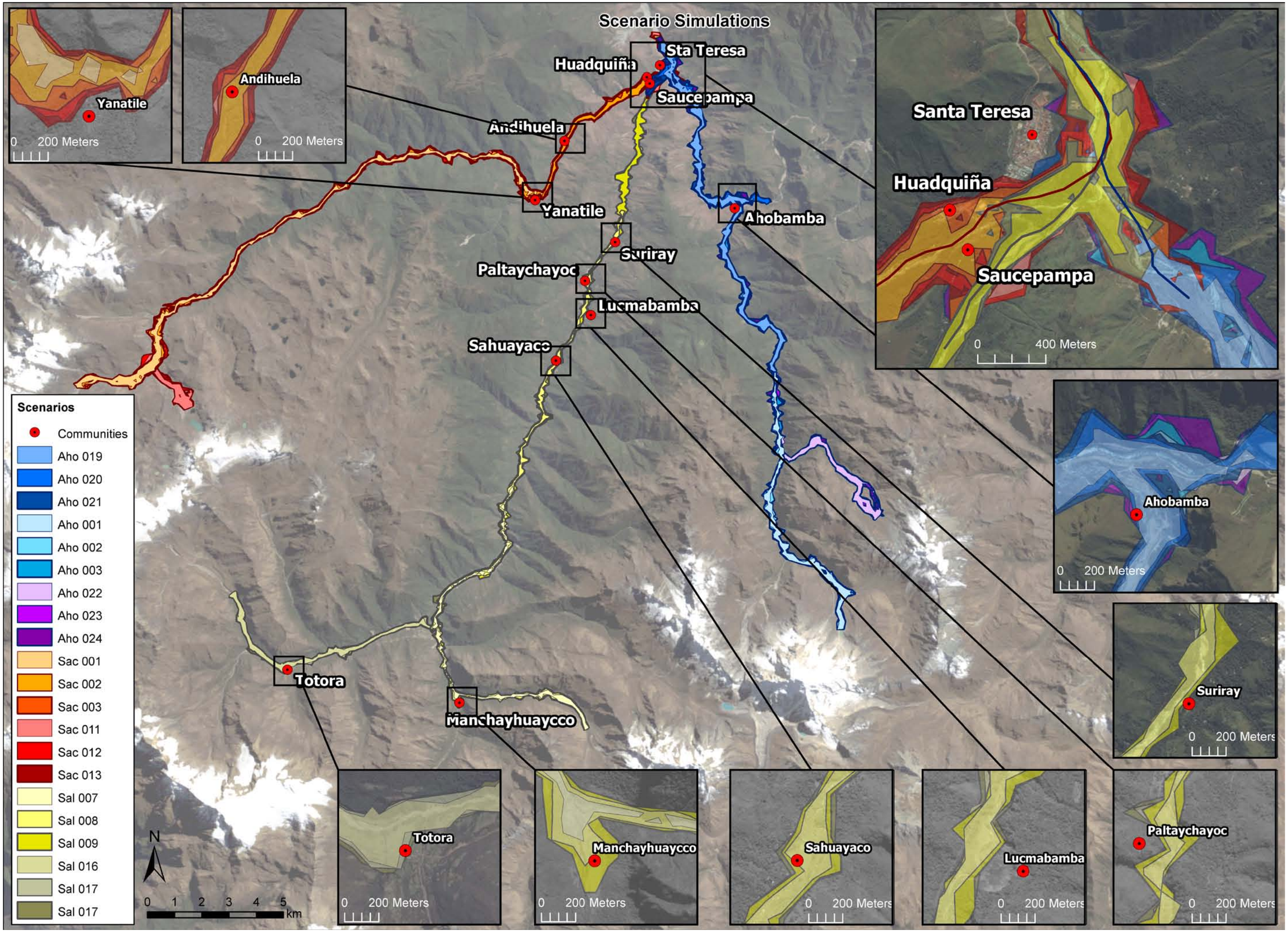
Scenario Simulations
Sta Teresa
Huadquiña
Saucepampa
Andihuela
Yanatile
Ahobamba
Suriray
Paltaychayoc
Lucmabamba
Sahuayaco
Totora
Manchayhuaycco
Yanatile
0 200 Meters
Andihuela
0 200 Meters
Santa Teresa
Huadquiña
Saucepampa
0 400 Meters
Ahobamba
0 200 Meters
Suriray
0 200 Meters
Totora
0 200 Meters
Manchayhuaycco
0 200 Meters
Sahuayaco
0 200 Meters
Lucmabamba
0 200 Meters
Paltaychayoc
0 200 Meters
Scenarios
Communities
Aho 019
Aho 020
Aho 021
Aho 001
Aho 002
Aho 003
Aho 022
Aho 023
Aho 024
Sac 001
Sac 002
Sac 003
Sac 011
Sac 012
Sac 013
Sal 007
Sal 008
Sal 009
Sal 016
Sal 017
Sal 017
N
0 1 2 3 4 5 km

Figure 8.1: All scenario simulations, colored depending on their origin: blue-violet for Ahobamba, red-orange for Sacsara and yellow-grey for Salcantay. Darker colors and bolder outlines represent larger scenarios. The bold lines in the inset map of Santa Teresa are the profile-lines used for flow heights and velocities of corresponding simulations (see Sections 8.1 - 8.3). Flow heights below 0.1 m were discarded.

The area of Santa Teresa is endangered by all three subcatchments. The highest hazard potential comes from Sacsara, followed by Salcantay and Ahobamba; as long as process interactions are not considered. The communities of Huadqiña and Saucepampa can be considered relatively save from Ahobamba and Salcantay; however Sacsara shows a large hazard potential. For more information on Santa Teresa area, see Section 8.4 “Hazard Map”.

8.1 Ahobamba

Simulations Aho 001 to Aho 003 model a GLOF from Laguna Sisaypampa (east of Rayancancha, with volumes of 300,000 m^3, 1 mill. m^3 and 2.5 mill. m^3 and a dam height of 5 m/10 m/ 20 m, resulting in discharges of 1,200 m^3/s, 2,600 m^3/s and 5,100 m^3/s. μ is 0.11. Simulations 002 and 003 can not be completely modeled as they take longer than 30,000 s to stop (after 30,000 s, still 11% and 14% of the mass was moving). Velocity seems reasonable in simulations but not calculation steps (see Section 9.3). Outflows of 4,000 m^3 (small scenario) and 270,000 m^3 (large scenario) along the flow path were registered.

Simulations Aho 019 to Aho 021 model a debris flow triggered by slope instability from 8 km upstream of the confluence with Urubamba with volumes of 500,000 m^3, 1 mill. m^3 and 3 mill. m^3, corresponding dam heights of 5 m/ 10 m and 20 m, resulting in discharges of 1,500 m^3/s, 2,600 m^3/s and 5,500 m^3/s. μ is 0.07. The largest single surge volume can come down maximum 13 times, assuming a total volume of 40 mill. m^3. No outflow along the flow path was detected.

Simulations Aho 022 to Aho 024 model a debris flow triggered by slope instability in Manamayo valley east of Ahobamba with volumes of 500,000 m^3, 1 mill. m^3 and 3 mill. m^3, corresponding dam heights of 5 m/ 10 m and 20 m, resulting in discharges of 1,500 m^3/s, 2,600 m^3/s and 5,500 m^3/s. μ is 0.15. Simulations 023 and 024 can not be completely modeled as they take longer than 30,000 s to stop (after 30,000 s, still 14% and 12% of the mass was moving). Velocity is very low. The starting zone was chosen on the lower boarder of a large debris accumulation below a glacier, not at a small lake nearby, as distance is comparable but the debris has a larger potential volume. The largest single surge volume can come down maximum 7 times, assuming a total volume of 20 mill. m^3. No outflow along the flow path was detected.

Fig. 8.2 shows flow height profiles for all scenarios from Ahobamba reaching Santa Teresa. A003 is a GLOF; the other scenarios are triggered by slope instability. Compared to the event in 1998, flow heights are much larger.

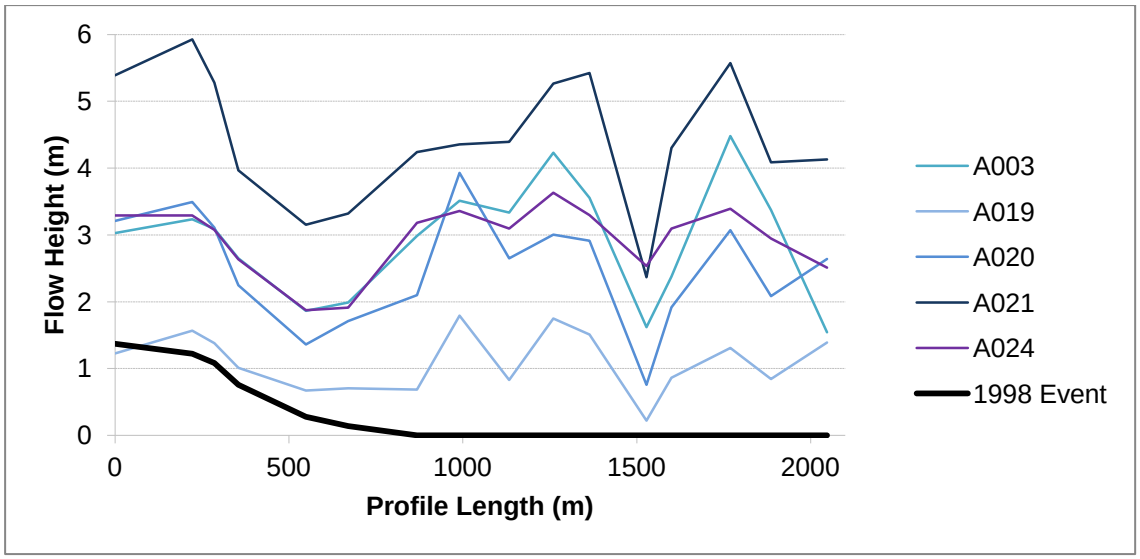

Figure 8.2: Flow heights in the deposition zone near Santa Teresa for different scenarios from Ahobamba.

The community of Ahobamba is endangered by future debris flows from Ahobamba, as scenario simulations show. Potential debris flows can damage Ahobamba or agricultural land in its surroundings. Ahobamba community is situated at the border of the hazard zone, but as stated before the hazard zone might be larger due to several succeeding surges or DEM errors. Monitoring is recommended.

8.2 Sacsara

Simulations Sac 001 to Sac 003 model a GLOF from a debris-covered glacier forming ponds, south of the starting zone of the 1998 event, with volumes of 300,000 m^3, 1 mill. m^3 and 2.5 mill. m^3, corresponding dam heights of 5 m/10 m and 20 m, resulting in discharges of 1,200 m^3/s, 2,600 m^3/s and 5,100 m^3/s. μ is 0.08. Velocity is low. This scenario is has larger runout than the calibration for the Sacsara event, due to lower μ. Outflows of 80,000 m^3 (small scenario) and 250,000 m^3 (large scenario) along the flow path were registered.

Simulations Sac 011 to Sac 013 model a GLOF from lake Hanpi K'ocha east of the Sacsara starting zone in 1998 with volumes of 1 mill. m^3, 5 mill. m^3 and 10 mill. m^3, corresponding dam heights of 10 m/ 20 m and 30 m, resulting in discharges of 2,600 m^3/s, 6,800 m^3/s and 10,900 m^3/s. μ is 0.09. Two lakes are located just next to each other, an outburst of the upper one (Volume: 4.3 mill. m^3) would consequently trigger an outburst of the lower one (Volume: 400,000 m^3). Velocity is low, as two tight curves in the valley slow the flow. Overall, velocity seems realistic. No outflow along the flow path was detected.

Fig. 8.3 shows flow height profiles for all scenarios from Sacsara reaching Santa Teresa. All modeled scenarios from Sacsara are GLOF dam failures, where the potential total volume was simulated to come down in one surge. This results in much higher flow heights compared to the 1998 event.

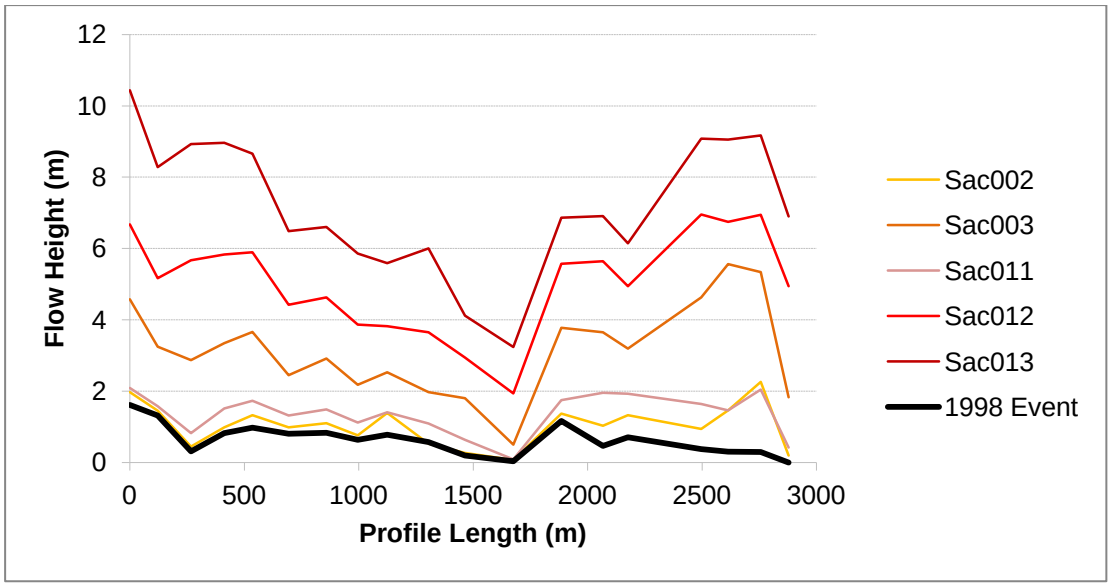

Figure 8.3: Flow heights in the deposition zone near Santa Teresa for different scenarios from Sacsara.

Yanatile and Andihuela are both endangered by future debris flows from Sacsara. The old community of Yanatile was completely destroyed by the 1998 debris flow from Sacsara. The new village was rebuilt outside the major hazard zone; no scenario was simulated to directly affect Yanatile. Andihuela on the other hand is located right in the middle of the potential debris flow path and shows high hazard potential. As hazard zones might be larger due to several succeeding surges or DEM errors, also Yanatile can not be considered safe. Except one scenario simulation only reaching Yanatile, all reach Andihuela and can potentially damage the communities or agricultural land in their surrounding. Monitoring for both communities is recommended.

8.3 Salcantay

Simulations Sal 007 to Sal 009 model a GLOF from a supra-glacial lake west of Nevado Tucarhuay and south of Huamantay valley, with volumes of 100,000 m^3, 500,000 m^3 and 2 mill. m^3, corresponding dam heights of 2 m/ 5 m and 10 m, resulting in discharges of 500 m^3/s, 1,500 m^3/s and 3,500 m^3/s. μ is 0.08. Simulations 008 and 009 can not be completely modeled as they take longer than 30,000 s to stop (after 30,000 s, still 22% and 20% of the mass was moving). The lake is very small, most is ice and debris. Outflows of 3 m^3 (small scenario) and 200,000 m^3 (large scenario) along the flow path were registered.

Simulations Sal 016 to Sal 018 model a debris flow triggered by slope instability in Totora valley in the west of Salcantay, with volumes of 500,000 m^3, 1 mill. m^3 and 3 mill. m^3, corresponding dam heights of 5 m/ 10 m and 20 m, resulting in discharges of 1,500 m^3/s, 2,600 m^3/s and 5,500 m^3/s. μ is 0.07. Simulations 016 and 017 can not be completely modeled as they take longer than 30,000 s to stop (after 30,000 s, still 13% and 15% of the mass was moving). Velocity is again low, due to some tight curves decreasing flow velocity. The lower erosion scar was taken as starting zone, as spreading on the upper area proved unrealistically large. However, μ was derived based on the erosion scar on the top, as the event would probably start there due to steeper slopes. The largest single surge volume can come down maximum 10 times, assuming a total volume of 30 mill. m^3. No outflow along the flow path was detected.

Fig. 8.4 shows flow height profiles for all scenarios from Salcantay reaching Santa Teresa. Flow heights for scenarios from Salcantay are very different, being smaller for a GLOF (Sal009) than a debris flow triggered by slope instability (Sal 018). However the total volume of a GLOF in Salcantay is limited, in contrast to large debris accumulations in side valleys. Note that the volume of Sal009 is 2 mill. m^3 and of Sal 018 3 mill. m^3. Flow heights seem realistic considering the large volumes involved.

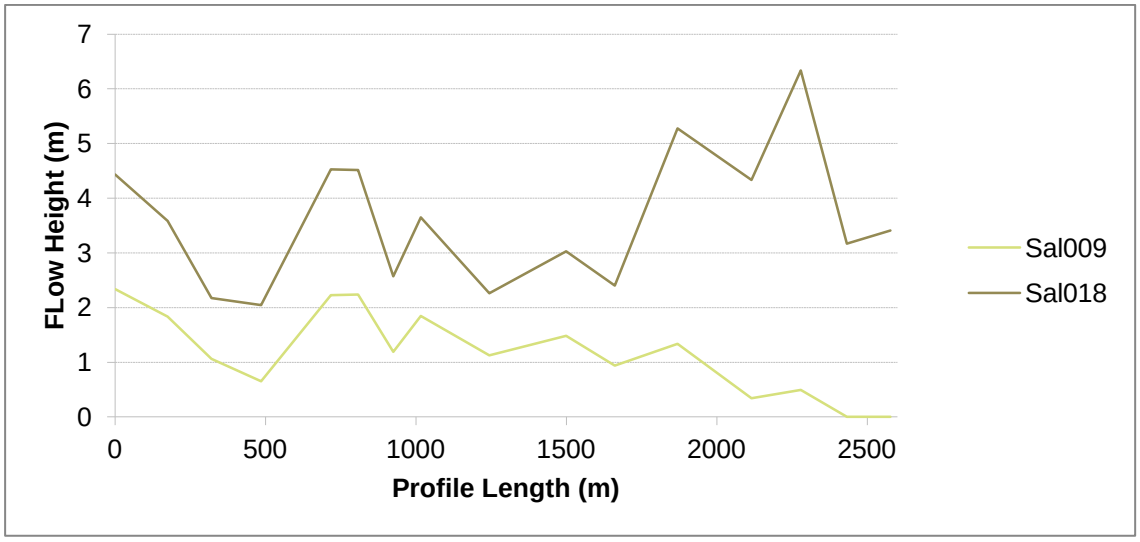

Figure 8.4: Flow heights in the deposition zone near Santa Teresa for different scenarios from Salcantay.

The communities of Totora, Manchayhuaycco, Sahuayaco and Suriray are endangered by potential debris flows from Salcantay. They are all located on the boarder of the hazard zone, but this does not mean they have no risk. Lucmabamba and Paltaychayoc are outside the modeled flow paths but could still be affected. Monitoring is recommended for both Salcantay starting zones.

8.4 Hazard Map

Fig. 8.5 shows a preliminary hazard map for Santa Teresa area. The highest hazard potential is exactly at the confluence between Sacsara, Salcantay and Urubamba, as debris flows from all three subcatchments (Ahobamba, Sacsara, and Salcantay) can reach this area. Note that the old village of Santa Teresa lies partly in a zone of high hazard potential (over 24). The part that got only partly destroyed is in a zone of medium hazard potential. Above hazard map shows that Santa Teresa village (and the communities of Saucepampa and Huadqiña) cannot be considered safe. Especially Saucepampa and Huadqiña are endangered, being in a similar hazard potential classification as the northern part of the old village Santa Teresa.

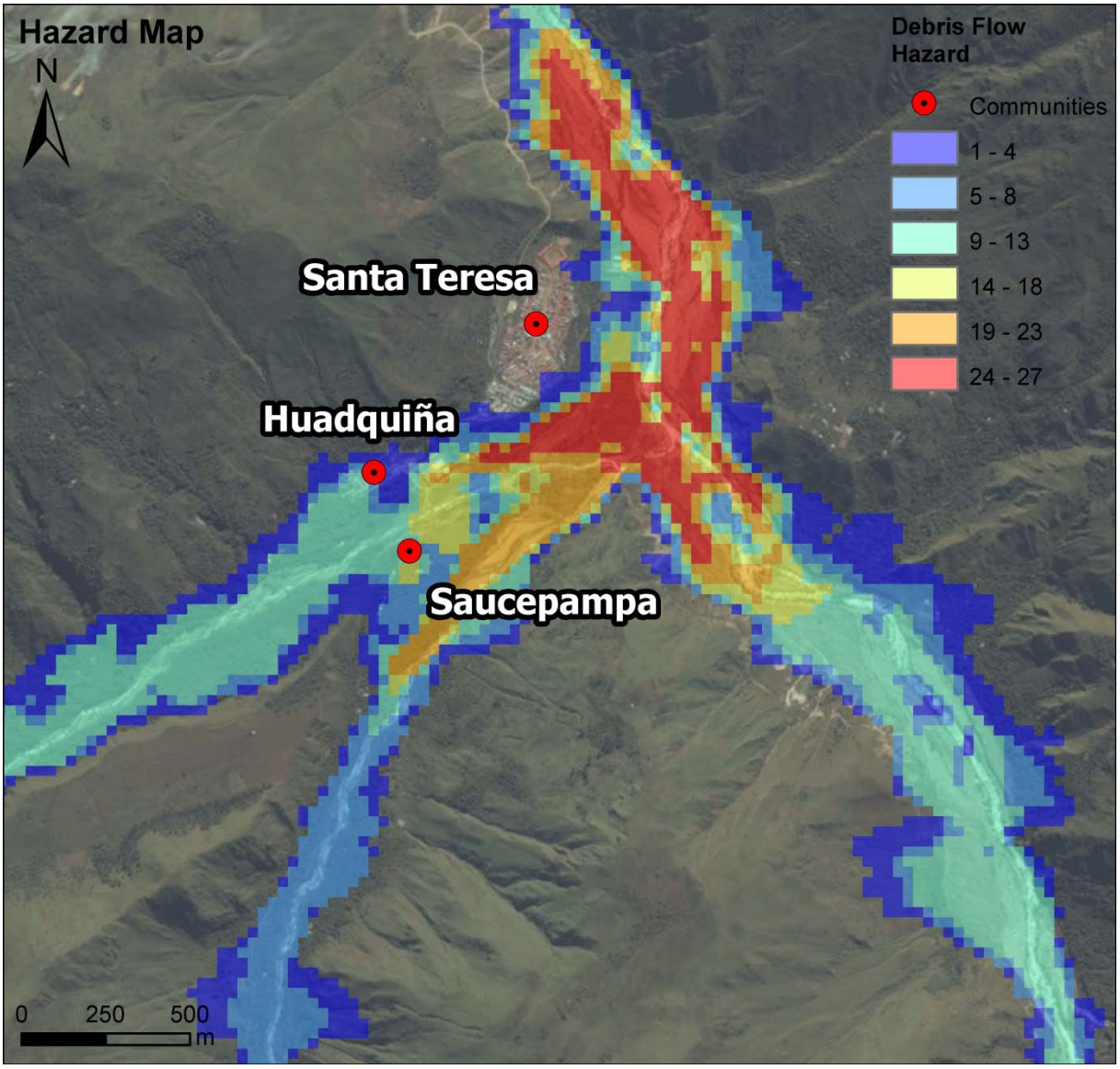

Figure 8.5: Preliminary hazard map for Santa Teresa. Affected areas are summed up, with a weighting of 3 for small, 2 for medium and 1 for large flows, which should qualitatively reflect their probability. Large values in the hazard map (red) correspond to a high danger of being affected by an event. Inundation depth is not shown in the hazard map, as intensity is more relevant and can be considered high wherever such large events affect an area.

The small areas indicating potential inundation of the new village of Santa Teresa is most likely a product of DEM inaccuracy, as Santa Teresa is located 40 m - 60 m above the river basin (based on Google Earth data, which is also afflicted with uncertainty). Although the new village appears safe from direct impact from future debris flows, an unknown residual risk exists due to potential DEM errors and multiple possible surges. Especially process interactions; mainly temporal dammings of either of the 3 subcatchments or Urubamba; could affect the new village of Santa Teresa. Also, as Giráldez et al. (2012) found, the hill Chilcapata, where Santa Teresa was rebuilt on, is slowly sliding, which is a further potential hazard.

Table 8.2 shows the reclassification of all scenarios and the 1998 events. Flow heights below 0.1 m were discarded. “Ignored” means that the debris flow did not reach Santa Teresa. “over 10” means that a simulation might have reached Santa Teresa, but did not as still over 10% of it's mass were moving. Whenever “over10” happened, the next largest simulation reaching Santa Teresa got a classification higher by 1. This was also done for scenarios stopping very close to Santa Teresa due to low mass movement, as runout could be slightly increased for several surges. Values 1, 2 and 3 correspond to large, medium and small scenarios (small ones having a higher “probability” of happening).

Table 8.2: Reclassification scheme for all scenario simulations.

Simulation	Size	Reclassification
A001	Small	ignored
A002	Medium	over10
A003	Large	2
A019	Small	3
A020	Medium	2
A021	Large	1
A022	Small	ignored
023	Medium	over10
A024	Large	2
Sac001	Small	ignored
Sac002	Medium	2
Sac003	Large	1
Sac011	Small	3
Sac012	Medium	2
Sac013	Large	1
Sal007	Small	ignored
Sal008	Medium	over10
Sal009	Large	2
Sal016	Small	over10
Sal017	Medium	over10
Sal018	Large	3
Sacs0047	Calibration	3
Aho0064	Calibration	ignored

Hazard analysis shows that potential debris flows can be as large as or even larger than what happened in 1998. The probability for these flows is not known, making hazard mitigation measures a challenging part of the CCA DRR project. Note that this hazard map is highly qualitative and but a rough assessment of potential hazards in Santa Teresa.

9 Discussion

This chapter discusses the results obtained in Chapters 6 - 8 based on the background provided by Chapters 2 and 3. Sections 9.1 - 9.5 correspond to the 5 goals of this thesis mentioned in Section 1.4.

9.1 Climatic and Geomorphologic Conditions in the Study Region

As seen in Chapters 2 and 3, the study region is highly vulnerable to mass movements (Carey, 2005). Slopes were very steep for both events and lowered the critical pore pressure for debris flow initiation (Iverson et al., 1997). Slopes over 40° are common in the area, and are most prone to slope failures (Lehmann & Or, 2012). A lot of morainic, loose material on fractured bedrock is present. Strong El Niño years (like from 1997 - 1999) can lead to higher temperatures and higher precipitation (Carlotto et al., 1999; Curtis et al., 2001). Glacier debuttressing in the starting zones destabilizes morainic material. Glacier retreat produced a lot of erodible sediment. El Niño and glacier debuttressing, together with glacier melt and permafrost thaw near the starting zones, influence variable disposition in the study region. Data is limited for all topics; none is available concerning vegetation, soil cover, grain size distribution, lithology and hydrological properties like porosity or permeability.

Potential starting zones (Section 3.5) were delineated by hand with Google Earth, as Landsats resolution is too low and Google Earth not freely available to allow for automatic delineation (as in Huggel et al., 2004). Slopes in some starting zones are rather low, but comparable to the 1998 starting zones. Starting zones are surrounded by steeper slopes that can produce other mass movements like ice- or rockfalls. The exact location of potential starting zones does not matter much for modeling (see Section 7.2.7), and communities are all farther downstream than the starting zones chosen. Potential starting zones can be considered representative of the event spectrum, with different positions, volumes and (simplified) trigger conditions (slope instabilities and dam-break).

9.2 Trigger Analysis

As seen in Section 2.2.3.3, precipitation and snowmelt are crucial for triggering debris flows, as they can increase pore water pressure (Costa, 1984; Iverson, 1997). These factors can be increased by both El Niño (Curtis et al., 2001) and climate change (see Section 3.3.1).

As Section 6.1.1 showed, quality of ground measurements of precipitation and temperature is limited. Only few SENAMHI stations containing data for 1998 exist in the study region; and they are often situated far from the starting zones. SENAMHI stations have different and sometimes changing acquisition techniques (Raissig, 2011). Errors from SENAMHI stations can not be visualized with error bars, as it is possible in manual stations that mistakes are absolute – e.g. a precipitation measure of 2.1 mm could have been recorded as 21mm, and vice versa (see also Section 4.3.1). As “no data” was sometimes reported as “0 precipitation”, climatic, monthly and yearly precipitation amounts can be higher than what SENAMHI data suggests. SENAMHI data errors can only be given qualitatively; no statistical tests were conducted. To better quantify data quality for SENAMHI stations, a direct visit with manual checking of the archives and the stations would be necessary.

Spatial correlation of SENAMHI stations is low, as precipitation in the study region is convective. Precipitation can fall very locally and some precipitation events might not be registered due to the limited number of stations in the area. This leads to strongly varying daily precipitation amounts, which induces large uncertainty on debris flow formation, as debris flows are local phenomena. Precipitation measurements are uncertain due to complex topography, convective precipitation, low data availability and uncertain data quality. Precipitation amounts can only be roughly estimated for the area. Estimates improve for longer time periods (e.g. for antecedent rainfall) and when compared with TMPA data.

TMPA data is a merged product and rarely directly measured; uncertainties are larger for short time periods and for high precipitation variability (Scheel et al., 2011), as is the case for this thesis. TMPA data is spatially plausible; tiles closer to each other have more similar values. Also, TRMM tiles close to SENAMHI stations show values comparable to the ground station (e.g. Ahobamba East has less precipitation, so has Urubamba). Nevertheless, TMPA and SENAMHI show different precipitation amounts, but precipitation event occurrence is comparable. Temporal aggregation increases correlation. Precipitation amounts are underestimated below 2 mm/d and are overestimated above, leading to a general overestimation of precipitation in TMPA (Scheel et al., 2011). Note that also SENAMHI data could be underestimated, as sometimes no data was being reported as 0 precipitation. Very low precipitation amounts can be the result of clouds included in TMPA estimates (Scheel et al., 2011). 3-hour TMPA errors are roughly twice the 3-hour precipitation (NASA, 2013a).

Results in Section 6.1.4 indicate that pre-event precipitation was high for both events. Concerning short-term precipitation (on the day of the event), no significant precipitation amounts were registered for the Ahobamba event. For the Sacsara event, TMPA data indicates that heavy rainfall affected the area. The values for 6-day precedent precipitation found by Klimeš et al. (2007) correspond well with the findings of this thesis, were a pre-event (1 week) precipitation of around 60 mm is estimated for the Sacsara event and 40 mm for Ahobamba. Daily precipitations for events evaluated by Klimeš et al. (2007) are not necessarily high. This means that short-term pre-event precipitation seems to play a more important role than precipitation on the event day, as was also concluded by Klimeš et al. (2007). From stations containing data for 1998, Quillabamba shows the most similar precipitation to Machu Picchu station (close to Santa Teresa). No weighted pre-event precipitation average was made, as Machu Picchu station is still far from the starting zones. Long-term pre event precipitation (from August to December 1997) was wetter than average in Quillabamba. It is possible that this played a role in the continuous saturation of the starting zones over a long period of time.

Section 6.1.5 indicates that daily precipitation over 50 mm is possible in the area, with up to 25 mm within an hour. A one-hour time interval is too short for being resolved in measurement stations, as precipitation in small, steep basins can strongly vary (Costa, 1984). As the study region is very mountainous, locally high hourly and sub-hourly precipitation peaks are possible, exceeding critical rainfall amount. It is possible that SENAMHI stations did not resolve locally high precipitation peaks before the events; which is also what Klimeš et al. (2007) assume. This fact is also funded by the TMPA showing consistently higher precipitation before the Sacsara event compared to most SENAMHI stations (situated farther away). In conclusion, locally much higher precipitation amounts than registered, falling within a short time period, were possible for both events. When also considering witness reports (Carlotto et al., 1999), high event-day precipitation for Sacsara and low event-day precipitation for Ahobamba are likely. The Sacsara event was therefore likely triggered by event-day precipitation, the Ahobamba event by pre-event precipitation.

Both low and high temperature influence debris flow activity. Low temperatures cause freeze-thaw cycles that increase erosion and debris production (the starting zones being located at 3,950 – 4,250 m a.s.l. (Ahobamba) and 4,200 – 4,450 m a.s.l. (Sacsara)). High temperatures are directly related to snowmelt rates (e.g. with the degree-day factor concept) and increase snowmelt and meltwater infiltration into loose debris.
Due to climate change and the El Niño phase of 1997 - 1999, temperatures were higher than average, increasing snow and ice melt (see e.g. Carlotto et al., 1999) and permafrost thaw. Meltwater percolating into the ground is an important trigger for debris flows (Saemundsson et al., 2003; Haeberli et al., 2010), especially when continuing over a long time, as is indicated by temperature data. As the starting zones of the 1998 are free of snow, ice and permafrost, permafrost thaw and snowmelt can be excluded as a direct trigger for both events. However, melt and thaw on the surrounding higher peaks added moisture, saturating the starting zones (see also Huggel et al., 2012d). Higher temperatures over a long time could have led to rock instabilities due to more freeze-thaw cycles, increasing debris production and decreasing its stability.

The earthquake of January 10th 1998 destabilized the loose debris accumulations of both starting zones. This effect was strengthened due to high precipitation amounts during the earthquake near the Sacsara starting zone. Earthquakes destabilize slopes for up to several years (Marui & Nadim, 2009; Kazuo et al., 2009) and thus certainly influenced Sacsara and probably also Ahobamba.

Although the El Niño phenomenon was argued to have caused the 1998 events (Hermoza et al., 1998), this is a strongly simplified explanation. Neither climate change can be “held responsible” for these flows. Much more, a critical combination of earthquakes, high temperatures, antecedent precipitation, strong short term-precipitation (for Sacsara) and a high basic and variable disposition caused these catastrophic events. The 1998 events are highly atypical, usually such large events are triggered by earthquakes or volcanic eruptions (see Section 9.2.4). Events like these occurring for the first time and/or with exceptionally high volume can be a sign of a system change (Huggel, 2004).

9.2.1 Ahobamba Reconstruction

Fig. 9.1 (page 81) shows all processes influencing the 1998 event in Ahobamba. Crucial for the Ahobamba event being triggered was the water input via groundwater flow and surface runoff from snow and glacier melt, permafrost thaw and long-term antecedent precipitation. All of these processes were increased due to El Niño. This water saturated the soil and increased its pore water pressure (Carlotto et al., 1999) on steep, debuttressed slopes. Debris was additionally destabilized by an earthquake, leading to slow landslides forming.
These landslides were deep-seated and did fail slowly, as local failed soil parts were supported by neighboring parts (Takahashi, 2007a) and complete liquefaction did not take place until the mass has moved some distance (Iverson et al., 1997). Finally, these landslides failed together and formed a debris flow, which accelerated quickly after the starting zone (Carlotto et al., 1999). Several lateral landslides in the valley lead to temporal dammings and their material got incorporated, explaining the very large volume of the event (see also Schuster, 2000; Cui et al., 2010). Finally, the Ahobamba event dammed the main river Urubamba up to 74 m (Carlotto et al., 1999). The artificial dam break initiated 4 months later produced a hyperconcentrated flow or debris flood (Hermoza et al., 1998).

The Ahobamba event fits well to the observations of Haeberli et al. (2010), who found that many slope failures occurred after exceptionally warm periods with subsequent refreezing of melt water in rock fissures, increasing pore water pressure additionally. Both Zimmermann et al. (1997) and Haeberli et al. (2012) state that landslides are the most common debris flow trigger in mountainous areas.

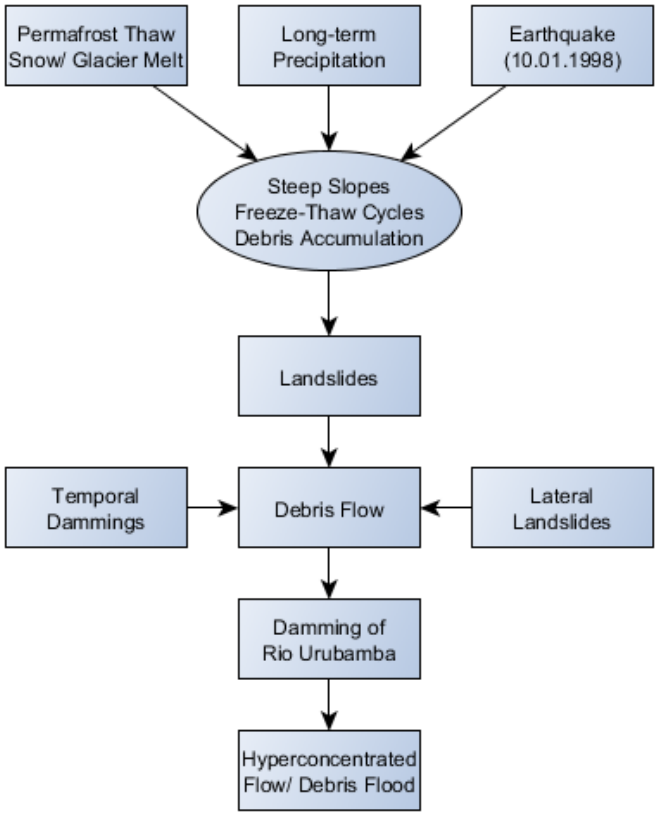

Figure 9.1: Processes involved in the Ahobamba event.

The Ahobamba event was the result of long-term precipitation. Critical water input for debris flow triggering decreases with increased duration of the input (Guzzetti et al., 2007b). Snowmelt could have increased the duration of constant water input significantly. This explains the Ahobamba event being triggered without notable short-term precipitation (from SENAMHI and TMPA data and witness reports). Long-term precipitation was higher than average for August to December 1997. Such long time spans can still influence debris flow triggering, saturating soils over long periods of time (M. Rohrer, pers. communication).

9.2.2 Sacsara Reconstruction

Fig. 9.2 shows the processes influencing the 1998 event in Sacsara. The Sacsara event had very similar triggers as the Ahobamba event. The main difference is that for Sacsara, no evidence of landslide activity was found and that short-term precipitation did play a much larger role.

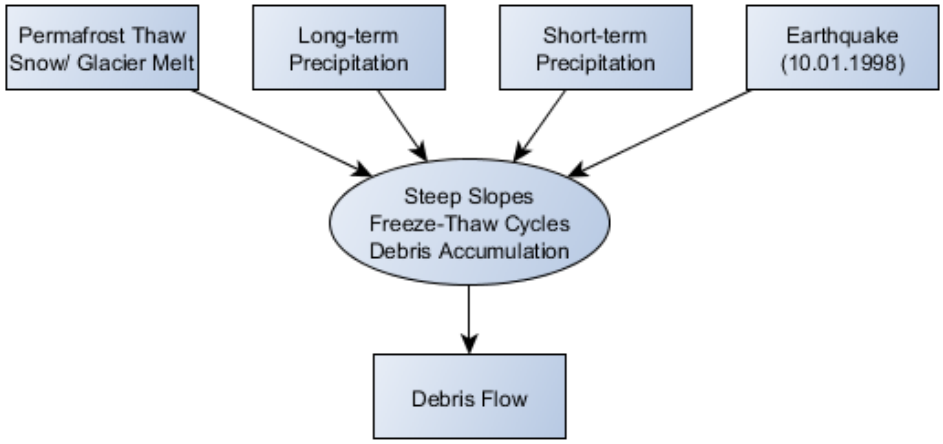

Figure 10.2: Processes involved in the Ahobamba event.

The Sacsara event started by sudden liquefaction of the whole slope (an "explosion-like" sound was heard by witnesses (Carlotto et al., 1999)). After the earthquake accompanied with high precipitation amounts 3 days prior to the event, another rainstorm on January 13th triggered the Sacsara debris flow, starting as a shallow landslide due to channel-bed erosion. Although data from TMPA and SENAMHI does not suggest very high precipitation, locally much higher amounts are possible (as suggested by witness reports) due to above-mentioned uncertainties. This second rainstorm was crucial. Marui & Nadim (2009) and Kazuo et al. (2009) state that the first rainstorm after an earthquake is most important, and Wieczorek & Glade (2005), Klubertanz et al.(2000) and Garland & Olivier (1993) all state that medium intensity, medium duration rainstorms raise pore water pressures above critical levels. Groundwater then rose until surface runoff appeared, started to incorporate debris and progressively destabilized the bed (see also Takahashi, 2007a; Tognacca & Bezzola, 1997).

9.2.3 Event Comparison

Table 9.1 below summarizes the most important characteristics of the 1998 events. First, general characteristics are listed, followed by starting zone characteristics and basic and variable disposition; flow behavior; deposition and triggers.

Table 9.1: Event comparison of the 1998 events.

Characteristics	**Ahobamba**	**Sacsara**
Type of Mass Movement	Debris-/ mudflow, then hyperconcentrated flow/debris flood	Debris flow
Debris flow Type	Viscous	Hybrid (between stony and viscous).
Volume (m^3)	25mill., then 50mill.	unknown (3 – 6 mill. estimated)
Starting Zone	saturated morainic material	
Starting Zone type	Type 1: Loose talus slope	
Catchment Slope	Mean 33°, Max 74°	Mean 29°, Max. 67°
Starting Zone Slope	between 10° and 40°	between 15° and over 50°
Material type	Water with mostly silty-sandy matrix, gravels	Water with mostly silty-sandy matrix, gravels, small blocks
Sediment Availability	Very high	
Stability of material	Very low	
Soil	no data	
Human impact	negligible	
Geology	First Cambrian, then Ordovician material	
Climate	Wet season, El Niño	
Glaciology	No Permafrost	
Vegetation	small bushes	
Velocity	no data, similar to Sacsara	Mean around 6 m/s, peak unknown
Intermittency	Very high (up to 300 surges)	Medium (5 larger surges, some minor)
Flow regime	Non-Newtonian, plastic, viscous, turbulent. later close to Newtonian	Non-Newtonian, plastic, Collisional-viscous, turbulent
Flow transformation	From deep-seated landslide to debris flow and hyperconcentrated flow/debris flood	From shallow landslide to debris flow
Runout	Around 50-200km	Around 30km
Antecedent Weekly P	around 40mm	Around 55mm
Event Day P	around 2mm	around 10mm
Antecedent T	21°C as compared to 19° (climatic average)	
Earthquake	Yes, 7 weeks prior	Yes, 3 days prior
Initiation	Slow failure	Sudden liquefaction
Main Trigger	Deep-seated slope instabilities (landslides)	Shallow slope instability due to precipitation

Both events showed a high degree of saturation. The large volume is explained by the large amount of erodible sediment in both starting zones but also (especially for Ahobamba) by large lateral erosion on the flow path. Also, glacier and permafrost thaw owned to climate change laid bare more morainic material, leading to debris flow volumes exceeding historical events (Zimmermann et al., 1997; Huggel, 2004). Intermittency is caused by the natural surging behavior of debris flows and in Ahobamba additionally by lateral landslides and temporal blockings. The very large runout of both events can be explained by the large volume, the friction reduction with velocity, fluidization and buoyancy effects, high water content, the shearing of the mixture, the velocity and reach dependency on slope and flow thickness. For antecedent and event day precipitation (P), the value is estimated based on results in Chapter 6 and witness reports ("high" or "low" precipitation). Temperature (T) is given for Anta Ancachuro on 3,340 m a.s.l..

9.2.4 Santa Teresa hazards in a worldwide comparison

Events in the scale of the ones analyzed in Santa Teresa region are scarce. However, several historic mass movements exist that were of comparable dimensions. USGS (2010) provides a good list of very large events. Triggers for debris flows or landslides of a reported magnitude of over 10 mill. m^3 were nearly always earthquakes or volcanic activity. For Peru however, various large mass movements triggered by rain, snowmelt or unknown causes are listed.
One of the most catastrophic mass movements in Peru was the Huaraz debris flow in 1941, where 4000 - 6000 people were killed. A debris flow with 10 mill. m^3 volume built a temporary river dam which later collapsed (Schuster & Highland, 2001). Two other large events originate from Nevado Huascarán in 1962 and 1970. Both mass movements transformed into a high-volume, high-velocity, mud-rich debris flow (Evans et al., 2009). While for the 1970 debris flow an earthquake of magnitude 7.9 was the trigger, the trigger for the 1962 event is unclear (Evans et al., 2009; Schneider, 2011) – similar to the event of Ahobamba.
In Argentina, a GLOF in 2009 produced a large debris flow transforming into a hyperconcentrated flow. The lake volume of 1×10^7 was emptied within 3 hours. The process chain probably was triggered by high antecedent rainfall, either causing the lake to overflow, ice blocks to break the dam or destabilizing the dam (Worni et al., 2012).
The largest known mass movements often show combinations and interactions between different processes, for example the Kolka-Karmadon rock-/ ice-avalanche, where interactions between unstable geology and geothermal conditions lead to a huge process chain with volumes exceeding 100 mill. m^3 (Haeberli et al., 2004).

9.3 Modeling

In order to simulate scenarios (Chapter 8), calibration of past events was made (see also Worni et al., 2012). Calibration was very challenging, as calibration criteria such as the exact runout, deposit, flow height or flow velocity are largely unknown. As no exact data is available, calibration is qualitative, based on visual assessment and designed to account for the worst case. Exact results are not possible without known input parameters (see also Walser, 2013). The exact reconstruction with all single surges is not possible due to the complexity of the process. In all simulations, it was evaluated if there is any outflow out of the calculation domain where this is not realistic. The influence of Mukayoc on debris flows in terms of potential impact dampening in Santa Teresa was not assessed.

Differences in flow height and flow velocity are larger in the valley part than in the deposition zone. However as the goal is to evaluate hazards for Santa Teresa (and to calibrate past events); this thesis is focused on flow height and velocity at the deposition zones. Note that the deposition zone does not

correspond to the largest runout, as the first surges of the flow did exceed the final estimated deposition area (C. Portocarrero, pers. communication). It is possible that the actual deposition area is larger, especially along Urubamba river, which eroded past deposition areas and rendered them invisible. As overall slope for Ahobamba and Sacsara was smaller than the minimum overall slope observed for coarse-grained debris flows in Switzerland (19%, Rickenmann & Zimmermann, 1993), it can be argued that the debris flows were rather muddy.

Simulated depositions correspond well with the estimated depositions at the confluence with Urubamba. Deposition zones were chosen to correspond to the area which was certainly flooded during the 1998 events. This means estimates are conservative and actual deposition zones were probably larger. Landslide scars on the opposite hill were not included, as these landslides were probably caused by erosion from the debris flow. Even if they were not, simulated debris flows would flow in these scars, as the DEM is from after the event. Exact depositions at the confluence with Urubamba are unknown and cut off, as fluvial erosion blurred deposition signs from the 1998 flows.

9.3.1 Input limitations

Modeling has several uncertainties, originating from the DEM, the model and the input parameters (see also Chapter 4). Concerning input parameters in general, a first major limitation is the limited data availability concerning input parameters and flow characteristics of historic events (see also Walser, 2013). Sensitivity analysis in Section 7.2 showed how this limiting knowledge of parameters can influence simulation results.

9.3.1.1 DEM

As shown in Sections 4.2 and 7.1, uncertainties for ASTER GDEM2 with 30 m resolution are considerable. The most problematic zones are steep northern slopes, where both starting zones are situated. In terrain as steep as in the study region, large uncertainties have to be expected. However, Christen et al. (2010a) state that large events such as the 1998 debris flows can be modeled with a DEM resolution lower than 25 m. It was found that the line with maximum flow height corresponds well to the lowest path in the GDEM. This means that based on the uncertain DEM, simulations itself show consistent results. In an ASTER GDEM2 with 30.7 m resolution; the flow took slightly longer to Santa Teresa with filled sinks and runout was reduced. Maximum velocity was significantly lower than without filled sinks. This is unrealistic, as a DEM with filled sinks should travel farther and faster with the same input parameters.

DEM evaluation (Section 7.1) showed that ASTER GDEM2 and SRTM DEM are of comparable quality. However, SRTM shows several voids which were (sometimes faulty) interpolated, and ASTER GDEM2 resolution is higher. This is why ASTER GDEM2 was chosen for this thesis. ASTER and SRTM have slightly different lowest flow.

The largest part of DEM uncertainty is probably added as the DEM was made after the events (the Terra spacecraft being launched in 1999). Pre-event topography is very different. After the events, the valley bottom filled up around 5 m. Also, artificial structures added after the events might have influenced simulation results. Huggel (2004) who used a self-made ASTER DEM concluded that close to infrastructure, ASTER DEMs might be unsuitable. Note that also the ArcGIS basemap and Google Earth might not be correctly georeferenced.

9.3.1.2 Model

The dynamic flow model RAMMS shows detailed results that can be viewed in fixed time intervals (Andres, 2010). RAMMS is a useful tool for estimates of potential runout distances and flow heights in complex terrain (Christen et al., 2008). A main advantage is that only 2 friction parameters need to be specified, which reduces uncertainty compared to other models needing more unconstrained input parameters (as in Worni et al., 2012). The Voellmy approach is robust in terms of numerical stability (Rickenmann, 2005). Although RAMMS generally yields good results, it induces several limitations:

- RAMMS does not implement erosion (Christen et al., 2012), although such a function will be implemented in the next version (RAMMS XChange, 2013).
- RAMMS is a single phase model, meaning that the interstitial fluid and solids are not treated separately and interactions are ignored (M. Christen, pers. communication). A two-phase approach is in planning (Hürlimann et al., 2008). As RAMMS is single-phase, water in front of a debris flow front is neglected. Flow deposits would change as water flows farther but solid parts stay. This can lead to an overestimation of runout (Walser, 2013).
- RAMMS cannot model levee generation (Walser, 2013).
- RAMMS does not implement debris flow density (Andres, 2010; M. Christen & C. Graf, pers. communication), but assumes a constant value of 2000 kg/m^3. This would be of use, as debris flow densities can vary between 2000 kg/m^3 (Berger et al., 2011) and 2500 kg/m^3 (Coussot & Meunier, 1996).
- RAMMS cannot model several surges of a debris flow. Each surge reduces the friction for the next surge (Scheuner, 2007) (see also section “Output Limitations” below). A workaround is only to add a surge to the DEM and then simulate the next surge with the modified DEM (Christen et al., 2010b). However, this is not applicable for Peru, as the DEM is made after the events and up to 300 surges are estimated for the Ahobamba event.
- Parameter calibration is subjective, requires expert knowledge and is often very uncertain. Calibration on passed events is recommended (Andres 2010; Walser, 2013).
- Forest is only implemented in RAMMS avalanche (Christen et al., 2010b), which might play a role in partly forested areas like Santa Teresa region. However, debris flows have a rather high density, which lessens the impact of forest on debris flow behavior.

RAMMS shows some numerical errors when calculating flow velocity. In RAMMS, flow velocities are highest at the front or boarders of the flow; in the middle of the flow path, velocities are mostly very low, which is unrealistic. Also, there is a discrepancy between the flow velocities seen in the results of RAMMS and the flow velocities manually reconstructed from the distance covered divided by the calculation time. While flow velocity is realistic, calculated velocity based on calculation steps often is unrealistically low (1.5 m/s) (see also Sections 7.3.1 and 7.3.2). The same problem affects discharge: With lower discharge, the flow takes much longer in terms of calculation steps needed to calculate. This mistake is probably also the reason that runout is much shorter for very large discharges (probably too short, when comparing to the same volume but lower discharge). RAMMS showed very sensitive for the DEM input (see above).

However, also with more sophisticated modeling approaches and larger data availability, better results are not necessarily obtained, as debris flows are highly complex phenomena. The complex physical behavior of debris flows is still a challenge in current research and widely disputed in literature. Field data is scarce, as field studies are hard to carry out and direct observation is rare (Lorenzini & Mazza, 2004). Useful regional precipitation thresholds are not yet available in all parts of the world (Guzzetti et al., 2007a und 200b). There is need for a new debris flow model that is able to calculate the horizontally and vertically varying internal structure of a debris flow (Kowalski, 2008).

RAMMS modeling can all the same help to assess hazard potential in Santa Teresa, due to very limited access to the area and largely lacking field investigations. RAMMS allows for a comparably quantitative and objective hazard mapping. Similar conclusions were obtained by Walser (2013). However, uncertainties can arise from the knowledge of the expert calibrating the parameters and interpreting the results (Christen et al., 2010a). As in all numerical models, the results must be checked carefully by experts for plausibility with empirical relations or field expeditions (Christen et al., 2012).

9.3.1.3 Input Parameters

All RAMMS input parameters show considerable uncertainty, but only the stop criterion, μ, volume and discharge showed large sensitivity (see Section 7.2).

The end time condition of 30,000 seconds used for calibration was defined by RAMMS, as no longer calculation times are possible. 30,000 s proved not sufficient for various simulations, as the debris flow continued farther downstream. It seems that in RAMMS, the moving momentum sometimes does not decrease as fast as it should. This can be explained by the uncommon magnitude of events, for which RAMMS was not designed.

μ was reduced by 10% for both Ahobamba and Sacsara, as both debris flows were rather muddy (C. Portocarrero, pers. communication). Although 0.1 showed slightly better results in Fig. 7.5 (SPI), 0.09 was chosen for Sacsara, as it resulted in faster and more realistic velocities.
Although ξ showed very low sensitivity in Section 7.2.2, it is generally considered a very uncertain parameter (D. Schneider, pers. communication). As for large debris flows, large ξ values were reported, ξ of 1500 seems reasonable and was chosen for sensitivity analysis and calibration. Scenarios were modeled with ξ of 1000, as most scenarios have lower volumes than the ones used in sensitivity analysis. As ξ dominates when the flow is fast, sensitivity can be assumed to be larger in the valley than in the deposition zone near Santa Teresa.

Simulated volume in sensitivity analysis was chosen too large (5 - 10mill.) and corresponds to the total event volume, not the largest single surge volume (see Section 9.3.2). However sensitivity of volume can still be well shown – if anything, volume sensitivity increases with larger volumes. A first estimate of total volume of 8 mill. m^3 was considered to have passed through the 8 km hydrograph in Sacsara in total.

Costa & Schuster's (1988) formula gave reasonable results for discharge for all simulations. Rickenmanns (1999) formula yields too large discharges in the order of up to 150,000 m^3/s for an event magnitude of 25 mill. m^3. As both debris flows observed consisted of several surges, a lower maximum discharge as proposed by Costa & Schuster (1988) for dam breaks proved more realistic. Also, discharges were found to decrease fast with flow propagation (Schneider et al., 2014). Lower discharges were found to have larger runout. This is probably due to the total material being spread over a longer period of time, meaning that the front is already a long way downstream until the last part passes the hydrograph. Dam heights for this formula were estimated based on event volume and debris-covered area. Note that peak discharge is empirically derived from event volume and not based on precipitation measurements (as in Walser, 2013). The same procedure was applied for scenario simulations.

9.3.2 Output limitations

Above-mentioned input limitations strongly influence simulation results. The most important input limitation is that surges can not be modeled. For surges, all mentioned input limitations come together: (1) only an after-event DEM is available; (2) RAMMS can not model several hundred surges; (3) single surge volumes, velocities, flow heights and runouts are unknown. Additionally, surges in debris flows strongly vary and do not have the same flow properties. Surges occur due to natural surging behavior of debris flows and temporal blockages due to boulders, logs and landslides (Costa, 1984).

Surges influence velocity, runout, as well as flow and deposition height. A simulation containing the total volume would result in runouts much too large and deposition heights too low. In reality, the total volume would not flow in one surge but in many smaller ones (see Coussot & Meunier, 1996). This is why runout calibration was chosen (see Section 5.2.4). However when taking only the largest single surge volume into account, velocity is much too low. This fact can be explained by the fact that the total volume would travel much faster than single surges, although a surge smoothens the valley bed for the following surges and several surges together can achieve higher velocities and larger runout than a single one.
Total runout distance of the whole event probably was larger than that of the largest single surge alone, as following surges partly overflow each other. However, runout is much lower as if the whole event went down in one surge only. The total volume coming down in several surges leads to the same volume being distributed over a smaller area, as runout is over all decreased for surges with lower volume (it is assumed that the volume effect is larger than the smoothening effect on runout distance). This leads to lower runout and higher deposition heights for several smaller surges with the same total volume than one single surge. This surging behavior increases deposition height for the events compared to their flow height, although deposition height is the flow height minus the water that flowed out (Walser, 2013) and should therefore be smaller than flow height. Mapped runouts of simulations can be an estimated 100 m larger or wider based on the DEM error alone, in addition to an estimated 10% larger extent due to larger volumes and multiple surges.

The strong surging behavior was detected during the calibration of the past events in Santa Teresa area and was therefore not considered for sensitivity analysis. In sensitivity analysis, the total event volume was taken as a reference. This means that several input parameters were chosen differently in calibration and scenario simulations as opposed to sensitivity analysis:

1) Time end condition was increased to 30,000 s (as opposed to 15,000 s), as simulations took longer for single surges due to lower volume.
2) The largest single surge volume was considered, as opposed to the total event volume. This means that the SPI for μ sensitivity is also based on total event volume, not a single surge volume. However the resulting μ value is still reasonable, as depositions would not fit at all when only considering the largest single surge volume – actual runout was larger due to overflowing of surges. As the largest single surge alone did not cover total runout, no SPI was made for calibration.
3) Flow heights below 0.1 m were discarded for calibration and scenario simulations, as opposed to 0.5 m, as several surges would add up in reality in calibration and scenario simulations.
4) The very high ξ was also tested for the total event volume, but sensitivity for the largest single surge volume was found to be similarly low.

Calibration showed that the largest single surge volume is of higher importance than the total volume of the events. As RAMMS cannot include surging behavior, either velocity is realistic but the volume much too large or the volume is correct but velocity too low (for the largest single surge). Surges also influence μ calibration and add uncertainty. Lower μ resulted in more realistic velocities but too large runout and vice versa. The most realistic μ values were not possible to obtain, as either velocity was too low or runout too large for the largest single surge volume. This as well can be explained with the smaller runout and larger velocities of many surges compared to one surge only.

9.3.3 Ahobamba Calibration

Ahobamba fits well to the deposits, except for reduced upflow in the model on the counter slope and to the east of the deposition zone compared to depositions. This is either due to the after-event DEM or because a lateral landslide was misinterpreted as part of the event. Also, all surges combined might lead to a higher upflow. Artificial structures built after the event could have added to this discrepancy.

Runout of the largest single surge volume (1 mill. m^3) is probably slightly overestimated, because of the after-event DEM, faulty input parameters or a volume too large for a single surge. However as no indications exist as to where the first surges actually went, this runout and volume was taken as "worst case" for the largest single surge volume. When considering that water input from Urubamba river probably increased runout of the first surges, simulated runout seems reasonable. The reduced runout observed in the simulation with the SRTM DEM can be explained by the artifacts in SRTM. Higher flow velocity is owned to lower resolution and smoother surfaces.

In Ahobamba, deposition height is known and compared to flow height. The many surges reported started depositing onto each other at the confluence with Urubamba. When the later surges are blocked by the previous ones, runout is reduced from around Santa Teresa to only the confluence with Urubamba. Due to this fact, it is likely that flow height can be extrapolated approximately linearly, meaning that with a mean flow height (not deposition height!) of 3 m, 24.667 surges of 1 mill. would be needed to add up to a deposition height of 74 m. This means that a total event volume of 25 mill. m^3 is realistic. This number is confirmed by C. Portocarrero (pers. communication). It can be expected that 5 - 20 surges were of similar or slightly smaller magnitude than the surge simulated (1 mill. m^3), with numerous smaller surges in between, in total up to 300. Based on this total volume, it is likely that around 10 mill. started from the top and then eroded large parts of lateral hillsides, whose scars can be seen on Google Earth.

The debris flow in the beginning and the hyperconcentrated flow/ debris flood 4 months later were simulated separately, as they can be considered two different processes. The simulation of the hyperconcentrated flow stopped after 30,000 s, with still 54% of the mass moving. This seems reasonable, as the flow continued downstream until past Quillabamba and the reason for stopping simply was that the calculation domain was cut off north of Santa Teresa. In contrast to the main event, no runout or deposition information is available except qualitative information in reports. No comparison with depositions can be made. The dam height of 0.1 m chosen with a volume of 50 mill. m^3 is of course not possible, but the best way to implement an artificial dam break, as the lake was drained over a long period. Flow heights seem to large, as actual discharge would probably be even longer, the lake being drained over a longer time. This would also reduce flow heights. Simulation results show an overestimation of the old part of Santa Teresa affected by the flow.

9.3.4 Sacsara Calibration

Also Sacsara fits well to deposits, but spreading is larger and the flow is not split in two south of Santa Teresa. This can be explained by the DEM being made after the event and the events filling up the valley bottom by several meters. Also, several surges would increase runout and spreading. Spreading is too large south of Santa Teresa and too low north of it (most of the flow north of Santa Teresa in Urubamba valley is below 0.1 m and can be discarded). This means that the largest single surge volume might be larger than 500,000 m^3. With larger volume, it is possible that more mass is deposited farther downstream, cancelling out the overestimation in the south and the underestimation in the north. Although spreading of the flow is too large, maximum flow height follows the center of the estimated depositions well. Due to after-event topography being smoother, runout distances can be overestimated (see above). Spreading of the Sacsara event is larger compared to the Ahobamba event, as the valley is broader and flatter.

For Sacsara no damming was reported, and flow height was compared (as opposed to deposition height in Ahobamba), which does not increase linearly. For 5 times the flow height, more than 5 times the volume has to come down. In total, 5 major surges (with 500,000 m^3 volume) and several small ones (with maybe 100,000 m^3 volume) totaling up to 3 – 6 mill. m^3 event volume are likely. The starting zone volume was estimated (based on measurements) to be around 1 mill. m^3, the rest of the total volume probably got eroded along the flow path. The deposition zone of Mukayoc might have dampened the impact of the Sacsara debris flow in Santa Teresa. On videos, flow velocity near Santa Teresa seems larger than 2 - 3 m/s. this can be explained by the incorporation of water from Sacsara river, which decreases velocity reduction on flatter slopes.

Runout is larger for SRTM than for ASTER, as surface is smoother due to lower resolution. It seems that artifacts in SRTM do not affect the Sacsara debris flow as strongly as the Ahobamba event. Lower runout and velocity for ASTER is confirmed by Andres (2010). Flow height differences are due to DEM differences, mainly differences in the lowest flow path of the DEM. When taking the lowest flow path of ASTER for both simulations, flow heights can vary strongly where SRTM has an only slightly different lowest flow path.

The exceptionally large volumes of both events in 1998 could also be explained by a system change (induced by climate change or El Niño), as magnitude and frequency are only inversely proportional as long as the physical system remains unchanged (Huggel, 2004).

9.4 Scenario Modeling and Preliminary Hazard Map

This section addresses the question whether events like in 1998 can happen again in the future. Scenarios were simulated to account for future uncertainty in hazard probability and magnitude and a preliminary hazard map was created for Santa Teresa. With the scenarios provided in this thesis, a broad variety of potential hazards are evaluated for Santa Teresa area. Probability of hazards can be given qualitatively, as it is no necessary input for scenario modeling (Wright & Cairns, 2011). Starting zones without lakes were found to have similar properties and size than the starting zones of the 1998 events and are triggered by slope instability; as opposed to triggered by dam break (e.g. GLOFs).

9.4.1 Scenarios

Flow height profiles were calibrated to follow the highest flow path of simulations. They correspond well; spreading from the Sacsara debris flow in Salcantay valley even follows the flow path of Salcantay. An exception is the maximum flow height of Ahobamba, where a bifurcation in Urubamba valley shortly before Santa Teresa was detected, probably caused by the after-event DEM.

Total volumes are qualitative and based on the estimated amount of water and debris present in the starting zones (on which no exact data is available). Although scenario volumes were chosen to account for the worst case, manual hazard zone delineation induces a large uncertainty in starting zone areas and volumes. As seen in Section 7.2, volumes have a large influence on results and add considerable uncertainty. Erosion and lateral landslides are not explicitly considered and could increase the total volume. However a largest single surge of 3 times the largest single surge volume of the events in 1998 is probably an overestimate and should cover the worst case (see Section 5.3.2). Outflow volumes adding up to less than 10% of the total volume were ignored. As volume sensitivity showed, influence on simulation results is not very large for amounts in the order of +- 10%. Precipitation (hourly, antecedent, rainfall thresholds) and snowmelt could not be taken into account for scenario volume estimates.

μ is lowered by 10% for debris flows triggered by slope instability or 20% for debris flows triggered by dam break; as Rickenmann (2005) found that μ is smaller for fine-grained debris flows and the 1998 events were rather muddy (C. Portocarrero, pers. communication). Smaller volumes would have larger μ (as friction is increased), muddier flows have lower μ. GLOFs can erode debris that was previously saturated, further lowering μ.

The extent of debris flows shown correspond to a height of over 0.1 m and a velocity of over 1 m/s in order to avoid unrealistic spreading due to DEM errors. These values (especially flow height) increase with multiple surges and larger total volume and can be an order of magnitude larger. Several hundred surges are possible in scenario simulations of debris flows triggered by slope instability, depending on the total erodible material present (see Section 3.5 for details). For GLOFs, the maximum possible number of surges is 1, the assumptions being that volumes correspond to total volume and no further temporal dammings occur. Also for GLOFs, various smaller surges are possible, but this procedure includes the worst case.

Those parts of simulations with lower velocity than 1 m/s were not computationally excluded from the simulations in ArcGIS, as RAMMS sometimes shows unrealistically small velocities in the middle of the flow (sometimes below 1 m/s), which would distort results. Flow velocity is underestimated in scenario simulations, as only a single surge is modeled and bed smoothening of various surges is ignored. Also, low velocity can be explained by tight curves in the valley which slow down the flow

(e.g. in Manamayo). In Salcantay, average and maximum velocities are lower than for Ahobamba and Sacsara, probably due to its lower overall slope (slope of 0.07 - 0.08 as opposed to 0.14 - 0.17 in Ahobamba and 0.1 - 0.11 in Sacsara). A strong velocity decrease at the confluence with Urubamba might also mean that runout was in fact shorter than modeled, even if still over 10% of the mass was moving. However, water from Urubamba would have increased runout for the first few surges, which is not taken into account in the simulation.

Flow heights from Ahobamba scenario simulations are generally larger compared to the 1998 events, as larger volumes are involved for the largest single surge from the calibration. The debris flow triggered by slope instability (simulation A019 - 021) in Ahobamba 8 km upstream from the confluence with Urubamba was created to summarize possible events in Ahobamba and to account for the worst case. 8 km corresponds to the lower boarder of landslide scars. μ is probably too low, but reflects the largest runout distance possible from a landslide dam 8 km upstream. μ also reduced by 20% to account for worst case (instead of -10%). The starting zone located much lower in the valley leads to higher flow heights, as the hydrograph was not adapted to a debris flow coming from above. It is more likely that a potential debris flow would start farther up and only pass through the 8 km - hydrograph, with flow heights more similar to the 1998 event.

All modeled scenarios from Sacsara are GLOFs, leading to large (but realistic) flow heights near Santa Teresa. The largest volume of Hanpi K'ocha was chosen to be only twice the total lake volume, as more debris incorporation than 5 mill. m^3 seems unrealistic. This would lead to a 10 mill. m^3 single surge, which is already very large, as such a lake volume probably would come down in several smaller surges. This scenario however was chosen in order to model the worst case scenario.

From Salcantay, most scenario simulations did not reach Santa Teresa. However this was mostly due to too long calculation times, simulations were stopped when over 20% of its mass were still moving. More scenarios could reach Santa Teresa in reality (see Section 8.4). As a μ of 0.07 in Totora is already quite low, it was not decreased by 10%.

All communities in Santa Teresa area can be affected by future hazards. The communities of Andihuela, Huadqiña, Saucepampa, Ahobamba, Sahuayaco and Manchayhuaycco are especially endangered. Strong surging behavior has to be expected – especially for debris flows triggered by slope instability – as many landslide scars exist and the 1998 debris flows both showed strong surging behavior.

Scenario simulations show flow heights and velocities comparable to the 1998 events with similar volumes (Table 8.1). However for "large" scenarios, larger flow heights are possible as the ones observed in 1998. In Urubamba river, maximum flow heights of 5 m (Ahobamba and Salcantay) to 8 m (Sacsara) are possible. This would probably lead to a temporal damming of Urubamba river, which could lead to cascading processes.

9.4.2 Preliminary Hazard Map

The preliminary hazard map obtained (Fig. 8.5) includes all simulations that reached Santa Teresa and seems consistent with historic data. The parts of the old village of Santa Teresa completely destroyed lie in high; the parts partly destroyed in medium hazard potential zones. As the highest hazard probability of the hazard map corresponds well to the destroyed parts of Sacsara, the preliminary hazard map can be considered a good estimate.

The new village of Santa Teresa is probably safe from direct impacts of debris flows, but not from process combinations or Chilcapata hill. Communities downstream of Santa Teresa were not looked at, but might be endangered. Monitoring is recommended for all three valleys and for all communities as well as Chilcapata hill above Santa Teresa. As seen from the scenario simulations, communities are not equally endangered, but all have some hazard potential. Debris flows in the future with larger flow heights than in 1998 are possible in Santa Teresa, even without temporal dammings of Urubamba.

Hazard maps never include all possible hazards, leaving a residual risk also in areas not mapped as endangered (Raetzo et al., 2002). To account for all these uncertainties, the hazard map is shown in a raster representation, as vector could lead to the misunderstanding of well-defined hazard boarders. Hazard maps have to be communicated carefully, as they have legal implications on land use (Gruber & Pike, 2008). Delineation should be reproducible (Jakob, 2005a). A hazard map cannot be validated, only evaluated (Gruber & Pike, 2008).

The reclassification for the hazard map is highly qualitative and can only give a rough estimate on hazard probability. It is on no account to be confused with an actual probability estimate for hazards at a given location. Of the 1998 events, only the Sacsara event was taken into account (given the highest "probability" of 3, as it already did happen in the past). The 1998 Ahobamba event could not be implemented, as it did not reach Santa Teresa in one surge (in the simulation, water from Urubamba increasing runout could not be modeled). However also in the simulation, still 14% of mass was moving and the simulation would have reached Santa Teresa when longer calculation times would have been possible.

The hazard assessment done in this thesis can not be treated as a full-scale hazard assessment, as data is too limited as yet (see Chapter 4). This, and the complex surging behavior of the debris flows observed, results in a preliminary hazard map only. This thesis merely gives a first order assessment of potential hazards in the study region. The hazard map does not include process chains, which can play a major role in mountainous environment. Temporal dammings can be considered most critical, especially at the confluence with Urubamba, and are possible from all simulations reaching the confluence with Urubamba. A temporal damming could strongly increase volume, peak discharge, velocity and flow height and thus the overall hazard potential, even for the new village of Santa Teresa.

10 Conclusion

The assessment of geomorphologic and climatic conditions of the study region (Chapter 3) showed that Santa Teresa region is prone to various mass movements. A lot of highly unstable sediment originating from debuttressed slopes is available at many locations.

Trigger analysis (Chapter 6) indicated that the Sacsara event was mainly triggered by a shallow slope instability induced by heavy rainfall; in combination with high antecedent rainfall and snowmelt. The earthquake prior to the event destabilized the slopes. Triggering processes for the Ahobamba event are less clear, but probably antecedent rainfall played an important role, together with enhanced snow and ice melt and permafrost thaw over several months. Several deep-seated slope instabilities started slowly and transformed into a debris flow.

Modeling of the events of 1998 (Chapter 7) showed that for runout, the largest single surge volume is more important than total event volume. Exact calibration of the Ahobamba and Sacsara events was not possible, due to the complex surging behavior and limited data availability.

Scenarios modeled in Chapter 8 indicate considerable hazard potential in all subcatchments of the study region. Even larger events than those in 1998 could happen in the future. Communities in the study region are endangered, monitoring and further data acquisition is strongly recommended.

The preliminary hazard map (Section 8.4) shows that Santa Teresa is comparably safe, in strong contrast to Huadqiña and Saucepampa. The largest danger for the study region originates from process interactions, including rock- and ice avalanches, GLOFs, landslides, temporal blockings, debris flows and hyperconcentrated flows. This conclusion is supported by Haeberli et al. (2012) and Frey et al. (2012). Such cascading processes are not included in the hazard map; the hazard assessment done in this thesis is not conclusive.

The methodology applied in this thesis proved suitable for the goals stated in Chapter 1 and lead to the desired results. The main limitation for a more conclusive hazard assessment is limited data availability concerning flow characteristics of past events, precipitation and temperature measurements, hazard potential of possible starting zones and DEM resolution.

10.1 Outlook

Potential debris flows in the future can be of similar or even larger volume than the events in 1998. The probability for these flows is not known, making suitable hazard mitigation measures a challenging part of the CCA DRR project. A monitoring and early warning system for Santa Teresa is in planning (CARE & UZH, 2011). Early warning systems are highly complex and should include monitoring sensors, data, and voice communication but also establish clear institutional responsibilities and response, involve local people (Huggel et al., 2012a). The only way to monitor temporal dammings are runout measurements down valley (Frey et al., 2012).

With further warming, lakes could increase in size and glaciers become temperate, decreasing the stability of ice and rock walls (Evans et al., 2006; Giráldez et al., 2012). This complex situation causes a need for further field work as well as an integrative and participatory approach (Haeberli et al., 2012).

10.2 Further Research

As hazard probability is unknown, continuous data acquisition is required to provide necessary data for future studies. A lot of data needed for monitoring and an early warning system is still unavailable. Further research about soil properties, deposits, hydrological and material properties as well as lake and debris volumes is absolutely essential; for both the starting zones of the 1998 events and potential future starting zones. Various locations chosen for potential starting zones in this thesis were never visited. Hazard analysis of potential starting zones needs to be made in situ and in more detail – for a possible procedure, see Jakob (2005a).

For future research, a new DEM currently being generated with data from the Advanced Land Observing Satellite (ALOS) could be used, which would enhance remote sensing data quality. Also, for hazard assessments after 2008, the Brazilian Weather service (CPTEC-INPE) developed a new merging approach for gauges and TRMM for daily precipitation, yielding better results than other reanalysis (Scheel et al., 2011).

As limited understanding of complex process interactions still is a drawback for modeling, it is vital that they are studied in more detail (Huggel, 2004). Process chains from ice- and rockfalls, landslides, floods, GLOFs and temporal dammings would help to assess potential hazards in Santa Teresa area and should be implemented in further studies. It is essential to find out what process combinations are possible and how they influence scenarios simulated here.

Based on more available data, more detailed scenario studies can be made for the area. Simulations could additionally be made with TIN instead of raster (D. Schneider, pers. communication), different dynamic flow models or other DEMs, such as ALOS (Schneider et al., 2008). Of course, the study region could also be extended to further endangered communities in the vicinity, such as Aguas Calientes (Machu Picchu village).

Further information to be implemented in future research could be gained from seismic data recordings (as done in Schneider et al., 2010), ASTER GDEM2 error analysis (see for example Andres, 2010), the automatic identification of steep debris reservoirs with high-resolution imagery (as done in Huggel et al., 2004) or the degree day factor concept used to interpolate temperature.

11 Literature

Adler, R.F., Huffmann, G.J., Chang, A., Ferraro, R., Xie, P.-P., Janowiak, J., Rudolf, B., Schneider, U., Curtis, S., Bolvin, D., Gruber, A., Susskind, J., Arkin, P. & Nelkin, E., 2003. The Version-2 Global Precipitation Climatology Project (GPCP) Monthly Precipitation Analysis (1979 – Present). Journal of Hydrometeorology, 4, 1147–1167.

Ancey, C., 2003. Role of particle network in concentrated mud suspensions. In: Rickenmann, D. & Chen, C.-L. (eds.). Debris-Flow Hazards Mitigation: Mechanics, Prediction, and Assessment, 1, Millpress, Rotterdam, 1335 pages.

Andres, N., 2010. Unsicherheiten von digitalen Geländemodellen und deren Auswirkungen auf die Berechnung von Gletscherseeausbrüchen mit RAMMS. Master Thesis, UZH.

Armento, M. C., Genevois, R. & Tecca, P.R., 2008. Comparison of numerical models of two debris flows in the Cortina d' Ampezzo area, Dolomites, Italy. Landslides, 5, 143–150. Springer Verlag.

Avalos, J.G., 2011. Evaluación geológica de los peligros naturales en el poblado de Santa Teresa y alrededores. Report, Ministerio del Ambiente, Instituto Geofisico del Perú, 1-30.

Ayotte, D. & Hungr, O., 2000. Calibration of runout prediction model for debris-flows and avalanches. In: Wieczorek & Naeser (eds.). Debris-Flow Hazards Mitigation: Mechanics, Prediction, and Assessment. Balkema, Rotterdam, 608 pages.

BAFU (Bundesamt für Umwelt), 1991: Ursachenanalyse der Hochwasser 1987. Schlussbericht. Mitteilung des Bundesamtes für Wasserwirtschaft Nr. 5, Mitteilungen der Landeshydrologie und –Geologie Nr. 15. 47 pages.

Bartelt, P., Buehler, Y., Christen, M., Deubelbeiss, Y., Graf, C., McArdell, B., Salz, M. & Schneider, M., 2013. RAMMS (rapid mass movements simulation). User Manual v1.5 Debris Flow. A numerical model for debris flows in research and practice. WSL Institute for Snow and Avalanche Research SLF, 126 pages.

Berger, C., McArdell, B.W. & Schlunegger, F., 2011. Direct measurement of channel erosion by debris flows, Illgraben, Switzerland. Journal of Geophysical Research, 116, 18 pages.

Bosilovich, M.G., Chen, J., Robertson, F.R., Adler, R.F., 2008. Evaluation of Global Precipitation in Reanalyses. Journal of Applied Meteorology and Climatology, 47, 2279–2299.

Bozhinskiy, A.N. & Nazarov, A.N., 2000. Two-phase model of debris-flow. In: Wieczorek & Naeser (eds.). Debris-Flow Hazards Mitigation: Mechanics, Prediction, and Assessment. Balkema, Rotterdam, 608 pages.

Bradley, R.S., Vuille, M. Diaz, H.F. and Vergara, W., 2006. Threats to water supply in the tropical Andes. Science, 312, 5781, 1755-1756.

Caine, N., 1980. The rainfall intensity-duration control of shallow landslides and debris flows. Geografiska Annaler, 62a, 23–27.

CARE, and UZH, 2011. ACC RRD Retroceso De Los Glaciares En La Cordillera De Los Andes. Internal project report, 41 pages.

CARE, and UZH. 2012. ACC RRD Retroceso De Los Glaciares En La Cordillera De Los Andes Informe Enero - Junio 2012. Internal project report, 40 pages.

CARE, UZH, 2013a. Sistema de gestion de riesgos santa teresa: base y conceptos. Santa Teresa. Internal project report, 14 pages.

CARE, UZH, 2013b. Línea de base climática – Cordillera Blanca y Santa Teresa. Internal project report, 17 pages.

CARE, and UZH, n.d.. Resumen Proyecto Glaciares. Internal project report, 5 pages.

Carey, M., 2005. Living and dying with glaciers: people's historical vulnerability to avalanches and outburst floods in Peru. Global and Planetary Change, 47(2-4), 122–134.

Carey, M., Huggel, C., Bury, J., Portocarrero, C., Haeberli, W., 2011. An integrated socio-environmental framework for glacier hazard management and climate change adaptation: lessons from Lake 513, Cordillera Blanca, Peru. Climatic Change, 112, 733–767.

Carlotto, V., Cárdenas, J., Romero, D., Valdivia, W. & Tintaya, D., 1999. Geología de los Cuadrángulos de Quillabamba y Machupicchu. Hojas 26-q y 27-q. Boletin N° 127, Serie A: Carta Geológica Nacional. INGEMMET (Instituto Geológico Minero y Metalúrgico). Report, 330 pages.

Cesca, M. & D'Agostino, V., 2008. Comparison between FLO-2D and RAMMS in debris-flow modelling: a case study in the Dolomites. In: Wrachien, de D., Brebbia, C.A. & Lenzi, M.A. (eds.): Monitoring, Simulation Prevention and Remediation of Dense and Debris Flows II. WIT Transactions on Engineering Sciences, 60, WIT Press, Southampton, Boston, 240 pages.

Chang, K. & Tsai, B. 1991. The Effect of DEM Resolution on Slope and Aspect Mapping. Cartography and Geographic Information Systems, 18, 1, 69–77.

Chen, Z.L., Liu, J.J. & Liu, J.K., 2010. Debris flow induced by glacial lake break in southeast Tibet. In: Wrachien, de D. & Brebbia, C.A. (eds.): Monitoring, Simulation Prevention and Remediation of Dense and Debris Flows III. WIT Transactions on Engineering Sciences, 67, WIT Press, Southampton, Boston, 288 pages.

Christen, M.: Personal Communication. WSL-Institut für Schnee- und Lawinenforschung, SLF, Davos, Switzerland.

Christen, M., Bartelt, P. & Gruber, U., 2002: AVAL-1D: An Avalanche Dynamics Program for the Practice. In: International Congress Interpraevent 2002 in the Pacific Rim – Matsumo, Japan. Congress publication, 2, 715 –725.

Christen, M., Bartelt, P., Kowalski, J. & Stoffel, L., 2008. Calculation of dense snow avalanches in three-dimensional terrain with the numerical simulation program RAMMS. International Snow Science Workshop Proceeding, 709–716.

Christen, M., Kowalski, J. & Bartelt, P., 2010a. RAMMS: Numerical simulation of dense snow avalanches in three-dimensional terrain. Cold Regions Science and Technology, 63, 1–14.

Christen, M., Bartelt, P. & Kowalski, J., 2010b. Back calculation of the "In den Arelen" avalanche with RAMMS: interpretation of model results. Annals of Glaciology, 51, 161–168.

Christen, M., Bühler, Y., Bartelt, P., Leine, R., Glover, J., Schweizer, A., Graf, C., McArdell, B.W., Gerber, W., Deubelbeiss, Y. & Feistl, T., 2012. Integral hazard management using a unified software environment numerical simulation tool „RAMMS" for gravitational natural hazards. In: Koboltsching, G., Hübl, J., Braun, J. (Eds.), 12th Congress INTERPRAEVENT, Grenoble, France, 77–86.

Clague, J.J. & Evans, S.G., 2000. A review of catastrophic drainage of moraine-dammed lakes in British Columbia. Quaternary Science Reviews, 19, 1763-1783.

Clague, J.J., 2009. Climate Change and Slope Instability. In: Sassa, K. & Canuti, P. (eds.). Landslides – Disaster Risk Reduction. Springer, Berlin, 649 pages.

Coe, J.A., Kinner, D.A. & Godt, J.W., 2008. Initiation conditions for debris flows generated by runoff at Chalk Cliffs, central Colorado. Geomorphology, 96, 270–297.

Costa, J. E., 1984. Physical Geomorphology of Debris Flows. In: Costa, J. E. & Fleisher, P. J. (eds.). Developments and Applications of Geomorphology. Springer, Berlin, 372 pages.

Costa, J.E. & Schuster, R.L., 1988. The formation and failure of natural dams. Geological Society of America Bulletin, 7, 1054-1068.

Coussot, P. & Meunier, M., 1996. Recognition, classification and mechanical description of debris flows. Earth-Science Reviews, 40, 209–227.

Crosta, G.B., Cucchiaro, S. & Frattini, P., 2003. Validation of semi-empirical relationships for the definition of debris-flow behaviour in granular materials. In: Rickenmann, D. & Chen, C.-L. (eds.). Debris-Flow Hazards Mitigation: Mechanics, Prediction, and Assessment, 2, Millpress, Rotterdam, 1335 pages.

Cui, P., Zhou, G.G.D., Zhu, X.H. & Zhang, J.Q., 2013. Scale amplification of natural debris flows caused by cascading landslide dam failures. Geomorphology, 182, 173–189.

Curtis, S., Adler, R., Huffman, G., Nelkin, E. & Bolvin, D., 2001. Evolution of tropical and extratropical precipitation anomalies during the 1997-1999 ENSO cycle. International Journal of Climatology, 21, 961–971.

Davies, T.R.H., 1988. Debris Flow Surges - A Laboratory Investigation. Mitteilungen der Versuchsanstalt für Wasserbau, Hydrologie und Glaziologie, 96, 1–121.

Davies, T.R.H., McSaveney, M.J. & Hodgson, K.A., 1999. A fragmentation-spreading model for long-runout rock avalanches. Canadian Geotechnical Journal, 36, 1096-1110.

DeGraff, J. V. & Ochiai, H., 2009. Rainfall, Debris Flows and Wildfires. In: Sassa, K. & Canuti, P. (eds.). Landslides – Disaster Risk Reduction. Springer, Berlin, 649 pages.

DesInventar (Disaster Inventory System), 2013. DesInventar online. Inventory system of the effects of disasters. <http:// online.desinventar.org> (update 2013, access 04.11.2013).

Díaz, A. C., 2010. Enfoque fisico de los procesos de remocion en masa en la microcuenca Tullumayu - Chicon. Centro de Estudios y Prevención de Desastres (PREDES). Project report, 13 pages.

EGEMSA (Empresa de Generación Eléctrica Machupicchu S.A.), 2011.<http://www.egemsa.com.pe/> (update 2011, access 17.12.2013).

Evans, S.G., 1986. The maximum discharge of outburst floods caused by the breaching of man-made and natural dams. Canadian Geotechnical Journal, 23, 385-387.

Evans, S.G., Scarascia Mugnozza, G., Strom, A.L., Hermanns, R.L., Ischuk, A. & Vinnichenko, S., 2006. Landslides from massive rock slope failure and associated phenomena. In: Evans, S.G., Scarascia Mugnozza, G., Strom, A.L. & Hermanns, R.L. (eds.). Landslides from Massive Rock Slope Failure. Series IV: Earth and Environmental Sciences, 49, Springer, Dordrecht, 662 pages.

Evans, S.G., Bishop, N.F., Fidel Smoll, L., Valderrama Murillo, P., Delaney, K.B. & Oliver-Smith, A., 2009. A re-examination of the mechanism and human impact of catastrophic mass flows originating on Nevado Huascarán, Cordillera Blanca, Peru in 1962 and 1970. Engineering Geology, 108, 96–118.

Fell, R., 1994. Landslide risk assessment and acceptable risk. Canadian Geotechnical Journal, 31, 261-272.

Fisher, P. & Tate, N. 2006. Causes and Consequences of Error in Digital Elevation Models. Progress in Physical Geography, 30, 4, 467–489.

Fleisher, P.J., 1984. Maps in Applied Geomorphology. In: Costa, J. E. & Fleisher, P. J. (eds.). Developments and Applications of Geomorphology. Springer, Berlin, 372 pages.

Francou, B., Vuille, M., Favier, V. & Cáceres, B., 2004. New evidence for an ENSO impact on low-latitude glaciers: Antizana 15, Andes of Ecuador, 0°28’S. Journal of Geophysical Research, 109, 17 pages.

Frey, H., Schneider, D. & Huggel, C., 2012. Satellite based analysis of the hazard situation of Santa Teresa, Peru. Internal project report. 21 pages.

Frey, H., & Paul, F., 2012. On the suitability of the SRTM DEM and ASTER GDEM for the compilation of topographic parameters in glacier inventories. International Journal of Applied Earth Observation and Geoinformation, 18, 480–490.

Frey, H., Giráldez, C., Huggel, C., Choquevilca, W. & Fernández, F., 2013. Mapa indicativa de amenazas. Project report, 18 pages.

Garland, G.G. & Olivier, M.J., 1993: Predicting landslides from rainfall in a humid, sub-tropical region. Geomorphology, 8, 165-173.

Ghilardi, P., Natale, L. & Savi, F., 2001. Modeling Debris Flow Propagation and Deposition. Physics and Chemistry of the Earth, Parts C 26, 651–656.

Ghilardi, P., Natale, L. & Savi, F., 2003: Experimental investigation and mathematical simulation of debris-flow runout distance and deposition area. In: Rickenmann, D. & Chen, C.-L. (eds.). Debris-Flow Hazards Mitigation: Mechanics, Prediction, and Assessment, 1, Millpress, Rotterdam, 1335 pages.

Giráldez, C., Cusipaucar, F.F., Farfán, N.C., Puma, R., Quispe, A., Barra, J.-C., Pinto, C.A., Elguera, H.B. & Lozono, G.A., 2012. Proyecto 'Glaciares'. Informe de la Expedición a la Quebrada Sacsara del 9 al 12 de Noviembre 2012. Internal project report, 18 pages.

Giráldez, C., Choquevilca, W., Fernández, F., Frey, H. & García, J., 2013. Large mass movements related to deglaciation effects in southern Peru (Cusco). European Geoscience Union, 15, 8183. EGU Abstract.

Graf, C.: Personal Communication. WSL-Institut für Schnee- und Lawinenforschung, SLF, Davos, Switzerland

Gruber, S., 2004. Permafrost thaw and destabilization of Alpine rock walls in the hot summer of 2003. Geophysical Research Letters, 31, 4 pages.

Gruber, S., Pike, R., 2008. Modelling mass movements and landslide susceptibility. In: Hengl, T., Reuter, H.I. (eds.). Geomorphometry. Elsevier, Amsterdam, 527–550.

Gruber, S., 2012. Derivation and analysis of a high-resolution estimate of global permafrost zonation. The Cryosphere, 6, 221–233.

Guzzetti, F., Peruccacci, S., Rossi, M., & Stark, C. P. (2007a). Rainfall thresholds for the initiation of landslides in central and southern Europe. Meteorology and Atmospheric Physics, 98 (3-4), 239–267.

Guzzetti, F., Peruccacci, S., Rossi, M., & Stark, C. P. (2007b). The rainfall intensity–duration control of shallow landslides and debris flows: an update. Landslides, 5 (1), 3–17.

Haeberli, W., Huggel, C., Ka, A., Zgraggen-Oswald, S., Polkvoj, A., Galushkin, I., Zotikov, I. & Osokin, N., 2004. The Kolka-Karmadon rock/ice slide of 20 September 2002: an extraordinary event of historical dimensions in North Ossetia, Russian Caucasus. Journal of Glaciology, 50, 533–546.

Haeberli, W., Clague, J.J., Huggel, C. & Kääb, A., 2010. Hazards from lakes in high-mountain glacier and permafrost regions: climate change effects and process interactions. Avances de la geomorfologia en España 2008-2010, pages 1–11.

Haeberli, W., Giráldez, C., Rohrer, M., Salzmann, N. & Schneider, D., 2012. Glacier CCA-DRR Project Jun 2012. Internal project report, Zurich, 28 pages.

Hebeler, F. & Purves, S. 2009. The Influence of Elevation Uncertainty on Derivation of Topographic Indices. Geomorphology, 111, 4–16.

Hegg, C. & Rhyner, J., 2007. Warnung bei aussergewöhnlichen Naturereignissen. Forum für Wissen, WSL, 96 pages.

Hegglin, E. & Huggel, C., 2008. An Integrated Assessment of Vulnerability to Glacial Hazards. Mountain Research and Development, 28, 299–309.

Heim, A., 1932: Bergsturz und Menschenleben. Fretz und Wasmuth, Zürich, 218 pages.

Hermoza, J., Ortiz, M., Benavente, R., Mattos, E., Portocarrero, C., Tamayo, W. & Villafuerte, J., 1998. Informe geológico glaciológico del aluvión de Aobamba-Cusco. EGEMSA (Empresa de generación electrica Machupicchu S.A.). Internal report, 89 pages.

Heuvelink, G.B.M., 1998. Error propagation in environmental modeling with GIS. Taylor & Francis, London, 150 pages.

Hubbard, B., Heald, A., Reynolds, J.M., Quincey, D., Richardson, S.D., Luyo, M.Z., Portilla, N.S. & Hambrey, M.J., 2005. Impact of a rock avalanche on a moraine-dammed proglacial lake: Laguna Safuna Alta, Cordillera Blanca, Peru. Earth Surface Processes and Landforms, 30, 1251–1264.

Huggel, C.: Personal Communication. Department of Geography, University of Zurich, Switzerland.

Huggel, C., 2004. Assessment of Glacial Hazards based on Remote Sensing and GIS Modeling. Dissertation, University of Zurich, 87 pages.

Huggel, C. & Salzmann, N., n.d.. ACC RRD project description. Internal project report, 2 pages.

Huggel, C. & Choquevilca, W., n.d.. Línea de base Santa Teresa. Sistema de Gestion de Riesgos: Base y Conceptos. Project report, 15 pages.

Huggel, C. & Schneider, D., 2012. Glacier CCA-DRR Project Oct-Dec 2011. Project report, 20 pages.

Huggel, C., Haeberli, W., Kääb, A., Hoelzle, M., Ayros, E. & Portocarrero, C., 2002. Assessment of glacier hazards and glacier runoff for different climate scenarios based on remote sensing data: A case study for a hydropower plant in the Peruvian Andes. Proceedings of EARSeL-LISSIG-Workshop Observing our Cryosphere from Space, Bern, 1–12.

Huggel, C., Kääb, A., Haeberli, W. & Krummenacher, B., 2003a. Regional-scale GIS-models for assessment of hazards from glacier lake outbursts: evaluation and application in the Swiss Alps. Natural Hazards and Earth System Sciences, 3, 647–662.

Huggel, C., Kääb, A. & Haeberli, W., 2003b. Vulnerability Study of the Central Hídroelectrica Machupicchu. Glacial Hazard Assessment and Modelling Based on Satellite Imagery. Report, 24 pages.

Huggel, C., Kääb, A. & Salzmann, N., 2004. GIS-based modelling of glacial hazards and their interactions using Landsat-TM and IKONOS imagery. Norwegian Journal of Geography, 58, 61-73.

Huggel, C., Encinas, C., Eugster, S. & Robledo, C., 2008. The SDC Climate Change Adaptation Programme in Peru: Disaster Risk Reduction within an Integrative Climate Change Context. IDRC Davos, pages 276–278.

Huggel, C., Cochachin, A., Frey, H., García, J., Giráldez, C., Gómez, J., Ludeña, S., Portocarrero, C., Price, K., Rohrer, M., Salzmann, N., Schneider, D. & Silvestre, E., 2012a. Integrated assessment of high mountain hazards, related risk reduction and climate change adaptation strategies in the Peruvian Cordilleras 2010–2013. GRF Davos, IDRC Davos, 4 pages.

Huggel, C., Allen, S., Deline, P., Fischer, L., Noetzli, J. & Ravanel, L., 2012b. Ice thawing, mountains falling-are alpine rock slope failures increasing? Geology Today, 28, 98–104.

Huggel, C., Vicuña, L., García, J. & Ludeña S.G., 2012c. Glacier CCA-DRR Project Aug 2012. Project report, 24 pages.

Huggel, C., Clague, J.J., Korup, O., 2012d. Is climate change responsible for changing landslide activity in high mountains? Earth Surface Processes and Landforms, 37, 77–91.

Huggel, C., Giráldez, C., Haeberli, W., Schneider, D. & Frey, H., 2013. Climatic extreme events combine with impacts of gradual climate change: recent evidence from the Andes and the Alps. Geophysical Research, 15, 2013. EGU Abstract.

Hungr, O., 2005. Ch2: Classification and terminology. In: Jakob, M. & Hungr, O. (eds.). Debris Flow Hazards and Related Phenomena. Springer, Berlin, 739 pages.

Hürlimann, M., Corominas, J., Moya, J. & Copons, R., 2003. Debris-flow events in the eastern Pyrenees: preliminary study on initiation and propagation. In: Rickenmann, D. & Chen, C.-L. (eds.). Debris-Flow Hazards Mitigation: Mechanics, Prediction, and Assessment, 1, Millpress, Rotterdam, 1335 pages.

Hürlimann, M., Rickenmann, D., Medina, V. & Bateman, A., 2008. Evaluation of approaches to calculate debris-flow parameters for hazard assessment. Engineering Geology, 102, 152–163.

IRPI (Instituto di Ricerca per la Protezione Idrogeologica), 2013. Rainfall Thresholds for the Initiation of Landslides. <http://rainfallthresholds.irpi.cnr.it/> (update 2013, access 05.12.2013).

Iverson, R.M., 1997. The physics of debris flows. Reviews of Geophysics, 35, 245–296.

Iverson, R.M., Reid, M.E. & Lahusen, R.G., 1997. Debris-Flow Mobilisation from Landslides. Annual Review of Earth and Planetary Sciences, 25, 85-138.

Iverson, R.M., Schilling, S.P., Vallance, J.W., 1998. Objective delineation of lahar-inundation hazard zones. Geological Society of America, 110, 972–984.

Iverson, R. & Denlinger, R. 2001. Flow of Variably Fluidized Granular Masses Across Three-Dimensional Terrain. 1. Coulomb Mixture Theory. Journal of Geophysical Research, 106, 537–552

Iverson, R. M., 2003. The debris-flow rheology myth. In: Rickenmann, D. & Chen, C. L. (eds.). Debris-Flow Hazards Mitigation: Mechanics, Prediction, and Assessment. Millpress, Rotterdam, 1335 pages.

Iverson, R.M., 2005. Ch6: Debris-flow mechanics. In: Jakob, M. & Hungr, O. (eds.). Debris Flow Hazards and Related Phenomena. Springer, Berlin, 739 pages.

Iverson, R.M., Logan, M., LaHusen, R.G. & Berti, M., 2010. The perfect debris flow? Aggregated results from 28 large-scale experiments. Journal of Geophysical Research, 115, 1–29.

Jakob, M., 2005a. Ch17: Debris-flow hazard analysis. In: Jakob, M. & Hungr, O. (eds.). Debris Flow Hazards and Related Phenomena. Springer, Berlin, 739 pages.

Jakob, M., 2005b. A size classification for debris flows. Engineering Geology, 79, 151–161.

Jan, C.-D. & Shen, H.W., 1997. Review dynamic modeling of debris flows. Recent Developments of Debris Flows, Lecture Notes in Earth Sciences, 64, 93-116.

Kazuo, K., Jorgen, J., Shigeki, T. & Takaaki, I., 2009. Huge Landslides Caused by Massive Earthquakes and Long-Lasting Geotechnical Risks. In: Sassa, K. & Canuti, P. (eds.). Landslides – Disaster Risk Reduction. Springer, Berlin, 649 pages.

Klenov, V.I., 2000. 2-D debris-flow simulation. In: Wieczorek & Naeser (eds.). Debris-Flow Hazards Mitigation: Mechanics, Prediction, and Assessment. Balkema, Rotterdam, 608 pages.

Klimeš, J., Vilímek, V. & Vlčko, J., 2007. Debris Flows in the Vicinity of Machu Picchu Village, Peru. In: Sassa, K. & Canuti, P. (eds.). Landslides – Disaster Risk Reduction. Springer, Berlin, 649 pages.

Klimeš, J., Vilímek, V., Benesova, M., Bouska, P. & Cochachin, A., 2011. Glacial lake outburst flood in the Chucchún watershed, Cordillera Blanca, Peru. Proceedings of the second world landslide forum, 4 pages.

Klubertanz, G., Laloui, L. & Vulliet, L., 2000. Parameters governing debris-flow initiation. In: Wieczorek & Naeser (eds.). Debris-Flow Hazards Mitigation: Mechanics, Prediction, and Assessment. Balkema, Rotterdam, 608 pages.

Konagai, K., Johansson, J. & Numada, M., 2007. Extracting Necessary Parameters from Real Landslide Mass for Mitigating Landslide Disaster. In: Sassa, K., Fukuoka, H., Wang, F. & Wang, G. (eds.). Progress in Landslide Science. Springer, Berlin, 378 pages.

Korup, O., Schneider, D., Huggel, C. & Dufresne, A., 2012. Long-Runout Landslides. In: Shroder, J.F. (ed.): Treatise on Geomorphology, 7. Academic Press, San Diego, 183-199.

Kowalski, J., 2008. Two-Phase Modeling of Debris Flows. Dissertation, ETH, Nr. 17827, 135 pages.

Legros, F., 2002. The mobility of long-runout landslides. Engineering Geology, 63, 3–4, 301-331.

Legros, F., 2006. Landslide mobility and the role of water. In: Evans, S.G., Scarascia Mugnozza, G., Strom, A.L. & Hermanns, R.L. (eds.): Landslides from Massive Rock Slope Failure. Series IV: Earth and Environmental Sciences, 49, Springer, Dordrecht, 662 pages.

Lehmann, P. & Or, D., 2012. Hydromechanical triggering of landslides: From progressive local failures to mass release. Water Resources Research, 48, 3, 24 pages.

Liu, K.F. & Lai, K.W., 2000. Numerical simulation of two-dimensional debris flows. In: Wieczorek & Naeser (eds.). Debris-Flow Hazards Mitigation: Mechanics, Prediction, and Assessment. Balkema, Rotterdam, 608 pages.

Lorenzini, G. & Mazza, N., 2004. Debris Flow. Phenomenology and Rheological Modelling. WIT-press, Southampton, Boston, 216 pages.

Marui, H. & Nadim, F., 2009. Landslides and Multi-Hazards. In: Sassa, K. & Canuti, P. (eds.). Landslides – Disaster Risk Reduction. Springer, Berlin, 649 pages.

MAXIMIXE Consult S.A., n.d. Subcuenca del Santa Teresa. Report, 150 pages.

McDougall, S. & Hungr, O., 2004. A model for the analysis of rapid landslide motion across three-dimensional terrain. Canadian Geotechnical Journal, 41, 1084–1097.

Mizuyama, T., Kobashi, S. & Ou, G., 1992. Prediction of debris flow peak discharge. Proceedings of the International Symposium Interpraevent, Bern, Switzerland, 4, 99–108.

NASA (National Aeronautics and Space Administration), 2013a: Giovanni – The Bridge Between Data & Science. <http://gdata1.sci.gsfc.nasa.gov/> (update 2013, access 10.11.2013).

NASA (National Aeronautics and Space Administration), 2013b. Readme for TRMM Product 3B42 (V7). < http://disc.sci.gsfc.nasa.gov/precipitation/documentation/TRMM_README/TRMM_3B42_readme.shtml> (update 18.03.2013, access 10.01.2014).

Navarro, C.Q., 2011. Estudio Geomorfológico-morfométrico de las microcuencas: Chaupimayo, Sacsara, Santa Teresa y Ahobamba. Project Report, 78 pages.

O'Brien, J.S., Julien, P.J. & Fullerton, W.T., 1993. Two-dimensional water flood and mudflow simulation. Journal of Hydraulic Engineering, 119, 244–261.

O'Callaghan, J. F. & Mark, D.M., 1984. The extraction of drainage networks from digital elevation data. Computer Vision, Graphics, and Image Processing, 28, 328-344.

Pack, R. T., 2005. Ch11: Application of airborne and spaceborn remote sensing methods. In: Jakob, M. & Hungr, O. (eds.). Debris Flow Hazards and Related Phenomena. Springer, Berlin, 739 pages.

Petrakov, D.A., Chernomorets, S.S., Evans, S.G. & Tutubalina, O. V, 2008. Catastrophic glacial multiphase mass movements: a special type of glacial hazard. Advances in Geosciences, 14, 211–218.

Pierson, C. T. & Costa, J. E., 1987. A rheologic classification of subaerial sediment-water flows. Geological Society of America, 7, 1-12.

Pirulli, M. & Sorbino, G., 2008. Assessing potential debris flow runout: a comparison of two simulation models. Natural Hazards and Earth System Science, 8, 961–971.

Portocarrero, C.: Personal Communication. Independent consultant, Peru.

Portocarrero, C., 2008. El evento de Ahobamba 1998. Internal report, 6 pages.

Portocarrero, C., Zapata, M., Gómez, R. J., Rapré, A.C., Tapia, G.E. & Portilla, N. S., 2010. Unidad de Glaciología y recursos hídricos (UGRH). Inventario de Glaciares Cordillera Blanca. Autoridad Nacional del Agua. Report, 121 pages.

Rabus, B., Eineder, M., Roth, A., & Bamler, R., 2003. The shuttle radar topography mission—a new class of digital elevation models acquired by spaceborne radar. ISPRS Journal of Photogrammetry and Remote Sensing, 57, 241–262.

Raetzo, H., Lateltin, O., Bollinger, D. & Tripet, J., 2002. Hazard assessment in Switzerland - Codes of Practice for mass movements. Bulletin of Engineering Geology and the Environment, 61, 263–268.

Raissig, A., 2011. Raum-zeitliche Analyse von klimatisch bedingten Extremereignissen in den südlichen Anden (Peru). Master thesis, University of Zurich, 140 pages.

RAMMS XChange, 2013: Workshop for RAMMS. WSL, November 2013.

Reid, M. E., Brien, D. L., LaHusen, R. G., Roering, J. J., de la Fuente, J. & Ellen, S. D., 2003. Debris-flow initiation from large, slow-moving landslides. In: Rickenmann, D. & Chen, C.-L. (eds.). Debris-Flow Hazards Mitigation: Mechanics, Prediction, and Assessment, 1, Millpress, Rotterdam, 1335 pages.

Rickenmann, D. & Zimmermann, M., 1993. The 1987 debris flows in Switzerland: Documentation and Analysis. Geomorphology, 8, 175–189.

Rickenmann, D., 1999. Empirical Relationships for Debris Flows. Natural Hazards, 19, 47–77.

Rickenmann, D., 2005. Ch13: Runout prediction methods. In: Jakob, M. & Hungr, O. (eds.). Debris Flow Hazards and Related Phenomena. Springer, Berlin, 739 pages.

Rienecker, M. M., Suarez, M. J., Gelaro, R., Todling, R., Bacmeister, J., Liu, E., Bosilovich, M. G., Schubert, S. D., Takacs, L., Kim, G.-K., Bloom, S., Chen, J., Collins, D., Conaty, A., da Silva, A., Gu, W., Joiner, J., Koster, R. D., Lucchesi, R., Molod, A., Owens, T., Pawson, S., Pegion, P., Redder, C. R., Reichle, R., Robertson, F. R., Ruddick, A. G., Sienkiewicz, M. & Woollen, J., 2011. MERRA: NASA's Modern-Era Retrospective Analysis for Research and Applications. Journal of Climate, 24 (14), 3624–3648.

Rohrer, M.: Personal Communication. Meteodat GmbH, Zurich.

Rohrer, M., 2012. Protokoll Vom Kickoff-Meeting Vom Gletscherprojekt 9.1.2012. Internal report, 11 pages.

Rosenfeld, C.L., 1984. Remote Sensing Techniques for Geomorphologists. In: Costa, J. E. & Fleisher, P. J. (eds.). Developments and Applications of Geomorphology. Springer, Berlin, 372 pages.

Saemundsson, T., Petursson, H.G. & Decaulne, A., 2003. Triggering factors for rapid mass movements in Iceland. In: Rickenmann, D. & Chen, C.-L. (eds.). Debris-Flow Hazards Mitigation: Mechanics, Prediction, and Assessment, 1, Millpress, Rotterdam, 1335 pages.

Salm, B., Burkard, A. & Gubler, H.U., 1990. Berechnung von Fliesslawinen. Eine Anleitung für Praktiker mit Beispielen. Mitteilungen des Eidgenössischen Instituts für Schnee- und Lawinenforschung, 47.

Salzmann, N., Huggel, C., Calanca, P., Díaz, A., Jonas, T., Jurt, C., Konzelmann, T., Lagos, P., Rohrer, M., Silverio, W. & Zappa, M., 2009. Integrated assessment and adaptation to climate change impacts in the Peruvian Andes. Advances in Geosciences, 22, 35–39.

Sassa, K., Fukuoka, H., Wang, F. & Wang, G., 2007. Landslides Induced by a Combined Effect of Earthquake and Rainfall. In: Sassa, K., Fukuoka, H., Wang, F. & Wang, G. (eds.). Progress in Landslide Science. Springer, Berlin, 378 pages.

Sassa, K., Fukuoka, H. & Carreno, R., 2009. Landslide Investigation and Capacity Building in the Machu Picchu – Aguas Calientes Area (IPL C101-1). In: Sassa, K. & Canuti, P. (eds.). Landslides – Disaster Risk Reduction. Springer, Berlin, 649 pages.

Savage, S.B. & Hutter, K., 1991. The dynamics of avalanches of granular materials from initiation to runout Part I: Analysis. Acta Mechanica, 86, 201-223.

Schatzmann, M., 2005. Rheometry for large particle fluids and debris flows. Dissertation, VAW (Versuchsanstalt für Wasserbau), ETH, Zurich, 192 pages.

Schauwecker, S., Lorenzi, D. & Rohrer, M., 2012. Línea de Base Santa Teresa. Clima. Project report, 21 pages.

Scheel, M.L.M., Rohrer, M., Huggel, C., Santos Villar, D., Silvestre, E. & Huffman, G.J., 2011. Evaluation of TRMM Multi-satellite Precipitation Analysis (TMPA) performance in the Central Andes region and its dependency on spatial and temporal resolution. Hydrology and Earth System Sciences, 15, 2649–2663.

Scheidl, C. & Rickenmann, D., 2009. Empirical prediction of debris-flow mobility and deposition on fans. Earth Surface Processes and Landforms, 35, 157-173.

Scheuner, T., 2007. Modellierung von Murgangereignissen mit RAMMS und Vergleich durch GIS-basiertes Fliessmodell. Master Thesis, University of Zurich, 122 pages.

Schneider, D.: Personal Communication. Tiefbauamt Kanton Bern, Burgdorf.

Schneider, D., Delgado Granados, H., Huggel, C. & Kääb, A., 2008. Assessing lahars from ice-capped volcanoes using ASTER satellite data, the SRTM DTM and two different flow models: case study on Iztaccíhuatl (Central Mexico). Natural Hazards and Earth System Sciences, 8, 559-571.

Schneider, D., Bartelt, P., Caplan-Auerbach, J., Christen, M., Huggel, C. & McArdell, B.W., 2010. Insights into rock-ice avalanche dynamics by combined analysis of seismic recordings and a numerical avalanche model. Journal of Geophysical Research, 115, 20 pages.

Schneider, D., 2011. On Characteristics and Flow Dynamics of Large Rapid Mass Movements in Glacial Environments. Dissertation, University of Zurich, 249 pages.

Schneider, D., Huggel., C., Cochachin, A., Guillén, S. & García, J., 2014. Mapping hazards from glacier lake outburst floods based on modeling of process cascades at Lake 513, Carhuaz, Peru. Advances in Geoscience, 35, 145-155.

Schuster, R.L., 2000. Outburst debris-flows from failure of natural dams. In: Wieczorek & Naeser (eds.). Debris-Flow Hazards Mitigation: Mechanics, Prediction, and Assessment. Balkema, Rotterdam, 608 pages.

Schuster, R.L. & Highland, L.M., 2001. Socioeconomic Impacts of Landslides in the Western Hemisphere: U.S. Geological Survey Open-File Report 01-0276, 47 pages.

Singhroy, V., 2009. Satellite Remote Sensing Applications for Landslide Detection and Monitoring. In: Sassa, K. & Canuti, P. (eds.). Landslides – Disaster Risk Reduction. Springer, Berlin, 649 pages.

Sosio, R., Crosta, G.B. & Hungr, O., 2008. Complete dynamic modeling calibration for the Thurwieser rock avalanche (Italian Central Alps). Engineering Geology, 100, 11–26.

Stricker, B., 2010. Murgänge im Torrente Riascio: Ereignisanalyse, Auslösefaktoren und Simulation von Ereignissen mit RAMMS. Master Thesis, University of Zurich, 110 pages.

Strom, A. L., 2009. Catastrophic Slides and Avalanches. In: Sassa, K. & Canuti, P. (eds.). Landslides – Disaster Risk Reduction. Springer, Berlin, 649 pages.

Suarez, W., 2010. SENAMHI (Servicio Nacional de Meteorología e Hidrología del Peru). Proyecto de Adactacion al Retroceso de los Glaciares Tropicales (PRAA). Reporte de Mision Cuenca del Rio Santa Teresa. Lima. Project report, 40 pages.

Suarez, W., Cerna, M., Ordoñez, J., Frey, H., Giráldez, C. & Huggel, C., 2013. Monitoring glacier variations in the Urubamba and Vilcabamba Mountain Ranges, Peru, using "Landsat 5" images. Geophysical Research Abstracts, 15, EGU General Assembly 2013.

Tachikawa, T., Kaku, M., Iwasaki, A., Gesch, D., Oimoen, M., Zhang, Z., Danielson, J., Krieger, T., Curtis, B., Haase, J., Abrams, M., Crippen, R. & Carabajal, C., 2011. ASTER Global Digital Elevation Model Version 2 – Summary of Validation Results. Available online on http://www.jspacesystems.or.jp/ersdac/GDEM/ver2Validation/Summary_GDEM2_validation_report_final.pdf (access 11.01.2014).

Takahashi, T., 2000. Initiation and flow of various types of debris-flow. In: Wieczorek, G. F. & Naeser, N. D. (eds.). Debris-Flow Hazards Mitigation: Mechanics, Prediction, and Assessment. Balkema, Rotterdam, 608 pages.

Takahashi, T., 2007a. Debris flow. Mechanics, Predictions and Countermeasures. Taylor & Francis, London, 440 pages.

Takahashi, T., 2007b. Progress in Debris flow modelling. In: Sassa, K., Fukuoka, H., Wang, F. & Wang, G. (eds.). Progress in Landslide Science. Springer, Berlin, 378 pages.

Takahashi, T., Satofuka, Y. & Kashimoto, S., 2003. Motion of landslide-induced debris flow. In: Rickenmann, D. & Chen, C.-L. (eds.). Debris-Flow Hazards Mitigation: Mechanics, Prediction, and Assessment, 1, Millpress, Rotterdam, 1335 pages.

Tarantino, A. & Bosco, G., 2000. Role of soil suction in understanding the triggering mechanisms of flow slides associated with rainfall. In: Wieczorek & Naeser (eds.). Debris-Flow Hazards Mitigation: Mechanics, Prediction, and Assessment. Balkema, Rotterdam, 608 pages.

Tognacca, C. & Bezzola, G.R., 1997. Debris-Flow Initiation by Channel-Bed Failure. In: Chen, C.-L. (ed.). Debris-Flow Hazards Mitigation: Mechanics, Prediction, and Assessment. ASCE (American Society of Civil Engineers), New York, 817 pages.

Tognacca, C., Bezzola, G.R. & Minor, H.-E., 2000. Threshold criterion for debris-flow initiation due to channel-bed failure. In: Wieczorek & Naeser (eds.). Debris-Flow Hazards Mitigation: Mechanics, Prediction, and Assessment. Balkema, Rotterdam, 608 pages.

Toutin, T. 2002. Three-Dimensional Topographic Mapping with ASTER Stereo Data in Rugged Topography. IEEE Transactions on Geoscience and Remote Sensing, 40, 10, 2241–2247.

Toutin, T, 2008.: ASTER DEMs for geomatic and geoscientific applications: a review, International Journal of Remote Sensing, 29, 1855–1875.

USGS (United States Geological Survey), 2010. Worldwide Overview of Large Landslides of the 20th and 21st Centuries. <http://landslides.usgs.gov/learning/majorls.php> (update: 2010, access 04.12.2013).

UZH, n.d.: ACC RRD Antrag. Internal report, 8 pages.

Valderrama Murillo, P., Vilca, O., 2010. Dinamica del aluvión de la laguna 513, Cordillera Blanca, Ancash Perú. Primeros alcances. Sociedad Geológica del Perú, 9, 336–341.

Varnes, D. J. 1978. Slope movement types and processes. In: Schuster, R. L. & Krizek, R. J. (eds.). Special Report 176, Landslides, Analysis and Control. Transportation and Road Research Board, National Academy of Science, Washington D. C., 11-33.

Vicuña, L., n.d. Línea de base Santa Teresa social. Internal report, 6 pages.

Vilímek, V., Zvelebil, J., Klimeš, J., Patzelt, Z., Astete, F., Kachlík, V., Hartvich, F., 2007. Geomorphological research of large-scale slope instability at Machu Picchu, Peru. Geomorphology, 89, 241–257.

Voellmy, A., 1955. Über die Zerstörungskraft von Lawinen. Schweizerische Bauzeitung, 53, 159-165, 212-217, 246-249, 280-285 (four parts).

Walder, J.S. & O'Connor, J.E., 1997. Methods for predicting peak discharge of floods caused by failure of natural and constructed earthen dams. In: Water resources research, 33, 10, 2337-2348.

Walser, M., 2013. Hazard mapping for debris-flows. Master thesis, University of Zurich, 66 pages.

Wieczorek, G.F., Coe, J.A. & Godt, J.W., 2003. Remote sensing of rainfall for debris-flow hazard assessment. In: Rickenmann, D. & Chen, C.-L. (eds.). Debris-Flow Hazards Mitigation: Mechanics, Prediction, and Assessment, 2, Millpress, Rotterdam, 1335 pages.

Wieczorek, G.F. & Glade, T., 2005. Ch14: Climatic factors influencing occurrence of debris flows. In: Jakob, M. & Hungr, O. (eds.). Debris Flow Hazards and Related Phenomena. Springer, Berlin, 739 pages.

Worni, R., Stoffel, M., Huggel, C., Volz, C., Casteller, A. & Luckman, B., 2012. Analysis and dynamic modeling of a moraine failure and glacier lake outburst flood at Ventisquero Negro, Patagonian Andes (Argentina). Journal of Hydrology, 444-445, 134–145.

Worni, R., Huggel, C., Dorren, L.K.A. & Jaboyedoff, M., 2013. Numerical Modeling of Flows and Falls. In: Shroder, J.J.F. (ed.), Treatise on Geomorphology, 7. Academic Press, San Diego, 273–283.

Wrachien, de D., 2006. Section 3 Debris and hyper-concentrated flows. Special session organised by D. De Wrachien. Scope, aims & topics. In: Lorenzini, G., Brebbia, C.A. & Emmanouloudis, D.E. (eds.). Monitoring, Simulation, Prevention and Remediation of Dense and Debris Flows. Millpress, Rotterdam, 400 pages.

Wrachien, de D., Mambretti, S. & Deangeli, C., 2010. Mechanical and fluid-dynamic behaviour of debris and hyper-concentrated flows: overview and challenges. In: Wrachien, de D. & Brebbia, C.A. (eds.): Monitoring, Simulation Prevention and Remediation of Dense and Debris Flows III. WIT Transactions on Engineering Sciences, 67, WIT Press, Southampton, Boston, 288 pages.

Wright, G. & Cairns, G. (eds.), 2011. Scenario Thinking. Practical Approaches to the Future. Palgrave Macmillan, Houndmills, Basingstoke, Hampshire, 192 pages.

WSL (Eidgenössische Forschungsanstalt für Wald, Schnee und Landschaft), 2013. RAMMS::DEBRIS FLOW. < http://ramms.slf.ch/ramms/> (Last update 2013, access 16.11.2013).

Zimmermann, M., 1990. Debris flows 1987 in Switzerland: geomorphological and meteorological aspects. In: Sinniger, R.O. & and Monbaron, M. (eds.). Proceedings of two Lausanne Symposia, Lausanne. IAHS, 387-393.

Zimmermann, M., Mani, P. & Gamma, P., 1997. Murganggefahr und Klimaänderung – ein GIS-basierter Ansatz. Schlussbericht NFP 31. vdf, Bern, 161 pages.

12 Appendix

Table 13.1: The most important simulations used for this thesis. Not all input parameters are given, more information can be found in chapter 7.2 and 7.3. In the tab "Stop", the reason for stopping is given: low flux (due to the stopping criterion) or end time (due to the end time condition).

All Simulations									
Simulation	**Volume (m^3)**	**Qmax (m^3/s)**	**t1 (s)**	**Velocity (m/s)**	ξ	μ	**Stop**	**Time (s)**	**Flux (%)**
sacsara_237	5000000	7500	180	15	1000	0.08	low flux	13800	
sacsara_238	5000000	38000	180	15	1000	0.08	low flux	6300	
sacsara_241	5000000	2500	180	15	1000	0.08	low flux	14500	
sacsara_245	5000000	7500	180	15	1000	0.08	low flux	8700	
sacsara_246	5000000	3750	180	15	1000	0.08	low flux	10500	
sacsara_247	5000000	5625	180	15	1000	0.08	low flux	9600	
sacsara_248	5000000	9375	180	15	1000	0.08	low flux	8700	
sacsara_249	5000000	11250	180	15	1000	0.08	low flux	7800	
Sacsara_0003	5000000	7500	180	15	1000	0.05	low flux	8700	
Sacsara_0004	5000000	7500	180	15	1000	0.06	low flux	11100	
Sacsara_0005	5000000	7500	180	15	1000	0.07	low flux	11100	
Sacsara_0006	5000000	7500	180	15	1000	0.08	low flux	14100	
Sacsara_0007	5000000	7500	180	15	1000	0.09	end time		0.12
Sacsara_0008	5000000	7500	180	15	1000	0.1	end time		0.2
Sacsara_0009	5000000	7500	180	15	1000	0.11	end time		0.2
Sacsara_0010	5000000	7500	180	15	1000	0.12	end time		0.22
Sacsara_0011	5000000	7500	180	15	1000	0.13	end time		0.31
Sacsara_0012	5000000	7500	180	15	1000	0.14	end time		0.35
Sacsara_0013	5000000	7500	180	15	1000	0.15	end time		0.41
Sacsara_0014	5000000	7500	180	15	500	0.09	end time		0.14
Sacsara_0015	5000000	7500	180	15	750	0.09	end time		0.15
Sacsara_0016	5000000	7500	180	15	1000	0.09	end time		0.12
Sacsara_0017	5000000	7500	180	15	1250	0.09	end time		0.14
Sacsara_0018	5000000	7500	180	15	1500	0.09	end time		0.11
Sacsara_0019	5000000	7500	180	15	1750	0.09	end time		0.11
Sacsara_0020	5000000	7500	180	15	2000	0.09	end time		0.13
Sacsara_0021	5000000	7500	180	15	2500	0.09	end time		0.12
Sacsara_0022	5000000	7500	180	15	3000	0.09	end time		0.13
Sacsara_0023	5000000	7500	180	15	1500	0.09	low flux	10500	
Sacsara_0024	6000000	8100	180	15	1500	0.09	low flux	10800	
Sacsara_0025	7000000	8700	180	15	1500	0.09	low flux	11100	
Sacsara_0026	8000000	9200	180	15	1500	0.09	low flux	11400	
Sacsara_0027	9000000	9600	180	15	1500	0.09	low flux	10500	
Sacsara_0028	10000000	10000	180	15	1500	0.09	low flux	11700	
Sacsara_0029	8000000	9200	180	3	1500	0.09	low flux	12000	
Sacsara_0030	8000000	9200	180	5	1500	0.09	low flux	10500	
Sacsara_0031	8000000	9200	180	10	1500	0.09	low flux	10800	
Sacsara_0032	8000000	9200	180	15	1500	0.09	low flux	11400	
Sacsara_0033	8000000	9200	180	20	1500	0.09	low flux	10500	
Sacsara_0034	8000000	9200	60	10	1500	0.09	low flux	10500	
Sacsara_0035	8000000	9200	120	10	1500	0.09	low flux	10200	
Sacsara_0036	8000000	9200	180	10	1500	0.09	low flux	10800	
Sacsara_0037	8000000	9200	240	10	1500	0.09	low flux	11100	
Sacsara_0038	8000000	9200	300	10	1500	0.09	low flux	10200	
Sacsara_0047	500000	1900	120	15	1500	0.09	low flux	22500	
ahobamba_0064	1000000	2600	120	15	1500	0.12	end time		0.14

All Simulations									
Simulation	**Volume (m^3)**	**Qmax (m^3/s)**	**t1 (s)**	**Velocity (m/s)**	ξ	μ	**Stop**	**Time (s)**	**Flux (%)**
ahobamba_0066	50000000	1900	300	15	1000	0.02	end time		0.54
Scenario_a001	300000	1200	120	15	1000	0.11	low flux	21000	
Scenario_a002	1000000	2600	120	15	1000	0.11	end time		0.11
Scenario_a003	2500000	5100	180	15	1000	0.11	end time		0.14
Scenario_a019	500000	1500	120	15	1000	0.07	low flux	22800	
Scenario_a020	1000000	2600	120	15	1000	0.07	low flux	18000	
Scenario_a021	3000000	5500	180	15	1000	0.07	low flux	12900	
Scenario_a022	500000	1500	120	15	1000	0.15	low flux	28200	
Scenario_a023	1000000	2600	180	15	1000	0.15	end time		0.14
Scenario_a024	3000000	5500	300	15	1000	0.15	end time		0.12
Scenario_sac001	300000	1200	120	15	1000	0.08	low flux	15900	
Scenario_sac002	1000000	2600	120	15	1000	0.08	low flux	20700	
Scenario_sac003	2500000	5100	180	15	1000	0.08	low flux	18600	
Scenario_sac011	1000000	2600	120	15	1000	0.09	low flux	28200	
Scenario_sac012	5000000	6800	180	15	1000	0.09	low flux	20400	
Scenario_sac013	10000000	10900	300	15	1000	0.09	low flux	18300	
Scenario_sal007	100000	500	60	15	1000	0.08	low flux	21900	
Scenario_sal008	500000	1500	120	15	1000	0.08	end time		0.22
Scenario_sal009	2000000	3500	120	15	1000	0.08	end time		0.2
Scenario_sal016	500000	1500	120	15	1000	0.07	end time		0.13
Scenario_sal017	1000000	2600	120	15	1000	0.07	end time		0.15
Scenario_sal018	3000000	5500	180	15	1000	0.07	low flux	26700	
srtm_s001	500000	1900	120	15	1500	0.09	low flux	13800	

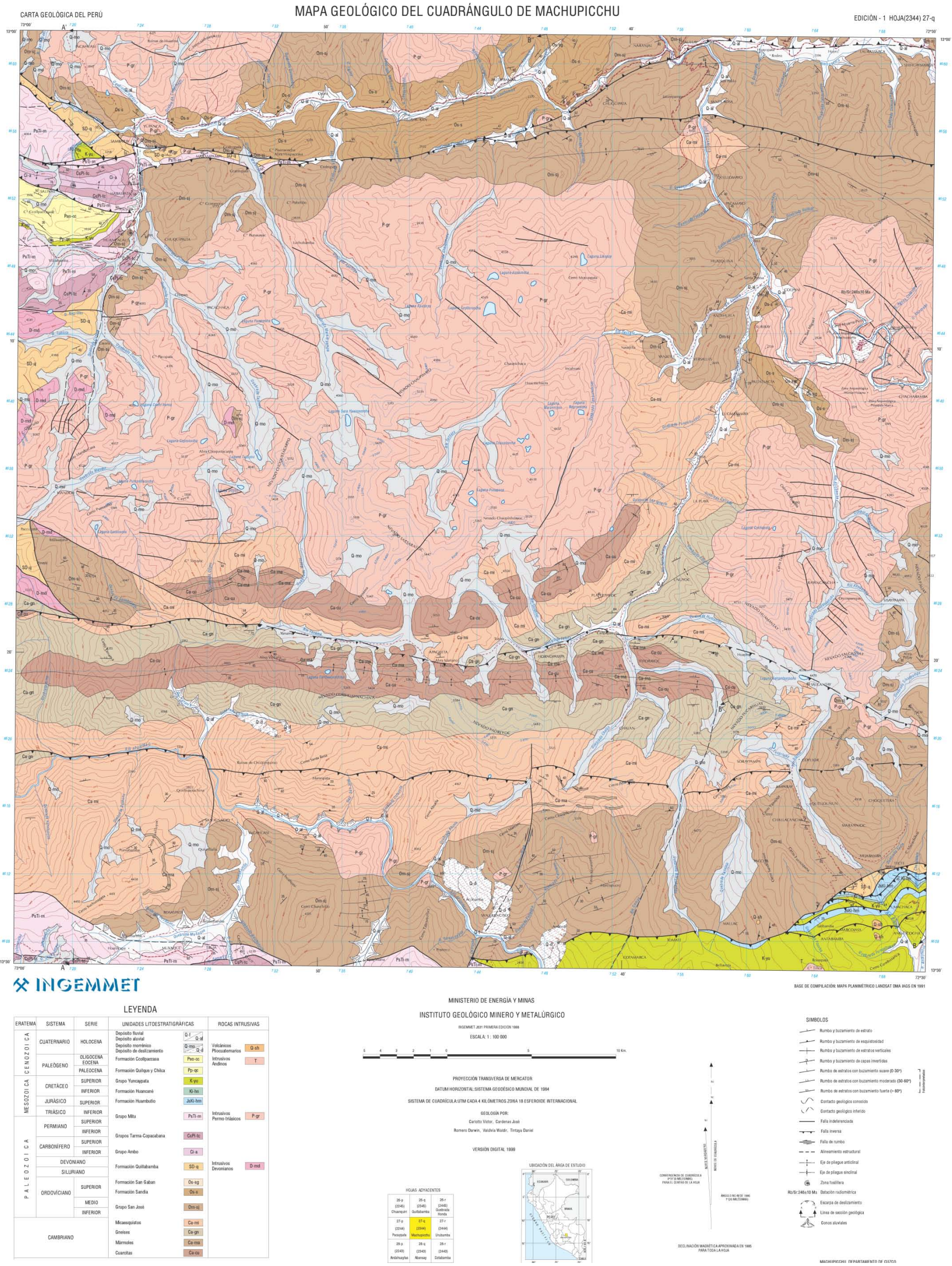

Figure 12.1: Geological Map of the study region (not in original size). Source: Carlotto et al., 1999.

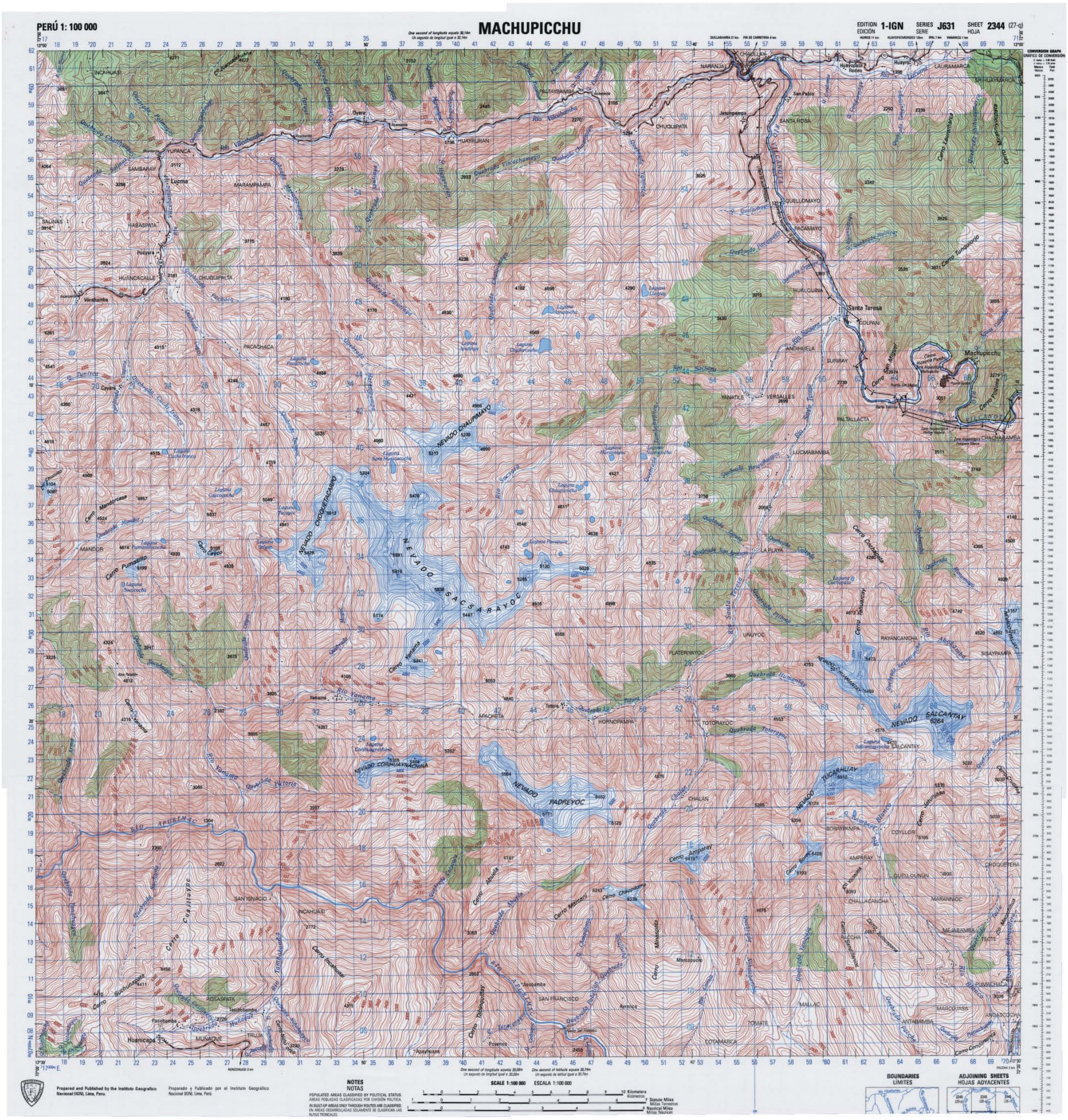

Figure 12.2: Topographic Map of the study region (not in original size). Source: IGN.

13 Personal Declaration

I hereby declare that the submitted thesis is the result of my own, independent, work. All external sources are explicitly acknowledged in the thesis.

Place and date_____ Signature_____

Daniel Buis